MS ZOE CUMBERPATCH (Orcid ID : 0000-0001-8253-8418)
MR MAX CASSON (Orcid ID : 0000-0003-4241-3447)

Article type : Original Article

Running Head: Cretaceous mixed system, Azerbaijan

Title: Evolution of a mixed siliciclastic-carbonate deep-marine system on an unstable margin: the Cretaceous of the Eastern Greater Caucasus, Azerbaijan

Authors: ZOË A. CUMBERPATCH[1*], EUAN L. SOUTTER[1], IAN A. KANE[1], MAX CASSON[1], STEPHEN J. VINCENT[2]

Institutions:

[1]Department of Earth and Environmental Sciences, University of Manchester, Oxford Road

[2]CASP, West Building, Madingley Rise, Madingley Road, Cambridge

Email: zoe.cumberpatch@manchester.ac.uk

Keywords: deep-marine, mixed system, siliciclastic-carbonate, Caucasus, Azerbaijan,

ABSTRACT

Mixed siliciclastic-carbonate deep-marine systems (mixed systems) are less documented in the geological record than pure siliciclastic systems. The similarities and differences between these systems are therefore poorly understood. A well-exposed Late Cretaceous mixed system on the northern side of the Eastern Greater Caucasus (EGC), Azerbaijan, provides an opportunity to study the interaction between contemporaneous siliciclastic and carbonate deep-marine deposition. Facies analysis reveals a Cenomanian–early Turonian siliciclastic submarine channel complex that abruptly transitions into a Mid Turonian–Maastrichtian mixed lobe-dominated succession. The channels are entrenched in lows on the palaeo-seafloor but are absent 10 km towards the west where an Early Cretaceous submarine landslide complex acted as a topographic barrier to deposition. By the Campanian, this topography was largely healed allowing extensive deposition of the mixed lobe-dominated succession. Evidence for irregular bathymetry is recorded by opposing palaeoflow indicators and frequent submarine landslides. The overall sequence is interpreted to represent the abrupt transition from Cenomanian–early Turonian siliciclastic progradation to c. Mid Turonian retrogradation, followed by a gradual return to progradation in the Santonian–Maastrichtian. The siliciclastic systems periodically punctuate a more widely extensive calcareous system from the Mid Turonian onwards, resulting in a mixed deep-marine system. Mixed lobes differ from their siliciclastic counterparts in that they contain both siliciclastic and calcareous depositional elements making determining distal and proximal environments challenging using conventional terminology and complicate palaeogeographic interpretations. Modulation and remobilisation also occurs between the two contemporaneous systems making stacking patterns difficult to decipher. The results provide insight into the behaviour of multiple contemporaneous deep-marine fans, an aspect that is challenging to decipher in non-mixed systems. The study area is comparable in terms of facies, architectures and the presence of widespread instability to offshore The Gambia, NW Africa, and could form a suitable analogue for mixed deep-marine systems observed elsewhere.

Introduction

Sedimentary successions characterised by contemporaneous deposition of both siliciclastic and carbonate lithologies, herein termed ‘mixed systems’, have been identified from the Cambrian (Osleger and Montañez, 1996) to the Quaternary (Dunbar & Dickens, 2003; Tucker, 2003). Mixed systems are defined as a system with at least 10% of a secondary source e.g. carbonate systems with a

> 10% siliciclastic component (Mount, 1985; Chiarella and Longhitano, 2012). Mixed systems are formed by a variety of depositional processes, such as river discharge in a shallow-marine area characterised by the presence of carbonate reefs, or gravity-driven siliciclastic flows eroding a carbonate-dominated slope (e.g., Mount, 1984; Chiarella et al., 2017). Mixed systems are consequently recognised in a variety of depositional environments, such as: lagoonal (Mitchell et al., 2001), shoreface (Zonneveld et al., 1997), shelfal (Mount, 1984; Zeller et al., 2015), slope (Gawthorpe, 1986) and deep-marine (Ditty et al., 1977; Yose & Heller, 1989; Bell et al., 2018a; Moscardelli et al., 2019). Recent research on mixed systems has focused on: 1) the relationships between the controlling sedimentary processes; 2) the environmental conditions influencing the carbonate factory; and 3) the distribution of mixed deposits in space and time (e.g., LaGasse and Read, 2006; Longhitano et al., 2010; 2012; Longhitano, 2011; Zeller et al., 2015; Moretti et al., 2016; Chiarella et al., 2016; 2017).

Mixed systems developed in deep-marine (below storm wave base) settings are usually formed of material shed from a shallower carbonate-producing shelf that periodically also received terrigenous input (Fig. 1) (Mount, 1984; Dunbar & Dickens, 2003; Crevello & Schlager, 1980). This material is deposited in the deep-marine by a spectrum of sediment gravity flows types, from turbidity currents to submarine landslides (Dorsey & Kidwell, 1999; Miller & Heller, 1994; Tassy et al., 2015; Moscardelli et al., 2019). Generic concepts have been proposed in the literature for mixed systems and their potential relationship with deep-marine systems (e.g., McNeill et al., 2004; Francis et al., 2007; 2008); while valuable, these studies rely on limited exposures and incomplete subsurface data sets leading to models that do not account for the vertical and lateral stratigraphic variabilities observed in recent subsurface studies of deep-marine mixed systems (Moscardelli et al., 2019; Casson et al., 2020).

Sediment-gravity-flows that lose confinement on the slope or basin-floor can build lobate depositional bodies, known generically as lobes (e.g., Prélat et al., 2009). Lobes can be important archives of palaeoclimatic and palaeogeographic information, and upstream changes in the source-to-sink system (e.g., Fildani et al., 2016; 2018; Hessler & Fildani, 2019). They may also record the palaeoenvironmental conditions that lead to margin instability and collapse, and thus aid interpretation of submarine landslide genesis (Clift and Gaedicke, 2002; Fildani et al., 2016; 2018). Exhumed deep-marine lobes have been studied in great detail, and a wide variety of stacking patterns, depositional processes and facies distributions have been described and interpreted (e.g., Mutti, 1983; Postma et al., 1993; Prélat et al., 2009; Terlaky et al., 2016; Kane et al., 2017; Bell et al., 2018a; Fildani et al., 2018; Fonnesu et al., 2018; Soutter et al., 2019). These studies typically focus on siliciclastic

systems, with few studies investigating the characteristics of lobes formed in mixed systems (Fig. 1). Recent work on mixed deep-marine systems is limited to subsurface data sets (Puga-Bernabéu et al., 2011; 2014 Moscardelli et al., 2019; Casson et al., 2020). It remains uncertain how exportable depositional models, documenting sub-seismic scale facies variability, stacking patterns and hierarchies, developed in siliciclastic deep-marine systems (e.g., Prélat et al., 2009; Spychala et al., 2017) are, to their mixed counterparts.

This study addresses this by describing exhumed Cretaceous submarine lobes from the Eastern Greater Caucasus (EGC), Azerbaijan (Fig. 2). The study aims to: 1) document characteristics of mixed lobes; 2) discuss processes that govern their deposition; 3) compare mixed lobes with their siliciclastic counterparts; 4) describe the sedimentological evolution of the EGC throughout the Cretaceous; and 5) provide insights into depocentres characterised by unstable margins.

Geological Setting and Basin Structure

Evolution of the Eastern Greater Caucasus (EGC)

The EGC forms the easternmost extent of the NW-SE trending Greater Caucasus orogenic belt, which runs from the Black Sea in the west to the Caspian Sea in the east (Fig. 2) (Phillip et al., 1989; Mosar et al., 2010). The EGC sits on the southern-edge of the Scythian Platform, which represents the southern margin of the Eastern European continent (Saintot et al., 2006b). The exposed EGC is mainly composed of Jurassic and Cretaceous deep-marine sediments that accumulated within the eastern strand of the Greater Caucasus Basin. Multiple phases of extension and compression are recorded in the basin fill and were driven by the sequential closure of the Tethys Ocean whose active margin was situated farther to the south (Golonka, 2004; Nikishin et al. 1998, 2001; Saintot et al., 2006a; Vincent et al., 2007, 2016; Adamia et al. 2011). Late Triassic-Early Jurassic compression was followed by the main rifting phase in the evolution of the Greater Caucasus Basin, in the Early- to Mid-Jurassic (Nikishin et al. 2001; Saintot et al., 2006a; Mosar et al. 2010; Vincent et al., 2016). This tectonic event is recorded by major thickness variations across the Middle Jurassic interval (Bochud, 2011). The Upper Jurassic succession is dominated by massive to well-bedded bioclastic limestones with fragments of echinoderms, corals and bivalves within a micritic matrix, which is interpreted to represent deposition in an open, moderate to high-energy proximal ramp (Khain, 1952; Shardanov, 1953; Alizadeh et al., 2016).

The Lower Cretaceous succession in the EGC was deposited within an unstable marine environment, as recorded by frequent mass-wasting events (Egan et al., 2009; Bochud, 2011). This was triggered by renewed rifting (e.g., Vincent et al., 2016; 2018). The rifting was potentially associated with opening phases in the Black Sea Basin farther to the west, although the exact timing of Black Sea Basin opening is still debated (e.g., Nikishin et al., 2015a; b; Sosson et al. 2016; Maynard and Erratt, 2020). This resulted in deep-marine deposition of extensive mudstones interspersed by submarine landslide deposits and terrigenous sediments.

The remainder of the Mid and Upper Cretaceous sequence was deposited during a period of thermal subsidence on a southward-dipping slope (Bochud, 2011). The Mid-Upper Cretaceous stratigraphy is dominated by calcareous and siliciclastic turbidites, and mass failure deposits, interbedded with hemipelagic marls and mudstones. A number of intra-Cretaceous unconformities occur within the Greater Caucasus Basin and are related to periods of compression (Egan et al., 2009) or sea-level fluctuations. The Cretaceous sequence is capped by a base-Cenozoic unconformity that may have formed during Paleogene compression (Bochud, 2011).

Cenozoic collision of the Arabian and Eurasian plates inverted the Mesozoic and early Cenozoic basinal succession (Saintot et al., 2006a; Vincent et al., 2007; 2016; Mosar et al., 2010). In the EGC a series of exhumed synclines are bound by major southerly-verging thrusts and associated back thrusts (Mosar et al., 2010). These faults separate distinct structural zones, including the Qonaqkend Zone in the northern EGC (Fig. 2) (Bochud, 2011).

The Buduq Syncline

This study focuses on Late Cretaceous strata exposed in the Buduq Syncline, or Buduq 'Trough' (Bochud, 2011), which is located between the NW-SE striking thrust faults that bound the Qonaqkend Zone (Fig. 3), and encompasses the villages of Buduq, Cek and Qonaqkend (Fig. 2). Late Cretaceous strata have been interpreted to be deposited in a 'palaeo-valley' incised into Early Cretaceous deep-marine sediments and Late Jurassic limestones (Bochud, 2011) following a period of Cretaceous compression (Fig. 2B) (Egan et al., 2009). The earliest fill of the palaeo-valley is represented by Cenomanian-early Turonian sandstones and conglomerates (the Kemishdag Formation) that crop out in the east (Kapaevitch et al., 2015, 2017). These sediments conformably

overlie Aptian-Albian sediments at Mt. Kelevudag (Kopaevich et al., 2015) but rest unconformably on Barremian strata at Khirt (Fig. 2). The overlying mid Turonian-Maastrichtian succession is represented by mixed turbidites and is conformable with the Cenomanian-early Turonian interval in the east. In the west, near Cek, the Cenomanian-Santonian interval is absent, with Campanian strata directly overlying Aptian-Albian thinly-bedded depsoits. Campanian-Maastrichtian strata consist of submarine landslide deposits, comprising remobilised Upper Jurassic blocks, and mixed siliciclastic-carbonate turbidites (Bochud, 2011; Kopaevich et al., 2015). Oceanic red beds (CORBs) occur throughout the Upper Cretaceous sequence, particularly in Coniacian–Campanian turbidites and marls, indicating periodically oxic deep-marine conditions (e.g., Hu et al., 2005). The overlying Paleogene succession has largely been removed by Cenozoic compression and erosion (Bochud, 2011), which folded the remaining Cretaceous into a shallow syncline (Figures 2 and 3). Recent erosion of the study area has carved a number of narrow valleys through this syncline exposing the Cretaceous succession (Fig. 2).

Data and Methods

The data set comprises 23 sedimentary logs, totalling 500 m, collected across the Buduq Syncline (see supplementary material). Logs were generally collected at 1:25 scale. Bedding, structural data (Fig. 3) and palaeocurrent data (Fig. 4) were collected to ground-truth the geological map and cross-sections of Khain and Shardanov (1958) and Bochud (2011). Palaeocurrent readings were quite rare and were taken only where sedimentary structures were clear enough to permit unambiguous data collection. Sparse biostratigraphic data hinders precise correlation across the study area. Chrono-stratigraphic subdivisions of the Buduq Syncline stratigraphy are still being refined (cf. Khain & Shardanov, 1958, Bochud, 2011; Bragina & Bragin, 2015; Kopaevich et al., 2015, 2017), due to the litho-stratigraphic similarities between the units and the complex palaeobathymetry in which they were deposited (Egan et al., 2009). Therefore, we use mapped stratigraphic units (J_1, J_2, K_1, K_2 etc.), lithostratigraphy and cross-cutting relationships to suggest associated ages. Combining the work discussed above, we group stratigraphy into early (Aptian-Albian), mid (c. Cenomanian-early Turonian) and late (c. mid Turonian and younger) Cretaceous units. Sedimentary logs were used to develop a lithofacies scheme (Fig. 5, Table 1) and facies associations (Fig. 6).

Over 10,000 sedimentological measurements (e.g. bed thickness, grain-size, facies) were collected and quantitatively analysed (see supplementary material). Stratigraphic logs were assigned one of seven facies associations (Fig. 6) in order to quantitively compare bed statistics across deep-marine sub-environments (Figures 7-10).

Results

Lithofacies

Carbonate and siliciclastic lithofacies presented in Table 1 and Figure 5 represent beds deposited by individual events (event beds) and are classified based on outcrop observations. For simplicity and ease of comparison to their siliciclastic gravity flow counterparts, here we define *calcareous mudstones/siltstone/sandstones* as resedimented mudstones-wackestones comprising detrital carbonate grains in accordance with the Dunham classification of limestones (Dunham, 1962). Grain-sizes range from silt- to very fine sand-sized in a micritic matrix. Lithofacies show evidence for bed-scale stratal mixing (*sensu* Chiarella et al., 2017) (Table 1).

Facies Associations

Facies associations have been interpreted based on the dominant lithofacies (Fig. 5, Table 1) and architecture of a given succession and are subdivided into siliciclastic and mixed associations (Fig. 6). Letters in brackets refer to lithofacies described in Table 1. Facies associations (FA) 1 is Aptian-Albian (early Cretaceous) in age, 2-3 are Cenomanian-early Turonian (mid Cretaceous) in age and FA 4-7 are mid Turonian-Maastrichtian (late Cretaceous) in age. Facies association nomenclature commonly used for lobes (Prélat et al., 2009; Spychala et al., 2017) and channels (Kane & Hodgson, 2011; Hubbard et al., 2014) best fit our observations.

Siliciclastic Facies Associations

FA 1: Lobe Fringe

Observations: FA 1 is dominated by metre-scale packages of thin-bedded siliciclastic siltstones to fine-grained sandstones (H) with subordinate mudstones (J) and medium-bedded siliciclastic sandstones (F) (Table 1, Fig. 6A). Beds are laterally extensive for 100's of metres and are commonly flat based and flat topped, often being normally-graded from fine-grained sandstone to siltstone. Planar and convolute laminations are observed in the upper part of many beds (Fig. 5E). Poorly-sorted clast-rich deposits, bi/tri-partite beds, conglomerates and thick-bedded sandstones are absent.

Interpretations: Thin-bedded, structured sandstones are interpreted to be deposited from low-concentration turbidity currents (Mutti et al., 1992; Jobe et al., 2012; Talling et al., 2012). The thin-bedded nature, lateral-extent and fine grain-size of these deposits (Mutti, 1977; Prélat et al., 2009;

Marini et al., 2015), along with the absence of bi/tri-partite beds and ripple-stratification indicate deposition in a lobe fringe (Fig. 8) (Spychala et al., 2017; Boulesteix et al. 2019; 2020).

FA 2: Channel Axis

Observations: FA 2 is composed of metre-scale conglomerates (A) and thick-bedded medium-grained to pebbly sandstones (C) with lesser medium-bedded sandstones (F) and rare thin-bedded sandstones (H), mudstones (J), poorly-sorted clast-rich deposits (B) and bi/tri partite beds (I) (Fig. 6C). FA 2 has the highest density of conglomerates (44%), thick-bedded sandstones (10%), and bi/tri partite beds (10%) of all Cenomanian-early Turonian facies associations (Fig. 8). Conglomerates often grade normally into thick-bedded sandstones, commonly associated with a grain-size break, with the granular-grade sandstone often missing. Where conglomerates do not grade into thick-bedded sandstones they are amalgamated or separated by thin beds of mudstone. Conglomerates are poorly-sorted, clast-supported and contain sub-angular – sub-rounded clasts of wackestone, micrite, sandstone and mudstone that often crudely grade from cobbles to pebbles upwards (Fig. 10). Conglomerates also often contain small amounts of disarticulated shelly fragments (<5% clasts). Sandstone and conglomerate bases are almost always erosional.

Thick-bedded sandstones are commonly normally-graded but can occasionally be massive or inversely-graded. Decimetre-scale mud-clasts are common throughout thick-bedded sandstones and low-angle cross-stratification is infrequently observed (Fig. 5H). Thin- to medium-bedded sandstones often have erosional bases and contain convolute, hummock-like and planar laminations, and are normally-graded, with rare examples of inverse- or non- grading. These sandstones are either amalgamated or separated by decimetre thick mudstone layers, and often contain mud-clasts throughout the bed with granules concentrated at the bed base (Fig. 5E). Sporadic poorly-sorted clast-rich deposits are also seen within FA 2; these have a deformed mudstone matrix and contain clasts of limestone and sandstone. Bi/tri-partite beds are amalgamated into 30-50 cm packages, with individual beds commonly consisting of a 2-4 cm thick fine- to medium- grained sandstone overlain by a clast and shelly fragment rich 8-12 cm thick muddy, very-fine sandstone poorly-sorted deposit.

Channel 'off-axis' sequences, are infrequently observed in outcrop, so are not divided into a separate facies association. Where interpreted to be present, they have fewer thick-bedded sandstones (C) and conglomerates (A) and more thin- to medium- bedded sandstones (H, E) than channel axis successions (Fig. 8).

Interpretations: The thick-bedded nature, coarse grain-size, amalgamation, erosion and entrainment of clasts within the sandstones suggests that the parent flows were highly energetic and capable of eroding and bypassing sediment (Mutti, 1992; Stevenson et al., 2015). Therefore, these beds are interpreted as high-density turbidites (Lowe, 1982). The poorly-sorted nature of the conglomerates suggests that they were initially deposited by laminar flows (Sohn, 2000), however apparent grading of conglomerates into thick-bedded sandstones could reflect the transition of hyper-concentrated submarine debris flows into highly-concentrated turbulent flows (Mulder and Alexander, 2001) due to entrainment of ambient water (Postma et al., 1988; Kane et al., 2009a). Limestone clasts are interpreted to have been remobilised from Jurassic platforms (Bochud, 2011).

The transition from conglomerates, to medium- to very coarse-grained sandstone is associated with a grain-size break, often missing the granule fraction, which could suggest bypass of flow (Stevenson et al., 2015). The coarse grain-size and basal location of the conglomerates with respect to thick-bedded sandstones suggests these beds could have been deposited as channel-base lags (Hubbard et al., 2014). Erosionally-based lenticular bodies grading from cobble-rich conglomerates to fine-grained sandstones are interpreted to represent submarine channel fills (Jobe et al., 2017; Bell et al., 2018a). This facies association is consistent with gravelly-conglomeratic deposits reported elsewhere to represent submarine channel axis deposition (Postma, 1984; Nemec & Steel, 1984; Surlyk, 1984; Dickie & Hein, 1995; Kane et al., 2009b; Li et al., 2018; McArthur et al., 2019; Kneller et al., 2020).

While typically related to storm deposits (e.g., Hunter & Clifton, 1982), hummock-like cross-lamination has been interpreted in deep-marine environments elsewhere as anti-dune stratification (Mulder et al., 2009), bottom current deposits (Basilici et al., 2012; Furhmann et al., 2020) and reworking of an initial deposit by a subsequent flow (Mutti, 1992; Tinterri et al., 2017). The channel axis interpretation of FA 2 speculatively suggests anti-dunes formed by supercritical flows may be the most probable interpretation of these hummock-like structures (Araya & Masuda, 2001; Alexander, 2008).

FA 3: Channel Margin

Observations: FA 3 comprises thin- to medium-bedded, fine-grained to granular- sandstones (H, F) in 30-80 cm packages interbedded with 10-90 cm thick dark mudstones (J) (Fig. 6C). Within the siliciclastic Cenomanian- early Turonian succession, FA 3 is dominated by thin- and to a lesser extent

medium-bedded sandstones (72%) (Fig. 8). Conglomerates (A) and thick-bedded sandstones (C) are rare in FA 3 (Fig. 8). Thin-bedded sandstones and the upper part of medium-bedded sandstones can be argillaceous and micaceous, and are often planar-, ripple- and convolute-laminated, with rarer hummock-like laminations. Sandstones are often normally-graded but inverse-grading is also observed. Beds of medium thickness are rich in mud-clasts and commonly amalgamated along mud-clast laden surfaces. Bed bases can be highly-erosive and scour-like, removing a significant proportion of the underlying bed. Thin-bedded sandstones can be flat or erosively based, and are commonly scoured; where bases are erosional the lowermost part of the bed is commonly rich in granule-grade material (Fig. 6C). Granules and coarser fragments are composed of limestone and sandstone. Infrequent bi/tri-partite beds (I) are composed of medium-coarse grained siliciclastic sandstone, overlain by a muddy, occasionally marly fine sandstone poorly-sorted deposit.

Interpretations: The thin-bedded nature and presence of tractional structures indicate that this facies association was deposited by a low-density turbidity current (Lowe, 1982). A deep-marine origin is interpreted based on the presence of thick, dark mudstones and frequent sediment gravity flow deposits (Mutti, 1992). Anti-dune formation (Mulder et al., 2009) and tractional reworking of an aggrading deposit (Mutti, 1992; Tinterri et al., 2017; Bell et al., 2018a) have both been interpreted to form similar hummock-like lamination in deep-marine environments, similar to those indicating storm-wave influenced deposition (Harms et al., 1975). Clean sandstones that grade into argillaceous, micaceous sandstones could indicate transitional flow deposits (Sylvester & Lowe, 2004; Baas et al., 2009; Kane & Pontén, 2012). The thin-bedded, coarse grain-size and erosive nature of these deposits, along with the presence of supercritical bedforms, is similar to the overbank deposits seen adjacent to bypass-dominated channels (Kane & Hodgson, 2011; Hubbard et al., 2014; Jobe et al., 2017; Lin et al., 2018; McArthur et al., 2019). These similarities, coupled with the along strike location of FA 3 adjacent to FA 2 (channel axis), has led to the interpretation of FA 3 as a channel margin (Fig. 8). The lateral transition of FA 2 and 3 is indicative of the continuum between axis and margin channel facies, and is similar to the 'on-axis' to 'off-axis' shifting of channel-belts (Kane et al., 2009b).

FA 4: Lobe Axis

Observations: FA 4 is dominated by > 1 m thick packages of amalgamated conglomerates (A) (Figures 6D and 8) interbedded with thin- to thick-bedded, very fine- to very coarse-grained sandstones (H, F, C). Within the mid Turonian-Maastrichtian succession, the thickest conglomerates are found within

FA 4 (Fig. 7). The conglomerates are laterally discontinuous over decametres, erosionally-based, and are either flat-topped when onlapping, or convex-up when downlapping the slope (Figures 6 and 11). Conglomerates increase in frequency, clast size (up to cobble-grade) and thickness up stratigraphy (Fig. 7) and contain sub-angular to rounded clasts of carbonate (wackestone and micrite) and siliciclastic (sandstone and mudstone) material (Fig. 10). Within the mid Turonian-Maastrichtian stratigraphy, the greatest number of amalgamated beds is in FA 4 (Fig. 9) and the largest grain-size range (majority of beds between very fine to medium-grained sandstone) is observed (Fig. 7). Within FA 4, a coarser grain-size class (of coarse-grained sandstone or above) is observed which is almost absent in other mid Turonian-Maastrichtian facies associations (FA 5, FA 6, FA 7) (Fig. 7).

Interpretations: Amalgamation of event beds suggests parent flows were energetic and capable of eroding sediment and incorporating it into the flow (Lowe, 1982; Stevenson et al., 2015). Amalgamation of conglomerates indicates deposition in an environment characterised by frequent debris-flows (Surlyk, 1984; Postma, 1984; Dickie & Hein, 1995), similar to the debris-flow dominated lobes described by McHargue et al. (2019). These conglomerates could also represent sediment bypass within lobe axes (Kane et al., 2009b) or channel fill conglomerates (Knaust et al., 2014). Their thickness, amalgamated nature, downlapping geometry, and association within a FA typical of lobe axis deposition (Spychala et al. 2017; Soutter et al. 2019) suggest they are most likely to represent deposition in the axis of a debris-flow dominated lobe (McHargue et al., 2019).

Mixed Facies Associations

Alternations between siliciclastic and carbonate beds in the mixed facies association indicates most mixing was on the stratal-scale (bed- to architecture-scale). Smaller-scale (lamination-scale) fluctuations between carbonate and siliciclastic are observed in the mixed siliciclastic and calcareous sandstones facies (D), indicating subordinate compositional mixing processes (Chiarella et al., 2017).

FA 5: Lobe Off-Axis

Observations: FA 5 is represented by erosively based, thin- to medium-bedded, fine- to coarse-grained siliciclastic sandstones (H, F), thin- to medium-bedded fine-grained calcareous siltstones (G, E), (A) and mudstones (J) (Figures 6 and 7). Sandstones with siliciclastic bases that appear to transition into calcareous topped are present throughout. They are often amalgamated with siliciclastic and calcareous sandstones, forming packages separated by mudstones and silty-mudstones. Calcareous beds are typically flat-based when overlying mudstones, whilst siliciclastic beds are commonly irregularly-based. Calcareous siltstones and sandstones are structureless (Figures 5B, 5D and 6D),

whilst siliciclastic sandstones may contain planar, convolute and ripple laminations, but can also be structureless (Figures 5D, 5E and 11B). Poorly-sorted clast-rich deposits (B) are interspersed, often comprising remobilised thin-bedded calcareous siltstones and sandstones. Bi/tri-partite beds (I) are rare (Fig. 8).

Interpretations: The presence of both calcareous and siliciclastic sandstones suggests deposition in a mixed system (Figures 1 and 9) (Al-Mashaikie & Mohammed, 2017; Chiarella et al., 2017; Walker et al., 2019). Structureless medium-bedded calcareous siltstones and sandstones with normal grading or tractional bedforms at the bed top are interpreted to record deposition from waning turbidity currents transitioning relatively continuously from higher- to lower-densities over a single point on the seabed (e.g. Talling et al., 2012), and are therefore termed 'medium-density' turbidites to differentiate them from high- and low-density turbidites (Soutter et al., 2019). These sandstones could also represent amalgamation of deposits formed by multiple low-density currents, with amalgamation surfaces difficult to decipher due to the lack of grain-size, colour and mineralogical variation within the sandstones (Imbrie & Buchanan, 1960). This depositional process is complicated within the calcareous medium-bedded deposits, which appear to have aggraded much more slowly than their siliciclastic counterparts, as evidenced by thin-bedded and medium-grained siliciclastic beds (D) being deposited within medium-bedded and fine-grained calcareous beds. These beds may therefore be derived from low-density carbonate-dominated flows that were depositional over long-time periods, resulting in thick, but fine-grained, beds. This may be driven by the presence of, and depositional distance from, two contemporaneously active sediment source areas (Chiarella et al., 2017; Moscardelli et al., 2019). The presence of medium-density turbidites, their relatively coarse grain-size and common amalgamation suggests lobe off axis deposition (Prélat et al., 2009; Spychala et al., 2017).

FA 6: Proximal Fringe

Observations: Primarily composed of normally-graded, thin- to medium-bedded, calcareous very-fine- to fine-grained sandstones and siltstones (G, E), with subordinate thin-bedded siliciclastic fine- to medium-grained sandstones (H) and mixed siliciclastic and calcareous sandstones (D) (Figures 6-8). Calcareous siltstones and sandstones are flat-based when overlying mudstones (J), but are often irregularly-based at amalgamation surfaces (Fig. 5D). Siliciclastic sandstones, either isolated or within mixed beds, are frequently < 3 cm thick, with flat to weakly-irregular bases (Fig. 5D). Poorly-sorted clast-rich deposits (B) are interspersed within FA 6 and often rework the thin-bedded calcareous siltstones and sandstones. Planar laminations are common within the thin-bedded siliciclastic and

calcareous sandstones (G) (Figures 5D and E). Less common ripple laminated sandstones show multiple and/or opposing palaeocurrent orientations (Figures 4 and 11B). Bi/tri-partite beds (I) are rare (Fig. 8).

Interpretations: The presence of both calcareous and siliciclastic sandstones suggests deposition in a mixed system (Figures 1 and 9) (Al-Mashaikie & Mohammed, 2017; Chiarella et al., 2017; Walker et al., 2019). Calcareous sandstones are interpreted to represent deposition from low- to medium-density turbidity currents based on their bed thickness, fine grain-size and internal sedimentary structures (Lowe, 1982; Mutti, 1992; Soutter et al. 2019). The thin-bedded siliciclastic sandstones could represent the depositional products of flow transformation from up-dip debris flows (i.e. the up-dip conglomerates) to turbulent flows following the entrainment of ambient water (Potsma, 1988; Haughton et al., 2009), which punctuate slowly aggrading calcareous turbidites, interpreted to represent the remnants of dilute flows (Remacha & Fernández, 2003). Opposing palaeocurrent orientation may suggest flow reflection and deflection due to the presence of topography (Kneller et al., 1991) or contour currents (e.g., Fuhrmann et al. 2020).

The preservation of both structured and structureless sandstones suggests an off-axis location of deposition because; similar preservation of both deposit types has been interpreted in proximal lobe fringes elsewhere (Prélat et al., 2009; Spychala et al., 2017; Soutter et al., 2019). FA 6 is differentiated from FA 5 based on its thinner beds and less abundant erosional events and is therefore interpreted as being more distal and deposited within the proximal fringe. Hybrid beds are rare throughout the studied system and a distinction between frontal fringe and lateral fringe is not possible (e.g., Spychala et al., 2017).

FA 7: Distal Fringe

Observations: Dominated by laterally extensive, metre-scale packages of thin-bedded amalgamated calcareous sandstones (H) that are normally-graded from very fine- or fine-grained sandstone to siltstone and are interbedded with metre-scale mudstones and silty mudstones (J) (Figures 6-8). Beds are flat-based, flat-topped and frequently contain both parallel and convolute laminations. Medium-bedded calcareous siltstones to fine-grained sandstones (E) are present and may reflect amalgamated thinner beds that are difficult to decipher. Poorly-sorted, clast-rich deposits (B), siliciclastic thin-bedded sandstones (H) and bi/tri-partite beds (I) are rare (Fig. 8). The smallest grain-size range (between siltstone and very fine-grained sandstone) is observed in FA 6 and FA 7 (Fig. 7) and

amalgamation is infrequent (Fig. 9). More thin beds are seen in FA 7 than elsewhere in the stratigraphy (Figures 6-8).

Interpretations: Thin-bedded laminated sandstones with tractional structures are interpreted to be deposited from low-concentration turbidity currents (Mutti et al., 1992; Jobe et al., 2012; Talling et al., 2012). The presence of thin- to medium-bedded calcareous siltstones and fine-grained sandstones and a lack of ripple laminations suggest slow aggradation rates from low velocity flows (Remacha & Fernández, 2003; Bell et al., 2018a). Alternatively, ripples may not have been preserved, or may be difficult to recognise due to a lack of grain-size or colour contrast (Imbrie & Buchanan, 1960). The infrequency of siliciclastic beds suggests deposition in a carbonate-dominated environment. The thin-bedded nature, lateral-extent, fine grain-size, rare hybrid beds and lack of ripple stratification suggest a distal lobe fringe depositional setting (Mutti, 1977; Prélat et al., 2009; Marini et al., 2015; Spychala et al., 2017).

Stratigraphic evolution

This section briefly describes the spatial and temporal distribution of facies associations (Fig. 6) and palaeocurrent changes throughout the Cretaceous (Fig. 4). These observations, along with evidence for palaeobathymetry (Figures 11-14) are later used to interpret the Cretaceous evolution of the Buduq Syncline (Fig. 15).

The Aptian-Albian succession comprises sheet-like stacked units of FA 1 which are extensive across the scale of the outcrop (100's of metres laterally) (Fig. 6A). Palaeocurrent data is not available due to limited accessibility.

An abrupt transition from distal fine-grained Aptian-Albian deposition to conglomeratic slope channels indicates a shallowing-upwards (regression) or change in sediment supply configuration into the Cenomanian. The Cenomanian-early Turonian succession is dominated by FA 2 and FA 3. FA 2 erosionally overlies FA 1, has a concave-up geometry and can be extensive for 100's metres, in both length and width (Fig. 6B). Metre-scale thick packages of FA 2 often erode into older channel axis facies below. The sheet-like architecture of FA 3 is laterally extensive for at least decametres, and is often laterally adjacent to FA 2. FA 2 can erosionally incise into FA 3 and appears to transition laterally into FA 3, in agreement with its interpretation as marginal channel deposition (e.g., Lin et al., 2018; McArthur et al., 2019). Cenomanian-early Turonian palaeocurrents are variable, consistent with

sinuosity in submarine channels (e.g., Peakall et al., 2000; 2012; Kane et al., 2008). There is a predominant SSW-trend in the Cenomanian – early Turonian (Fig. 4), consistent with the presence of a terrigenous sediment source to the NNE (Gómez-Pérez et al., 2005). A significant amount of northerly dominated flow indicators could indicate palaeoflow reflections in agreement with flow deflection from a bathymetric high to the south (Fig. 11B) (e.g., Kneller et al., 1991).

From the mid Turonian onwards mixed facies associations are common and the percentage of carbonate intraclasts in conglomerates increases (Fig. 10) illustrating a transition from Mid Cretaceous terrigenous to Late Cretaceous chalk dominated shallow-water carbonate Scythian and southern Russian platforms (Baraboshkin et al., 2003). This, coupled with a change from slope channels to submarine lobes, indicates sea-level rise or a reduction in sediment supply. FA 4-7 are laterally extensive and stack together. The facies associations often transition vertically into each-other in a non-predictable manner (Fig. 17). FA 6 and 7 are extensive at Cek, in the NW of the Buduq Syncline. FA 4 and 5 are more common in the centre, in agreement with Cek being at a more distal location with respect to the proposed Scythian Platform source. FA 6 and 7 are sheet-like and laterally extensive across 100s-1000s of metres. Where FA 6 and 7 are in contact with trough margins or Jurassic clasts, units are steepened and thin towards the contacts (Figures 11A, 12A and 12B), suggesting slopes of up to 6° in places.

Conglomeratic bodies within FA 4 and FA 5 (Figures 6D and 6E) are discontinuous over metres-decametres and can be convex-up or down in geometry and amalgamated or erosive with the beds below. These small conglomeratic channel fills have similar composition to the underlying, Cenomanian-early Turonian, more extensive slope channels (100s metres wide) (FA 2). Conglomerate body frequency increases throughout the mid Turonian to Maastrichtian stratigraphy, suggesting progradation (Figures 6D and 7).

Limited palaeocurrent observations from the mid Turonian-Santonian stratigraphy at Qonaqkend (Fig. 4) indicate E-W flow. This may reflect the interruption of siliciclastic input immediately to the north and the continued presence of a bathymetric high to the south resulting in the axial flow of mixed systems within a sub-basin. Given the limited number of palaeocurrent measurements, however, this hypothesis must be considered speculative. Campanian-Maastrichtian palaeocurrent data support palaeoflow in a broadly SW to WNW direction (Fig. 4). This is consistent with palaeoflow measurements from older strata and is in broad agreement with regional palaeogeographic

maps (e.g., Nikishin et al., 1998; Barrier et al., 2008). It is considered to represent flows derived directly from a northerly Scythian Platform source, along with those from input points farther east that were deflected to flow parallel to the structural grain of the Greater Caucasus Basin. Southerly-verging folds in debrites (Fig. 11E) are further evidence for the presence of a northerly-slope.

Changes in the geometry, exact extent and thus source area of the platform are probably linked to the compositional transition from a terrigenous to a carbonate-dominated platform (Nikishin et al., 1998; 2001) rather than a geographical shift in source area. The majority of palaeocurrent measurements were from siliciclastic units, and therefore the change in palaeocurrent could reflect a switching of dominance of various siliciclastic point-feeding conduits on the platform through time, rather than a change in overall platform geometry or position (e.g., Tcherepanov et al., 2008; Casson et al., 2020).

Discussion

Nature of the Late Cretaceous Bathymetry

In the western part of the study area, Late Cretaceous deep-marine sandstones are observed to thin-towards, and onlap, Late Jurassic platform limestones (Figures 11-13). Stratigraphy is observed to thin from metres to centimetres across the scale of the outcrop (10's – 100's metres) towards Late Jurassic limestones around Cek (Figures 11A, 12B and 13). Late Jurassic limestones must therefore have formed 100s of metres of relief on the Cretaceous seafloor. The most likely mechanism for the generation of seafloor topography is through allochthonous block emplacement. These blocks, or 'megaclasts' (e.g., Blair & McPherson, 1999), were likely derived from Late Jurassic carbonate platform limestones (Figures 12-14). The presence of decametre-scale allochthonous blocks and submarine landslide deposits throughout the Cretaceous stratigraphy indicates a highly unstable margin (Fig. 12). Interpretations of basin-scale submarine landslide deposits, which partially form the Qizilqaya and Shahdag mountains farther west, further validates this interpretation (Bochud, 2011; Gavrilov, 2018) (Fig. 14), with the mega-clasts in the west of the study area possibly forming part of this deposit (Figures 13-15). Similar onlap relationships to those formed as the Cretaceous stratigraphy infilled the irregular surface created by earlier submarine landslide deposits, have been observed elsewhere at outcrop (e.g., Burbank et al., 1992; Armitage et al., 2009; Kneller et al., 2020) and in the subsurface (Fig. 16) (e.g., Soutter et al., 2018; Casson et al., 2020). These Late Jurassic blocks (Figures 12 and 14) within the Cretaceous stratigraphy can be interpreted as either: 1) Late

Cretaceous failures from an exposed Jurassic shelf; 2) out-running blocks from Early Cretaceous failures (e.g., De Blasio et al., 2006) that were subsequently onlapped during the Late Cretaceous, or; 3) blocks that were periodically remobilised throughout the Late Cretaceous from high-relief Early Cretaceous slope submarine landslides identified in the west (Figures 13 and 15).

Differential compaction around these rigid blocks will have resulted in the steepening of strata adjacent to the block, which may contribute to the gradual rotation and steepening of stratigraphy identified (Figure 11 and 13). This has been reported elsewhere around allochthonous blocks (e.g., Burbank et al., 1992).

Late Cretaceous evolution of the Buduq Syncline

Late Cretaceous deep-marine deposition within the Buduq Syncline began following a period of compression and folding in the mid-Cretaceous (Fig. 15) (Egan et al., 2009, Bochud, 2011). Evidence of this compression is preserved in the east of the study area. The early fill is represented by Cenomanian-early Turonian conglomeratic slope channels that either eroded into Barremian deep-marine mudstones or are conformable with thin-bedded Aptian-Albian siliciclastic turbidites. These basal Cenomanian stratigraphic relationships are suggested to be caused by channels preferentially infilling lows present on the seafloor, forming entrenched channel axes that pinch-out laterally against Barremian mudstones (Fig. 15). These lows may have formed during mid-Cretaceous compression and folding (Egan et al., 2009; Bochud, 2011) or through submarine slope failure and seafloor erosion.

It is possible that poorly-preserved thin-bedded Aptian-Albian turbidites (FA 1) represent the distal extents of the slope channel systems evident in the Cenomanian that were either eroded by the channels during progradation or deposited within isolated lows on the Barremian slope. These lows may have formed in response to similar processes to those that entrenched the Cenomanian channels (FA 2 and 3). The abrupt nature of the transition from distal fine-grained turbidite deposition to conglomeratic slope channels may correspond to either tectonic rejuvenation during the Mid-Cretaceous compressional event (Fig. 15) (Egan et al., 2009) and/or an abrupt relative sea-level fall. Such a sea-level fall has been identified in the mid-Cenomanian (Miller et al., 2003; Baraboshkin et al., 2003), resulting in a mid Cenomanian-early Turonian hiatus or condensed section on the Russian Platform to the north.

Evidence for bathymetry is present during deposition of the Cenomanian–early Turonian interval, with the sequence almost entirely absent 10 km to the west at Cek, indicating the presence of a relative high in this location (Figures 2, 12 and 15). Submarine landslide thicknesses also increase toward this high in the Barremian, suggesting the high influenced deposition from the Early Cretaceous until the Turonian. Previous work has shown the presence of a large c. Early Cretaceous submarine landslide, composed of remobilised Late Jurassic blocks, toward the west (Fig. 15) (Bochud, 2011; Gavrilov, 2018). The exact timing of this failure is uncertain, with Gavrilov (2018) suggesting this event may have occurred in the Late Cretaceous. The stratigraphic observations made by this study indicate that this failure occurred prior to the Cenomanian, with this submarine landslide complex, or a related basin-scale mass-failure, forming the westerly high and the complex stratigraphic relationships described previously (Figures 12-14). It is also likely that this submarine landslide, and other more minor ones in the area, were emplaced during an earlier period of tectonism and instability related to Early Cretaceous compression (Fig. 15). Evidence for topography (Fig. 11) in the Late Cretaceous also exists on a smaller-scale through palaeocurrent reversals in low-density turbidites indicating a northward-dipping slope confining southward-directed flows (Figures 4 and 11), and through the deposition of Late Jurassic blocks within the Turonian succession, indicating slope instability during this period (Figures 12 and 14).

Following the Cenomanian regression, the study area began to deepen again during the mid Turonian, as represented by the deposition of laterally-extensive, thin- to medium-bedded, mixed turbidites overlying the slope channels (Fig. 15). The mixed-lithology of the turbidites contrasts with the dominantly siliciclastic Aptian-Albian turbidites underlying the slope channels, indicating the development of a carbonate factory along the northern margin of the Greater Caucasus Basin in the Late Cretaceous (Figure 15). The presence of thinning and facies changes toward the present-day syncline margins, frequent debrites and out-runner blocks, and divergent palaeocurrent distributions indicates that basinal topography had an impact on mid Turonian and later deposition (Figures 4, 11, 12 and 14). This topography may have been formed by differential compaction over the rigid limestone megaclast, or external compression (Figures 13-15). Erosional contacts are seen within the succession at the base of metre-scale channel fills, which occur with increasing frequency through time. These small channel fills (FA 4) are filled by conglomerates and high-density turbidites with similar compositions to the underlying and much more extensive slope channels (FA 2). These metre- to decametre-scale channels are therefore interpreted as small distributary channels in the axes of

lobes (FA 4 and 5) that formed at the distal ends of the underlying 100s metre-scale slope channels (e.g., Normark et al., 1979). The increasing frequency and thickness of these conglomerates through the mid Turonian to Maastrichtian succession (Fig. 7) may therefore represent gradual progradation of the slope channels following their abrupt backstep in the mid Turonian. Clasts within these younger conglomerates are also more carbonate-dominated, which fits with the transition to a more carbonate-dominated system through the Late Cretaceous (Figures 10, 15 and 17). Mixed-deep-marine deposition continues in the Buduq Syncline throughout the remainder of the Cretaceous and into the Paleocene (Bochud, 2011).

A Subsurface Analogue for the Buduq Syncline

A seismic-scale mixed system analogous to the Cretaceous succession in the Buduq Syncline has been identified and is used to support and increase 3D visualisation of the outcrop-based model. The continental margin offshore The Gambia, NW Africa, developed through the Late Cretaceous (summarised in Casson et al., 2020; Fig. 16). Unconfined mixed systems developed on the deep-marine basin floor are interpreted to have been line-fed through canyons developed on an unconformity surface (Fig. 16C). Seismic geomorphology reveals the strata mixing (*sensu* Chiarella et al., 2017) of interdigitating siliciclastic-dominated and carbonate-dominated systems (i.e. at X and Y in Fig. 18), similar to that observed at outcrop- (facies and facies architecture) scale in the EGC (Figures 5 and 6).

Sediment-gravity-flows passing through the submarine canyons eroded into the underlying carbonate platform redepositing hundreds of metre-scale, seismically-resolvable carbonate mega-clasts 20+ km from the escarpment, above the unconformity surface (Figures 16B and D). Our field work suggests that these blocks may be associated with a multitude of different types and sizes of submarine landslides and blocks that are below seismic scale (Figures 12 and 14). The presence of carbonate blocks, lobe-morphology and similarity in run-out length and volume to debris dominated lobes documented elsewhere (McHargue et al. 2019) suggests the carbonate dominated systems were deposited by debris-flows. Hence, two stages of mixing occurs, firstly during erosion to form mixed lithology flows (bed-scale strata mixing), and then through deposition of interdigitating systems (lithofacies-scale strata mixing; *sensu* Chiarella et al., 2017). Pervasively channelised siliciclastic-systems with single feeder channels show a distinct seismic geomorphological response to their carbonate counterparts (Figures 16D and 16E). The lateral location along the margin of siliciclastic-dominated systems is conceivably related to sediment input points (i.e. shelf-incising canyons) capturing an extra-

basinal source of siliciclastic sediment from the shallow marine environment, away from shelfal carbonate factories. Basin floor topography is created by early deposits and influences subsequent lobe deposition (Fig. 16), causing stacking and lateral migration of lobes, which cannot be resolved in the Buduq Syncline (Fig. 17) probably because the scale of the study area is smaller than the scale at which migration occurred.

Ancient subsurface mixed systems have been described from seismic reflection data (e.g., Moscardelli et al., 2019; Casson et al., 2020). It may also be possible that transitions from calcareous-dominated to siliciclastic-dominated deep-marine systems, which are commonly associated with the rapid arrival (progradation) of the siliciclastic system (e.g., Scott et al., 2010; Kilhams et al., 2012; 2015; Soutter et al., 2019), may have been overlooked as 'transition zones', and in fact represent short-lived mixed systems, which are often below the scale of seismic resolution. The role of mixed system interactions on a grain-scale and its implications in terms of reservoir quality remain unclear until such systems are studied in detail in the subsurface (Chiarella et al., 2017; Moscardelli et al., 2019), or at outcrop (Bell et al. 2018b).

Mixed lobes

Source area and mixing origin: Palaeoflow indicators are limited within the calcareous system due to a lack of ripple laminations developed in the fine-grained and likely slowly accumulating deposits that build this system (Baas et al., 2016), and because of a lack of contrasting mineralogies, which prevented preservation of defined structures in the fine-grained carbonates (Imbrie & Buchanan, 1960). It is therefore difficult to decipher whether these siliciclastic and calcareous systems were perpendicular, oblique or parallel to each-other. The palaeoflow indicators that were collected, however, are consistent with a provenance to the north (Figures 4, 11 and 14). A northern provenance is also suggested from palaeographic maps for the Cretaceous, suggesting a Scythian-Russian Platform source area (e.g. Nikishin et al., 1998; Barrier et al., 2008). In Figure 15 it is assumed that the simplest explanation is the most likely, and that both systems are sourced from the Scythian Platform to the north. This is in agreement with the Mid-Cretaceous transition from terrigenous to chalk-rich deposition (Baraboshkin et al., 2003).

Disentangling specific types of mixing and interactions of mixing is possible in stratigraphy with excellent time constraints (e.g., Chiarella et al., 2019) or well-established shelf-basin floor seismic data sets (e.g., Tcherepanov et al., 2008; Moscardelli et al., 2019; Casson et al., 2020). These remain

uncertain in the study area which has a poorly-exposed source to sink relationship and limited temporal constraints, however it is possible to identify two different scales of stratal mixing (*sensu* Chiarella et al., 2017) of the two separate systems. Outcrop identification of mixed siliciclastic and calcareous sandstones (Lithofacies D, Table 1) indicate bed-scale stratal mixing, and observations of mixed facies associations (Figures 6 and 9), suggest facies-scale stratal mixing.

The offshore analogue (Figure 16 and 18) discussed above also exemplifies two separate systems interdigitating under two different scales of stratal mixing (*sensu* Chiarella et al., 2017), but due to well-established source to sink relationships and regionally extensive data coverage source areas are more certain. Two different sources for separate components of a mixed system have been documented elsewhere (Figures 1, 16 and 18A) (e.g., Ditty et al., 1977; Ahmad & Afzal, 2012; Poprawski et al., 2014; 2016).

Below we speculate how these mixed lobes differ from their siliciclastic counterparts in terms of sub-environments, stacking patterns and controlling parameters.

Lobe sub-environments: In the study area, when independently observed, the siliciclastic part of the mixed system could be interpreted as stacked lobes with axis, off-axis and fringe sub-environments all being identified (e.g., Spychala et al., 2017). The calcareous part of the system in the study area, however, would be interpreted as being predominantly the product of lobe fringe deposition (Remacha & Fernández, 2003; Bell et al., 2018a). Since the systems are mixed, it is difficult to assign a single lobe sub-environment to a sequence of beds as they represent the inter-fingering of two interacting systems (Fig. 18). Hence, siliciclastic lobe elements (*sensu* Prélat et al., 2009) are likely to occur within calcareous lobe elements forming a succession of mixed event beds (Lithofacies D, Table 1) (Figures 1, 16 and 18) The succession is further complicated by the often highly-erosive siliciclastic turbidity currents reworking calcareous beds, as evidenced by calcareous rip-up clasts within siliciclastic turbidites. This reworking may remove individual calcareous lobe elements from the rock record and make stacking interpretations and correlations more difficult (Fig. 17) (Braga et al., 2001). Similar observations offshore of erosion and re-working of carbonate deposits have been made offshore The Gambia (Casson et al., 2020).

Due to these complexities it is perhaps necessary to refer to such systems with a more specific descriptor (e.g., mixed axis-fringe), or broadly refer to them as 'mixed systems' in order to allude to

their heterogeneity and contrast them from siliciclastic-dominated systems (Fig. 18). Use of the siliciclastic lobe hierarchy of Prélat et al. (2009) is possible in mixed systems, but calcareous and siliciclastic descriptors are required (Fig. 18). It is possible to decipher the different systems in our field and subsurface examples, due to their lithological differences being visually resolvable at outcrop (Figures 5 and 6), and showing different seismic characteristics in the subsurface (Figures 16 and 18). However, without detailed provenance and geochemical analysis it would be very difficult to decipher the mixing of two siliciclastic systems or two calcareous systems, due to similarity in depositional facies and thus seismic character. Unless an individual system can be followed from source to sink in outcrop or subsurface, the possibility of multiple systems interdigitating, interacting, modulating each other and complicating stacking patterns must always considered (Fig. 18).

Stacking patterns: Deep-marine stacking motifs can show either aggradational, progradational, retrogradational or unorganized stacking patterns (Stow & Mayall, 2000; Deptuck et al., 2007; Straub et al., 2009; Prélat & Hodgson, 2013). These can be modulated by both external and internal processes (e.g., Ferguson et al., 2020). Mixed systems are influenced not only by the conventional controlling factors in siliciclastic-settings (e.g., climate, tectonics, sea-level), but also by ecological factors that influence carbonate production such as: salinity, latitude, nutrients and temperature (e.g., Mount, 1984; Chiarella et al. 2017; 2019).

Our study shows that in mixed interdigitating systems it can be difficult to decipher stacking patterns within each individual system due to the interdigitation of each system by the other (Figures 17 and 18). Bed thickness trends within the calcareous turbidites are difficult to interpret, possibly due to their narrow grain-size range, lack of contrasting mineralogies and early pseudo-lithification preventing the identification of thinner-beds, and amalgamation within thicker beds (Fig. 17). A lack of defined structures in fine-grained carbonates also hinders the identification of bed tops (Imbrie & Buchanan, 1960).

In 'pure' siliciclastic systems, stacking patterns are frequently deciphered based on grain-size and bed thickness trends. Progradational cycles, for example, are often manifested in deposits as coarsening- and thickening- upwards packages (e.g., Prélat et al., 2009; Prélat and Hodgson, 2013; Hodgson et al., 2016). However, bed thickness and grain-size analysis for the mid Turonian-Maastrichtian do not show any thickness trends or stacking patterns within the calcareous or siliciclastic turbidites when treated separately, or the combined mixed deposits (Fig. 17). This suggests that in mixed systems it is

difficult to disentangle the evolution of the systems individually, or together. It therefore may not be possible to describe the progradation or retrogradation of an individual system, and only possible to describe the relative ratio between the two; the apparent dominance of the mixed system (e.g., if siliciclastic (s) > carbonate (c) this could be due to progradation of s or by the retrogradation of c, both of which are controlled by a number of external and internal forcings (e.g., Chiarella et al., 2017; 2019; Moscardelli et al., 2019).

It is also a possibility that the influence of topography promotes predominately aggradational stacking, explaining the lack of statistical significance between grain-size or bed thickness and bed number. However, aggradational stacking is often associated with a consistent bed thickness and grain-size throughout evolution (Hodgson et al., 2011; Grundvåg et al., 2014; Spychala et al., 2017) which is not observed in the Buduq Syncline (Fig. 17). Siliciclastic conglomerates become more frequent and thicker throughout the mid Turonian-Maastrichtian, perhaps reflecting a progradation of the siliciclastic system (Figures 7 and 15). These observations, rather than bed thickness or grain-size alone, are more helpful in disentangling these interdigitating systems and understanding subsurface spatial and temporal distribution of depositional elements.

On the scale of the outcrop (100s m), calcareous turbidites appear to be sheet-like, while the siliciclastic turbidites show more thickness variation, representing more typical channel and lobe geometries (e.g. Prélat et al., 2009). Conglomerates in FA 4 appear to be confined to isolated depocentres and pinch-out across meters or decametres, indicating the presence of subtle topography (Fig. 11). This suggests the deposition of the conglomerates may have been controlled by depositional topography, i.e. compensational stacking, and that the underlying calcareous turbidites do exhibit subtle, long-wavelength thickness changes over a greater scale than observed at outcrop, influencing subsequent sediment routing. Alternatively, the thinning of conglomerates is due to the basinal topography present at this time, preventing these highly-concentrated flows running-out over great distances (Fig. 11).

In both cases the calcareous system is likely to represent the 'background' sedimentation, dominated by suspension fall out and very low-density gravity flow deposits (*sensu* Boulesteix et al., 2019; 2020) derived from a calcareous platform, most likely the Late Cretaceous chalk-dominated Scythian and Russian platforms (Baraboshkin et al., 2003; Barrier et al., 2008). The siliciclastic system is interpreted to have punctuated this slowly aggrading 'background' deposition via canyonised conduits on the

platform in agreement with the subsurface example (Casson et al., 2020). The extensive existence of the calcareous deposits throughout the study area, at the margins and adjacent to topographic highs, versus the siliciclastic deposits localised isolation in the central syncline, further supports this hypothesis.

Previous work on mixed systems has correlated alternations in calcareous and siliciclastic turbidites to 3rd order sea-level cycles (Yose & Heller, 1989; Miller & Heller, 1994). The alternations in the Buduq Syncline are lower frequency than these cycles but could be interpreted as fifth-sixth order sea-level cycles (parasequences) occurring on a 10,000 – 100,000 year cycle (Fig. 15) (Van Wagoner et al., 1990), related to Milankovitch orbital cycling (Goldhammer et al., 1990; D'Argenio et al., 1999). Elsewhere mixed systems have been interpreted to represent alternating cool-wet and cold-dry, possibly monsoonal, climate cycles driven by precession orbital cycles (García-García et al., 2009). No obvious stacking can be deduced in the study area (Fig. 17) preventing a confident interpretation to be made regarding the controls on the high-frequency lithological variations. Locations where k-ys. cyclicity can be determined, are controlled by excellent stratigraphic frameworks (e.g., Saller et al., 2004; Chiarella et al., 2019), which the Buduq Syncline is lacking.

The overall change in composition of the Scythian-Russian Platform, from terrigenous to calcareous (Baraboshkin et al., 2003) is controlled by a high order sea-level rise, and associated climatic warming. Bed-scale mixing could suggest very high frequency sea-level cycles, which are impossible to decipher without better age control (Moscardelli et al., 2019). Individual gravity flow deposits, are known to represent very short periods of deposition (hours, days) (e.g., Paull et al., 2018; Maier et al., 2019) highlighting the importance of keeping time scales in perspective when studying such high-frequency variations (Moscardelli et al., 2019).

Scalloped and serrated carbonate platform margins (e.g., Saller et al., 1989; Grant et al., 2019, Casson et al., 2020), like those that may characterise the northern margin of the Greater Caucasus Basin (Figures 12, 15 and 16), have been proposed as conduits for siliciclastic sediments without requiring a sea-level change (Francis et al., 2008; Braga et al., 2008; Puga-Bernabéu et al., 2014; Al-Mashaikie & Mohammed, 2017; Walker et al., 2019). The high-frequency variation in composition within the Buduq Syncline mixed stratigraphy are therefore likely to be best explained by this model rather than by sea-level fluctuations discussed above. This indicates that the calcareous deep-marine system exposed in the Buduq Syncline is part of a much more extensive and line-fed system (the Scythian and Russian platforms) derived from shedding of active carbonate factories perched on the shelf (Fig. 16).

The contemporaneous siliciclastic system may therefore have been derived from multiple point source conduits along this margin that either: 1) periodically punctuated this larger carbonate system or; 2) were long-lived conduits, fed by the uplifting siliciclastic hinterland, permanently bound by, or incising into, carbonate highs on the platform (Fig. 15) (Mueller et al., 2017; Moscardelli et al., 2019). Once sediment reached the upper slope, gravity flows would have been funnelled through sedimentary pathways, the location of which were controlled by the presence of underlying structures and topography (e.g., Moscardelli et al., 2019).

Conclusion

This study of the Upper Cretaceous stratigraphy of the Buduq Syncline, Azerbaijan documents the characteristics of an unstable and mixed siliciclastic-carbonate sedimentary system. Deposition in the syncline is represented by a Cenomanian-early Turonian submarine channel complex, which transitions into a mid-Turonian to Maastrichtian mixed lobe succession. This sequence represents an abrupt Cenomanian regression, probably related to an abrupt mid-Cenomanian eustatic sea-level fall and/or a mid-Cretaceous compressional event; followed by a mid Turonian transgression. Siliciclastic systems fed to the deep-marine via point-sourced conduits along a carbonate platform and are interpreted to punctuate a more extensive calcareous system throughout the remainder of the Cretaceous, resulting in the deposition of a mixed deep-marine system.

A westerly bathymetric high, likely formed by an Early Cretaceous submarine landslide complex deposited during earlier compression, is interpreted to have prevented deposition of Cenomanian–Turonian sediments toward the west. This submarine landslide complex may also have provided a lateral source for landslides through secondary remobilisation perpendicular to the regional palaeoflow from the north. Bed pinch-out, thinning, ripple reflections and frequent debrite deposition provides further evidence for the presence of basinal topography during deposition.

The mid Turonian-Maastrichtian mixed siliciclastic-calcareous deep-marine system contains both siliciclastic and calcareous lobe elements, which represent different lobe sub-environments, requiring modification of terminology developed for siliciclastic lobes. Mixed systems are also shown to have unique facies, both at outcrop and in a subsurface analogue from offshore The Gambia, reflecting differing depositional processes between the systems operating contemporaneously. Interaction

between the two deep-marine environments characterising the mixed systems has also made stacking patterns difficult to decipher, with each system attenuating the other.

Acknowledgments

We are grateful to CASP for awarding an Andrew Whitham Fieldwork Award to support this project. We thank Chris Van Baak and Rashad Gulmammadov for their logistical support and Muslim Gazibayov for his hospitality. Nigel Mountney is thanked for suggesting this study area in 2010. Jack Stacey and Ross Grant are thanked for input on carbonate sedimentology. TGS are thanked for permission to publish the seismic data. Yvonne Spychala, Domenico Chiarella and Hilary Corlett are thanked for their constructive and detailed reviews which greatly improved the manuscript. Basin Research Editor Atle Rotevatn and the editorial team are thanked for their handling of the manuscript.

Conflict of Interest Statement: The authors have no conflict of interest to declare.

Data Availability Statement: The data that support the findings of this study are provided in the supplementary material, further data is available from the corresponding author upon request.

References

ADAMIA, S.A., ZAKARIADZE, G.S., CHKHOTUA, T., SADRADZE, N., TSERETELI, N., CHABUKIANI, A., & GVENTSADZE, A. (2011) Geology of the Caucasus: a review: Turkish Journal of Earth Sciences, 20, 489-544.

AHMAD, R. & AFZAL, J. (2012) Sequence Stratigraphy of the Mixed Carbonate-Siliciclastic System of the Eocene Nisai Formation, Pishin Basin. Distribution of Source Rocks and Reservoir Facies.

AL-MASHAIKIE, S. Z.A.K. & MOHAMMED, Y. A. (2017) Anatomy of carbonate breccias, turbidite facies and depositional systems of Gercus Formation, in Donkan Area, Northern Iraq. Iraqi Geological Journal, 50 (1). 90-103.

ALEXANDER, J. (2008) Bedforms in Froude-supercritcal flow. Marine and River Dune Dynamics.

ALIZADEH, A., GULIYEV, I.S., KADIROV, F.A. & EPPELBAUM, L.V. (2016). Geosciences of Azerbaijan. Springer Switzerland. 237.

ARAYA, T. & MASUDA, F. (2001) Sedimentary structures of antidunes: An overview. Journal of the Sedimentological Society of Japan, 53, 1-15.

ARMITAGE, D.A., ROMANS, B.W., COVAULT, J.A. & GRAHAM, S.A. (2009) The influence of mass-transport-deposit surface topography on the evolution of turbidite architecture: The Sierra Contreras, Tres Pasos Formation (Cretaceous), southern Chile. Journal of Sedimentary Research, 79(5), 287-301.

BAAS, J.H., BEST, J.L., PEAKALL, J. & WANG, M. (2009) A phase diagram for turbulent, transitional and laminar clay suspension flows. Journal of Sedimentary Research, 79, 162-183.

BAAS, J., BEST, J. & PEAKALL, J. (2016) Predicting bedforms and primary current stratification in cohesive mixtures of mud and sand. Journal of the Geological Society, 173(1), 12-45.

BARABOSHKIN, E.Y., ALEKSEEV, A.S., & KOPAEVICH, L.F. (2003) Cretaceous palaeogeography of the North-Eastern Peri-Tethys. Palaeogeography Palaeoclimatology Palaeoecology, 196, p. 177-208.

BARKER, S.P., HAUGHTON, P.D.W., MCCAFFREY, W.D., ARCHER, S.G. & HAKES, B. (2008) Development of rheological heterogeneity in clay-rich high-density turbidity currents: Aptian Britannia Sandstone Member, UK continental shelf. Journal of Sedimentary Research, 78, 45–68.

BARRIER, E., VRIELYNCK, B., BERGERAT, F., BRUNET, M-F, MOSAR, J., POISSON, A. & SOSSON, M. (2008) Paleotectonic maps of the Middle East – Tectono-sedimentary-palinplastic maps from Late Norian to Pliocene.

BASILICI, G., VIEIRA DE LUCA, P. H. & POIRÉ, D. G. (2012) Hummocky cross-stratification-like structures and combined-flow ripples in the Punta Negra Formation (Lower-Middle Devonian, Argentine Precordillera): A turbiditic deep-marine or storm-dominated prodelta inner-shelf systems? Sedimentary Geology, 267-268, 73-92.

BELL, D., STEVENSON, C.J., KANE, I.A., HODGSON, D.M. & POYATOS-MORÉ, M. (2018a) Topographic Controls On the Development of Contemporaneous but Contrasting Basin-Floor Depositional Architectures. Journal of Sedimentary Research, 88(10), 1166-1189.

BELL, D., KANE, I., PONTÉN, A., FLINT, S., HODGSON, D. & BARRETT, B. (2018b) Spatial variability in depositional reservoir quality of deep-marine channel-fill and lobe deposits. Marine and Petroleum Geology, 98, 97-115.

BLAIR, T.C. & MCPHERSON J.G. (1999) Grain-size and textural classification of coarse sedimentary particles. Journal of Sedimentary Research, 69 (1), 6-19.

BOCHUD, M. (2011) Tectonics of the Eastern Greater Caucasus in Azerbaijan (Doctoral Dissertation, University of Freiburg). p. 202.

BOULESTEIX, K., POYATOS-MORE, M., FLINT, S.S, TAYLOR, K.G., HODGSON, D.M. AND HASIOTIS, S.T. (2019) Transport and Deposition of Mud in Deep-marine Environments: Processes and Stratigraphic Implications. Sedimentology, 66 (7), 2894-2925.

BOULESTEIX, K., POYATOS-MORE, M., FLINT, S.S, HODGSON, D.M. & TAYLOR, K.G. (2020) Sedimentary facies and stratigraphic architecture of deep-water mudstones beyond the basin-floor fan sandstone pinchout. Journal of Sedimentary Research, in press. EarthArXiv.

BRAGA, J., MARTIN, J. & WOOD, J. (2001) Submarine lobes and feeder channels of redeposited,temperate carbonate and mixed siliciclastic-carbonate platform deposits (Vera Basin, Almeria, southern Spain). Sedimentology v. 48(1), 99-116.

BRAGINA, L. G. & BRAGIN, N.Y. (2015) New data on Albian-Coniacian radiolarians from the Kelevudag section (northeastern Azerbaijan). Stratigraphy and Geological Correlation, 23 (1), 45-56.

BRUNET M. F., KOROTAEV M.V., ERSHOV A.V. & NIKISHIN A.M. (2003) The South Caspian Basin: a review of its evolution from subsidence modelling. Sedimentary Geology, 156 (1-4), 119-148.

BURBANK, D.W., VERGÉS, J., MUNOZ, A. & BENTHAM, P. (1992) Coeval hindward- and forward-imbricating thrusting in the south-central Pyrenees, Spain: Timing and rates of shortening and deposition. Geological Society of America Bulletin, 104, 3-17.

CASSON, M.A., CALVÈS, G., REDFERN, J., HUUSE, M. & SAYERS, B. (2020) Cretaceous continental margin evolution from quantitative seismic geomorphology, offshore NW Africa. Basin Research, online early.

CHIARELLA, D. & LONGHITANO, S.G. (2012) Distinguishing Depositional Environments In Shallow-Water Mixed, Bio-Siliciclastic Deposits On the Basis Of The Degree Of Heterolithic Segregation (Gelasian, Southern Italy). Journal of Sedimentary Research, 82, 969-990.

CHIARELLA, D., MORETTI, M., LONGHITANO, S.G. & MUTO, F. (2016) Deformed cross-stratified deposits in the Early Pleistocene tidally-dominated Catanzaro strait fill succession, Calabrian

Arc (Southern Italy): triggering mechanisms and environmental significance. Sedimentary Geology. 344, 277-289.

CHIARELLA, D., LONGHITANO, S.G. & TROPEANO, M. (2017) Types of mixing and heterogeneities in siliciclastic-carbonate sediments. Marine and Petroleum Geology, 88, 617-627.

CHIARELLA, D., LONGHITANO, S.G. & TROPEANO, M. (2019) Different stacking patterns along an active fold-and-thrust belt-Acerenza Bay, Southern Appennines (Italy). Geology, 47 (2), 139-142.

CLIFT, P. & GAEDICKE, C. (2002) Accelerated mass flux to the Arabian Sea during the middle to late Miocene. Geology, 30, 207-210.

CREVELLO, P.D. & SCHLAGER, W. (1980) Carbonate debris sheets and turbidites, Exuma Sound, Bahamas. Journal of Sedimentary Research, 50(4), 1121-1147.

D'ARGENIO, B., FERRERI, V., RASPINI, A., AMODIO, S. & BUONOCUNTO, F. (1999) Cyclostratigraphy of a carbonate platform as a tool for high-precision correlation. Tectonophysics, 315(1-4), 357-384.

DEPTUCK, M.E., SYLVESTER, Z., PIRMEZ, C. & O'BYRNE, C. (2007) Migration-aggradation history and 3-D seismic geomorphology of submarine channels in the Pleistocene Benin-major Canyon, western Niger Delta slope. Marine and Petroleum Geology, 24 (6-9), 406-433.

DE BLASIO, F.V., ENGVIK, L.E. & ELVERHØI, A. (2006) Sliding of outrunner blocks from submarine landslides. Geophysical Research Letters, 33(6).

DICKIE, J. & HEIN, F. (1995) Conglomeratic fan deltas and submarine fans of the Jurassic Laberge Group, Whitehorse Trough, Yukon Territory, Canada: fore-arc sedimentation and unroofing of a volcanic island arc complex. Sedimentary Geology, 98(1-4), 263-292.

DITTY, P.S., HARMON, C.J., PILKEY, O.H., BALL, M.M. & RICHARDSON, E.S. (1977) Mixed terrigenous—Carbonate sedimentation in the Hispaniola—Caicos turbidite basin. Marine Geology, 24(1), 1-20.

DORSEY, R.J. & KIDWELL, S.M. (1999) Mixed carbonate-siliciclastic sedimentation on a tectonically active margin: Example from the Pliocene of Baja California Sur, Mexico. Geology, 27(10), 935-938.

DUNBAR, G.B. & DICKENS, G.R. (2003) Late Quaternary shedding of shallow-marine carbonate along a tropical mixed siliciclastic–carbonate shelf: Great Barrier Reef, Australia. Sedimentology, 50(6), 1061-1077.

DUNHAM, R.J. (1962) Classification of carbonate Rocks according to depositional texture. American Association of Petroleum Geologists Memoir, 108-121.

EGAN, S.S., MOSAR, J., BRUNET, M.F. & KANGARLI, T. (2009) Subsidence and uplift mechanisms within the South Caspian Basin: insights from the onshore and offshore Azerbaijan region. Geological Society, London, Special Publications, 312(1), 219-240.

FERGUSON, R.A., KANE, I.A., EGGENHUISEN, J.T., POHL, F., TILSTON, M., SPYCHALA, Y.T. & BRUNT, R.L. (2020) Entangled external and internal controls on submarine fan evolution: an experimental perspective: The Depositional Record, online early.

FILDANI, A., McKAY, M.P., STOCKLI, D., CLARK, J., DYKSTRA, M.L., STOCKLI, L. & HESSLER, A.M. (2016) The ancestral Mississippi drainage archived in the late Wisconsin Mississippi deep-sea fan. Geology, 44, 479-482.

FILDANI, A., CLARK, J., COVAULT, J.A., POWER, B., ROMANS, B. W. & AIELLO, I. W. (2018) Muddy sand and sandy mud on the distal Mississippi fan: Implications for lobe depositional processes: Geosphere, 14(3), 1051-1066.

FISHER, R.V. (1971) Features of coarse-grained, high concentration fluids and their deposits: Journal of Sedimentary Petrology, 41, 916- 927.

FONNESU, M., FELLETTI, F., HAUGHTON, P.D., PATACCI, M. & MCCAFFREY, W.D. (2018) Hybrid event bed character and distribution linked to turbidite system sub-environments: The North Apennine Gottero Sandstone (north-west Italy). Sedimentology, 65(1), 151-190.

FRANCIS, J.M., DUNBAR, G.B., DICKENS, G.R., SUTHERLAND, I.A. & DROXLER, A.W. (2007) Siliciclastic sediment across the north Queensland margin (Australia): A Holocene perspective on reciprocal versus coeval deposition in tropical mixed siliciclastic-carbonate systems. Journal of Sedimentary Research, 77 (7), 572–586.

FRANCIS, J., DANIELL, J., DROXLER, A., DICKENS, G., BENTLEY, S., PETERSON, L. BRADLEY, N. & BEAUFORT, L. (2008) Deep water geomorphology of the mixed siliciclastic-carbonate system, Gulf of Papua: Journal of Geophysical Research: Earth Surface, 113(1).

FUHRMANN, A., KANE, I., CLARE, M.A., FERGUSON, R., SCHOMACKER, E., BONAMINI, E. & ARISTIZABAL, F. (2020) Hybrid turbidite-drift channel complexes: An integrated multiscale model: Geology, in press.

GAVRILOV, Y.O. (2018) Architecture of the Southern Marginal Zone of the Upper Jurassic-Valanginian Carbonate Platform of the Northeastern Caucasus (Dagestan, Shakhdag Massif). Lithology and Mineral Resources, 53 (6), 460-472.

GARCÍA-GARCÍA, F., SORIA, J., SAR VISERAS, C. & FERNÁNDEZ, J. (2009) High-frequency rhythmicity in a mixed siliciclastic-carbonate shelf (Late Miocene, Guadix Basin, Spain): A model of interplay between climatic oscillations, subsidence and sediment dispersal. Journal of Sedimentary Research, 79, 302-315.

GAWTHORPE, R.L. (1986) Sedimentation during carbonate ramp-to-slope evolution in a tectonically active area: Bowland Basin (Dinantian), northern England: Sedimentology, 33(2), 185-206.

GOLDHAMMER, R.K., DUNN, P.A. & HARDIE, L.A. (1990) Depositional cycles, composite sea level changes, cycle stacking patterns, and the hierarchy of stratigraphic forcing - examples from platform carbonates of the Alpine Triassic. Geological Society of America Bulletin, 102, 535-562.

GOLONKA, J. 2004. Plate tectonic evolution of the southern margin of Eurasia in the Mesozoic and Cenozoic. Tectonophysics, 381(1-4), 235-273.

GÓMEZ-PÉREZ, I., MORTON, A.C., KELLY, S.R.A. & STEWART, J.C. (2005) Integrated Mesozoic sediment dispersal patterns from Azerbaijan and Kazakstan: implications for the Central Caspian Basin, CASP, Central Caspian Project, 16, 68 p.

GRANT, R., UNDERHILL, J., HERNÁNDEZ-CASADO, J., BARKER, S. & JAMIESON, R. (2019) Upper Permian Zechstein Supergroup carbonate-evaporite platform palaeomorphology in the UK Southern North Sea. Marine and Petroleum Geology, 100, 484-518.

GRUNDVÅG, S-A., JOHANNESSEN, E.P., HELLAND-HANSEN, W. & PLINK-BJÖRKLUND, P. (2014) Depositional architecture and evolution of progradationally stacked lobe complexes in the Eocene Central Basin of Spitsbergen. Sedimentology, 61(2), 535-569.

HAQ, B.U. (2014) Cretaceous eustacy revisited. Global and Planetary Change, 113, 44-58.

HAUGHTON, P.D.W., DAVIS, C., MCCAFFREY, W. & BARKER, S. (2009) Hybrid sediment gravity flow deposits - Classification, origin and significance. Marine and Petroleum Geology, 26, 1900-1918.

HU, X., JANSA, L., WANG, C., SARTI, M., BAK, K., WAGREICH, M., MICHALIK, J. & SOTAK, J. (2005) Upper Cretaceous oceanic red beds (CORBs) in the Tethys: occurrences, lithofacies, age, and environments. Cretaceous Research, 26(1), 3-20.

HARMS, J., SOUTHARD, J., SPEARING, D., & WALKER, R. (1975) Depositional Environments as Interpreted from Primary Sedimentary and Stratigraphic Sequences. SEPM.

HESSLER, A.M. & FILDANI, A. (2019) Deep-sea fans: tapping into Earth's changing landscapes. Journal of Sedimentary Research, 89(11), 1171-1179.

HODGSON, D.M., DI CELMA, C.N., BRUNT, R.L. & FLINT, S.S. (2011) Submarine slope degradation and aggradation and the stratigraphic evolution of channel-levee systems. Journal of the Geological Society, 168(3), 625-628.

HODGSON, D.M., KANE, I.A., FLINT, S.S., BRUNT, R.L. & ORTIZ-KARPF, A. (2016) Time-transgressive Confinement On the Slope and the Progradation of Basin-floor Fans: Implications For the Sequence Stratigraphy of Deep-water Deposits. Journal of Sedimentary Research, 86 (1), 73-86.

HUBBARD, S.M., COVAULT, J.A., FILDANI, A. & ROMANS, B.W. (2014) Sediment transfer and deposition in slope channels: Deciphering the record of enigmatic deep-sea processes from outcrop. Geological Society of America Bulletin, 126, 857-871.

HUNTER, R.E. & CLIFTON, E.H. (1982) Cyclic deposits and hummocky cross-stratification of probable storm origin in Upper Cretaceous rocks of the Cape Sebastian area, southwestern Oregon. Journal of Sedimentary Research, 52(1), 127-143.

IMBRIE, J. & BUCHANAN, H. (1960) Sedimentary structures in modern carbonate sands of the Bahamas. Special Publications of SEPM, 12.

INVERSON, R.M. (1997) The physics of debris flows. Reviews of Geophysics, 35, 245-296.

INVERSON, R.M., LOGAN, M., LAHUSEN, R.G. & BERTI, M. (2010) The perfect debris flow? Aggregated results from 28 largescale experiments. Journal of Geophysical Research: Earth Surface, 115, 1-29.

JOBE, Z.R., LOWE, D.R. & MORRIS, W.R. (2012) Climbing-ripple successions in turbidite systems: depositional environments, sedimentation and accumulation times. Sedimentology, 59, 867-898.

JOBE, Z.R., SYLVESTER, Z., HOWES, N., PIRMEZ, C., PARKER, A., CANTELLI, A., SMITH, R., WOLINKSKY, M.A., O'BRYNE, C., SLOWEY, N. & PRATHER, B. (2017) High-resolution,

millennial-scale patterns of bed compensation on a sand-rich intraslope submarine fan, western Niger Delta slope. GSA Bulletin, 129, 23-37.

KANE, I.A. & PONTÉN, A.S.M. (2012) Submarine transitional flow deposits in the Paleogene Gulf of Mexico. Geology, 40, 1119–1122.

KANE, I.A. & HODGSON, D.M. (2011) Sedimentological criteria to differentiate submarine channel levee subenvironments: Exhumed examples from the Rosario Fm. (Upper Cretaceous) of Baja California, Mexico, and the Fort Brown Fm. (Permian), Karoo Basin, S. Africa. Marine and Petroleum Geology, 28, 807-823.

KANE, I.A., McCAFFREY, W.D. & PEAKALL, J. (2008) Controls on sinuosity evolution within submarine channels. Geology, 36 (4), 287-290.

KANE, I.A., MCCAFFREY, W.D. & MARTINSEN, O.J. (2009a) Allogenic vs. Autogenic Controls on Megaflute Formation. Journal of Sedimentary Research, v. 9, 643-651.

KANE, I.A., DYKSTRA, M.L., KNELLER, B.C., TREMBLAY, S. & MCCAFFREY, W.D. (2009b) Architecture of coarse-grained channel-levée system: the Rosario Formation, Baja California, Mexico. Sedimentology, 56 (7), 2207-2234.

KANE, I.A., PONTÉN, A.S., VANGDAL, B., EGGENHUISEN, J.T., HODGSON, D.M. & SPYCHALA, Y.T. (2017) The stratigraphic record and processes of turbidity current transformation across deep-marine lobes. Sedimentology, 64(5), 1236-1273.

KHAIN, V.E. (1952) Tectonic structure of Azerbaijan. Proceedings of the Conference on Geological Problems of the Transcaucasian. Academy of Science, Baku, Azerbaijan, 162-175 (in Russian).

KHAIN, V.E. & SHARDANOV, A.N., 1958, Geological map of the USSR, Caucasus series sheet K-39-XXV, Ministry of Geology, 1:200,000.

KILHAMS, B., HARTLEY, A., HUUSE, M. & DAVIS, C. (2012) Characterizing the Paleocene turbidites of the North Sea: The Mey Sandstone Member, Lista Formation, UK Central Graben. Petroleum Geoscience, 18(3), 337-354.

KILHAMS, B., HARTLEY, A., HUUSE, M. & DAVIS, C. (2015) Characterizing the Paleocene turbidites of the North Sea: Maureen formation, UK Central Graben. Geological Society Special Publication, 403, 43-62.

KNAUST, D., WARCHOL, M. & KANE, I.A. (2014) Ichnodiversity and ichnoabundance: revealing depositional trends in a confined turbidite system. Sedimentology, 61 (7), 2218-2267.

KNELLER, B. C. & BRANNEY, M.J. (1995) Sustained high-density turbidity currents and the deposition of thick massive sands. Sedimentology, 42, 607-616.

KNELLER, B., EDWARDS, D., MCCAFFREY, W. & MOORE, R. (1991) Oblique reflection of turbidity currents. Geology, 19(3), 250-252.

KNELLER, B., BOZETTI, G., CALLOW, R., DYKSTRA, M., HANSEN, L., KANE, I., LI, P., MCARTHUR, A., CATHARINA, A.S., SANTOS, T.D. & THOMPSON, P (2020) Architecture, process, and environmental diversity in a late Cretaceous slope channel system. Journal of Sedimentary Research, 90, 1-26.

KOPAEVICH, L.F., BENIAMOVSKII, V.N. & BRAGINA, L.G. (2015) Upper Albian-Turonian foraminifers and radiolarians from the Kelevudag section, northeastern Azerbaijan. Stratigraphy and Geological Correlation, 23(6), 580-599.

KOPAEVICH, L.F., BRAGIN, N.Yu. & BRAGINA, L.G. (2017) New data on the planktonic foraminifers from the Yunusdag Formation (Coniacian-Santonian) in the Kelevudag section, northeastern Azerbaijan. Stratigraphy and Geological Correlation, 25(6), 627-637.

LaGASSE, J. & READ, J.F. (2006) Updip sequence development on a wave- and current-dominated, mixed carbonate-siliciclastic continental shelf: paleogene, North Carolina, eastern U.S.A. Sedimentary Geology, 184, 155-182.

LI, P., KNELLER, B.C., THOMPSON, P., BOZETTI, G. & DOS SANTOS, T. (2018) Architectural and facies organisation of slope channel fills: Upper Cretaceous Rosario Formation, Baja California, Mexico. Marine and Petroleum Geology, 92, 632–649.

LONGHITANO, S.G. (2011) The record of tidal cycles in mixed silic-bioclastic deposits: examples from small Plio-Pleistocene peripheral basins of the microtidal Central Mediteranean Sea. Sedimentology. 58, 691-719.

LONGHITANO, S.G., SABATO, L., TROPEANO, M. & GALLICCHIO, S. (2010) A mixed bio-clastic siliciclastic flood-tidal delta in a microtidal setting: depositional architectures and hierarchical internal organization (Pliocene, southern apennine, Italy). Journal of Sedimentary. Research.80, 36-53.

LONGHITANO, S.G., CHIARELLA, D., DI STEFANO, A., MESSINA, C., SABATO, L. TROPEANO, M. (2012) Tidal signatures in Neogene to Quaternary mixed deposits of southern Italy straits and bays. Sedimentary Geology, 279, 74-96.

LOWE, D.R. (1982) Sediment gravity flows: Depositional models with special reference to the deposits of high-density turbidity currents. Journal of Sedimentary Research, 52, 279-297.

MAIER, K.L., GALES, J.A., PAULL, C.K., ROSENBERGER, K., TALLING, P.J., SIMMONS, S.M., GWIAZDA, R., McGANN, M., CARTIGNY, M.J.B., LUNDSTEN, E., ANDERSON, K., CLARE M.A., XU J., PARSONS, D., BARRY, J.P., WOLFSON-SCHWEHR, M., NIEMINSKI, N.M. & SUMNER, E.J. (2019) Linking Direct Measurements of Turbidity Currents to Submarine Canyon-Floor Deposits. Frontiers in Earth Science. 7, 144.

MARINI, M., MILLI, S., RAVNAS, R. & MOSCATELLI, M. (2015) A comparative study of confined vs. semi-confined turbidite lobes from the Lower Messinian Laga Basin (Central Apennines, Italy): implications for assessment of reservoir architecture. Marine and Petroleum Geology, 63, 142–165.

MAYNARD, J.R. & ERRATT, D. (2020) The Black Sea, a Tertiary basin: Observations and insights. Marine and Petroleum Geology, 118. Online Early.

MCARTHUR, A., KANE, I., BOZETTI, G., HANSEN, L. & KNELLER, B. (2019) Supercritical flows overspilling from bypass-dominated submarine channels and the development of overbank bedforms: The Depositional Record. Online Early.

MCHARGUE, T. R., HODGSON, D. M. & SHELEF, E. (2019) Architectural Diversity of Submarine Lobes. EarthArXiv.

McNEILL, D.F., CUNNINGHAM, K.J., GUERTIN, L.A. & ANSELMETTI, F.S. (2004) Depositional themes of mixed carbonate-siliciclastics in the south Florida Neogene: Application to ancient deposits. AAPG Memoir, 80, 23–43.

MILLER, R.P. & HELLER, P.L. (1994) Depositional framework and controls on mixed carbonate-siliciclastic gravity flows: Pennsylvanian-Permian shelf to basin transect, south-western Great Basin, USA. Sedimentology, 41(1), 1-20.

MILLER, K.G., SUGARMAN, P.J., BROWNING, J.V., KOMINZ, M.A., HERNÁNDEZ, J.C., OLSSON, R.K., WRIGHT, J.D., FEIGENSON, M.D. & VAN SICKEL, W. (2003) Late Cretaceous chronology of large, rapid sea-level changes: Glacioeustasy during the greenhouse world. Geology, 31(7), 585-588.

MITCHELL, S.F., PICKERILL, R.K. & STEMANN, T.A. (2001) The Port Morant Formation (Upper Pleistocene, Jamaica): high resolution sedimentology and paleoenvironmental analysis of a mixed carbonate clastic lagoonal succession. Sedimentary Geology, 144(3-4), 291-306.

MORETTI, M., TROPEANO, M., VAN LOON, A.J., ACQUAFREDDA, P., BALDACCONI, R., FESTA, V., LISCO, S., MASTRONUZZI, G., MORETTI, V. & SCOTTI, R. (2016) Texture and composition of the Rosa Marina beach sands (Adriatic coast, southern Italy): a sedimentological/ecological approach. Geologos, 22, 87-103.

MOSAR, J., KANGARLI, T., BOCHUD, M., GLASMACHER, U.A., RAST, A., BRUNET, M.-F. & SOSSON, M., (2010) Cenozoic-Recent tectonics and uplift in the Greater Caucasus: a prespective

from Azerbaijan, in Sosson, M., Kaymakci, N., Stephenson, R.A., Bergerat, F., and Starostenko, V., eds., Sedimentary basin tectonics from the Black Sea and Caucasus to the Arabian Platform: London: Geological Society Special Publication, 340, p. 261-280.

MOSCARDELLI, L., OCHOA, J., LUNT, I. & ZAHM, L. (2019) Mixed siliciclastic–carbonate systems and their impact for the development of deep-marine turbidites in continental margins: A case study from the Late Jurassic to Early Cretaceous Shelburne subbasin in offshore Nova Scotia. AAPG Bulletin, 103(10), 2487-2520.

MOUNT, J.F. (1984) Mixing of siliciclastic and carbonate sediments in shallow shelf environments. Geology, 12, 432-435.

MULDER, T. & ALEXANDER, J. (2001) Abrupt change in slope causes variation in the deposit thickness of concentrated particle-driven density currents. Marine Geology, 175(1-4), 221-235.

MULDER, T., ZARAGOSI, S., RAZIN, P., GRELAUD, C., LANFUMEY, V. & BAVOIL, F. (2009) A new conceptual model for the deposition process of homogenite: Application to a cretaceous megaturbidite of the western Pyrenees (Basque region, SW France). Sedimentary Geology, 222(3-4), 263-273.

MUELLER, P., PATACCI, M. & DI GIULIO, A. (2017) Hybrid event beds in the proximal to distal extensive lobe domain of the coarse-grained and sand-rich Bordighera turbidite system (NW Italy). Marine and Petroleum Geology, 86, 908-931.

MUTTI, E. (1977) Distinctive thin-bedded turbidite facies and related depositional environments in the Eocene Hecho Group (South-central Pyrenees, Spain). Sedimentology, 24, 107–131.

MUTTI, E. (1983) The Hecho Eocene submarine fan system, south-central Pyrenees, Spain. GeoMarine Letters, 3(2-4), 199-202.

MUTTI, E. (1992) Turbidite sandstones: AGIP- Instituto di Geologia, Università di Parma, p. 275.

NARDIN, T.R., HEIN, F.J., GORSLINE, D.S. & EDWARDS, B.D. (1979) A review of mass movement processes, sediment and acoustic characteristics, and contrasts in slope and base-of-slope systems versus canyon-fan-basin floor systems. SEPM Special Publications, 27, 61-73.

NEMEC, W. & STEEL, R.J. (1984) Alluvial and Coastal Conglomerates: Their Significant Features and Some Comments on Gravelly Mass-Flow Deposits.

NIKISHIN, A.M., CLOETINGH, S., BRUNET, M-F., STEPHENSON, R.A., BOLOTOV, S.N. & ERSHOV, A.V. (1998). Scythian Platform, Caucasus and Black Sea region: Mesozoic-Cenozoic tectonic history and dynamics. In: Peri-Tethys Memoir 3: stratigraphy and evolution of Peri-Tethyan platforms (Ed. by Crasquin-Soleau, S. and Barrier, É.) Mémoires du Muséum national d'Histoire naturelle, Paris, 177, 163-176.

NIKISHIN A.M., ZIEGLER P., PANOV, D.I., NAZAREVICH B.P., BRUNET M., F., STEPHENSON R.A., BOLOTOV S.N., KORATAEV M.V. & TIKHOMROV P.L. (2001) Mesozoic and Cainozoic evolution of the Scythian Platform - Black Sea - Caucasus domain. In: Peri-Tethys Memoir 6 - Peri-Tethyan rift/wrench basins and passive margins (Ed. by Ziegler P., Cavazza W., Robertson A.H.F. & Crasquin-Soleau S.), Mémoires du Muséum national d'Histoire naturelle, Paris, 186, 295-346.

NIKISHIN, A. M., POKAY, A. I., TÜYSÜZ, O., DEMIRER, A., AMELIN, N. & PETROV, E. (2015 a) The Black Sea basins structure and history: New model based on new deep penetration regional seismic data. Part 1: Basins structure and fill. Marine and Petroleum Geology, 59, 638-655.

NIKISHIN A.M., OKAY A., TÜYSÜZ O., DEMIRER A., WANNIER M., AMELIN, N. & PETROV E. (2015 b) The Black Sea basins structure and history: New model based on new deep penetration regional seismic data. Part 2: Tectonic history and paleogeography. Marine and Petroleum Geology, 59, 656-670.

NORMARK, W.R., PIPER, D.J.W. & HESS, G.R. (1979) Distributary channels, sand lobes, and mesotopography of Navy submarine fan, California Borderland, with applications to ancient fan sediments. Sedimentology, 26(6), 749-774.

PATACCI, M., HAUGHTON, P.D. & MCCAFFREY, W.D. (2014) Rheological complexity in sediment gravity flows forced to decelerate against a confining slope, Braux, SE France. Journal of Sedimentary Research, 84, 270-277.

PAULL, C.K., TALLING, P.J., MAIER, K.L., PARSONS, D., XU, J., CARESS, D.W., GWIAZDA, R., LUNDSTEN, E.M., ANDERSON, K., BARRY, J.P., CHAFFEY, M., O'REILLY, T., ROSENBERGER, K.J., GALES, J.A., KIEFT, B., McGANN, M., SIMMONS, S.M., McCANN, M., SUMNER, E.J., CLARE M.A. & CARTIGNY, M.J. (2018) Powerful turbidity currents driven by dense basal layers. Nature communications, 9, 4114.

PEAKALL, J., MCCAFFREY, B. & KNELLER, B. (2000) A process model for the evolution, morphology, and architecture of sinuous submarine channels: Journal of Sedimentary Research, 70, 434–448.

PEAKALL, K., KANE, I.A., MASSON, D.G., KEEVIL, G., McCAFFREY, W. and CORNEY, R. (2012) Global (latitudinal) variation in submarine channel sinuosity. Geology, 40 (1), 11-14.

PHILIP, H., CISTERNAS, A., GVISHIANI, A. & GORSHKOV, A. (1989) The Caucasus: an actual example of the initial stages of continental collision. Tectonophysics, 161, 1-21.

POPRAWSKI, Y., BASILE, C., AGIRREZABALA, L., JAILLARD, E., GAUDIN, M. & JACQUIN, T. (2014) Sedimentary and structural record of the Albian growth of the Bakio salt diapir (the Basque Country, northern Spain). Basin Research, 26(6), 746-766.

POPRAWSKI, Y., BASILE, C., JAILARD, E., GAUDIN, M., AND LOPEZ, M. (2016) Halokinetic sequences in carbonate systems: An example from the Middle Albian Bakio Breccias Formation (Basque Country, Spain). Sedimentary Geology, 334, 34-52.

POSTMA, G. (1984) Mass-flow conglomerates in a submarine canyon: Abrioja fan-delta, Pliocene, southeast Spain. In: Sedimentology of Gravels and Conglomerates, Canadian Society of Petroleum Geologists Memoir (Ed. by Koster, E.H. & Steel, R.J.), 10, 237-258.

POSTMA, G. (1984) Slumps and their deposits in fan delta front and slope (sedimentation model,

Spain). Geology, 12(1), 27-30.

POSTMA, G., NEMEC, W. & KLEINSPEHN, K. (1988) Large floating clasts in turbidites: a mechanism for their emplacement. Sedimentary Geology, 58 (1), 47-61.

POSTMA, G., HILGEN, F.J. & ZACHARIASSE, W.J. (1993) Precession-punctuated growth of a late Miocene submarine-fan lobe on Gavdos (Greece). Terra nova, 5(5), 438-444.

PRÉLAT, A., HODGSON, D.M. & FLINT, S.S. (2009) Evolution, architecture and hierarchy of distributary deep-water deposits: a high-resolution outcrop investigation from the Permian Karoo Basin, South Africa. Sedimentology, 56(7), 2132-2154.

PRÉLAT, A. & HODGSON, D.M. (2013) The full range of turbidite bed thickness patterns in Submarine lobes: Controls and implications. Journal of the Geological Society, v. 170(1), pp. 209-214.

PUGA-BERNABÉU, Á., WEBSTER, J., BEAMAN, R. & GUILBAUB, V. (2011) Morphology and controls on the evolution of a mixed carbonate-siliciclastic submarine canyon system, Great Barrier Reef margin, north-eastern Australia. Marine Geology, 289, 100–116.

PUGA-BERNABÉU, Á., WEBSTER, J., BEAMAN, R., REIMER, P. & RENEMA, W. (2014) Filling the gap: A 60ky record of mixed carbonate-siliciclastic turbidite deposition from the Great Barrier Reef. Marine and Petroleum Geology, 50, 40-50.

REMACHA, E. & FERNÁNDEZ, L.P. (2003) High-resolution correlation patterns in the turbidite systems of the Hecho Group (South-Central Pyrenees, Spain). Marine and Petroleum Geology, 20, 711–726.

OSLEGER, D.A. & MONTAÑEZ, I.P. (1996) Cross-platform architecture of a sequence boundary in mixed siliciclastic-carbonate lithofacies, Middle Cambrian, southern Great Basin, USA. Sedimentology, 43(2), 197-217.

SAINTOT, A., BRUNET, M.-F., YAKOVLEV, F., SÉBRIER, M., STEPHENSON, R., ERSHOV, A., CHALOT-PRAT, F., & MCCANN, T. (2006a) The Mesozoic-Cenozoic tectonic evolution of the Greater Caucasus, *in* Gee, D., and Stephenson, R., eds., European Lithosphere Dynamics: Geological Society, London, Memoir, 32, 277-289.

SAINTOT, A., STEPHENSON, R.A., STOVBA, S., BRUNET, M.F., YEGOROVA, T. & STAROSTENKO, V. (2006b) The evolution of the southern margin of Eastern Europe (Eastern European and Scythian platforms) from the latest Precambrian-Early Palaeozoic to the Early Cretaceous: Geological Society, London, Memoirs, 32(1), 481-505.

SALLER, A.H., BARTON, J.W. & BARTON, R.E. (1989) Slope sedimentation associated with a vertically building shelf, Bone Spring Formation, Mescalero Escarpe field, southeastern New Mexico. In: Controls on carbonate platform and basin development (Ed. by P.D. Crevello, J.J. Wilson, J.F. Sarg, and J.F. Read), Society of Economic Paleontologists and Mineralogists, pp. 275-288.

SALLER, A.H., NOAH, J.T., RUZUAR, A.P. & SCHNEIDER, R. (2004) Linked lowstand delta to basin-floor fan deposition, offshore Indonesia: An analogue for deep-water reservoir systems: AAPG Bulletin, 88 (1), 21-46.

SCOTT, E., GELIN, F., JOLLEY, S., LEENAARTS, E., SADLER, S. & ELSINGER, R. (2010) Sedimentological control of fluid flow in deep-marine turbidite reservoirs: Pierce Field, UK Central North Sea. Geological Society Special Publication, 347, 113-132.

SHARDANOV, A.N. (1953) On the problem of effects of nappe tectonics in the South-Eastern Caucasus. Doklady Academy of Science Azerbaijan, 9, 439-444 (In Russian).

SOHN, Y.K. (2000) Depositional processes of submarine debris flows in the Miocene fan deltas, Pohang Basin, SE Korea with special reference to flow transformation. Journal of Sedimentary Research, 70, 491–503.

SOHN, Y., CHOE, M. & JO, H. (2002) Transition from debris flow to hyperconcentrated flow in a submarine channel (the Cretaceous Cerro Toro formation, southern Chile). Terra Nova, 14(5), 405-415.

SOSSON, M., STEPHENSON, R., SHEREMET, Y., ROLLAND, Y., ADAMIA, S., MELKONIAN, R., KANGARLI, T., YEGOROVA, T., AVAGYAN, A., GALOYAN, G. & DANELIAN, T. (2016) The eastern Black Sea-Caucasus region during the Cretaceous: New evidence to constrain its tectonic evolution. Comptes Rendus Geoscience, 348(1), 23-32.

SOUTTER, E.L., KANE, I.A. & HUUSE, M. (2018) Giant submarine landslide triggered by Paleocene mantle plume activity in the North Atlantic. geology, 46(6), 511-514.

SOUTTER, E.L., KANE, I.A., FUHRMANN, A., CUMBERPATCH, Z.A. & HUUSE, M. (2019) The Stratigraphic Evolution of Onlap in Clastic Deep-marine Systems: Autogenic Modulation of Allogenic Signals. Journal of Sedimentary Research, 89 (10), 890-917.

SPYCHALA, Y.T., HODGSON, D.M., PRÉLAT, A., KANE, I.A., FLINT, S.S. & MOUNTNEY, N.P. (2017) Frontal and lateral submarine lobe fringes: comparing sedimentary facies, architecture and flow processes. Journal of Sedimentary Research, 87, 75-96.

SPYCHALA, Y.T., HODGSON, D.M., STEVENSON, C.J. & FLINT, S.S. (2017) Aggradational lobe fringes: The influence of subtle intrabasinal seabed topography on sediment gravity flow processes and lobe stacking patterns. Sedimentology, 64(2), 582-608.

STEVENSON, C.J., JACKSON, C.A-L., HODGSON, D.M., HUBBARD, S.M. & EGGENHEISEN, J.T. (2015) Deep-marine sediment bypass. Journal of Sedimentary Research, 85, 1058-1081.

STOW, D.A.V. & MAYALL, M. (2000) Deep-marine sedimentary systems: new models for the 21st Century. Marine and Petroleum Geology, 17, 125-135

STRAUB, K., PAOLA, C., MOHRIG, D., WOLINSKY, M. & GEORGE, T. (2009) Compensational stacking of channelized sedimentary deposits. Journal of Sedimentary Research, 79, 673-688.

SURLYK, F. (1984) Fan-delta to submarine fan conglomerates of the Volgian-Valanginian Wollaston Forland Group, East Greenland. In: Sedimentology of Gravels and Conglomerates: Canadian Soc. of Petroleum Geologists, Memoir (Ed. by E. H. Koster & R. J. Steel), 10, 359-382.

SYLVESTER, Z. & LOWE, D.R. (2004) Textural trends in turbidites and slurry beds from the Oligocene flysch of the East Carpathians, Romania. Sedimentology, 51, 945–972.

TALLING, P., MASSON, D. SUMNER, E. & MALGESINI, G. (2012) Subaqueous sediment density flows: Depositional processes and deposit types. Sedimentology, 59, 1937-2003.

TASSY, A., CROUZY, E., GORINI, C., RUBINO, J.L., BOUROULLEC, J.L. & SAPIN, F. (2015) Egyptian Tethyan margin in the Mesozoic: Evolution of a mixed carbonate-siliciclastic shelf edge (from Western Desert to Sinai). Marine and Petroleum Geology, 68, 565-581.

TCHEREPANOV, E.N., DROXLER, A.W., LAPOINTE, P., DICKENS, G.R., BENTLEY, S.J., BEAUFORT, L., PETERSON, L.C., DANIELL, J. & OPDYKE, B.N. (2008) Neogene evolution of the mixed carbonate-siliciclastic system in the Gulf of Papua, Papua New Guinea. Journal of Geophysical Research Earth Surface, 113 (F1).

TERLAKY, V., ROCHELEAU, J. & ARNOTT, R.W.C. (2016) Stratal composition and stratigraphic organization of stratal elements in an ancient deep-marine basin-floor succession, Neoproterozoic Windermere Supergroup, British Columbia, Canada. Sedimentology, 63(1), 136-175

TINTERRI, R., LAPORTA, M. & OGATA, K. (2017) Asymmetrical cross-current turbidite facies tract in a structurally-confined mini-basin (Priabonian–Rupelian, Ranzano Sandstone, northern Apennines, Italy). Sedimentary Geology, 352, 63–87.

TUCKER, M.E. (2003) Mixed clastic–carbonate cycles and sequences: Quaternary of Egypt and Carboniferous of England. Geologia Croatica, 56(1), 19-37.

VAN WAGONER J.C., MITCHUM R.M., CAMPION K.M. & RAHMANIAN V.D. (1990) Siliciclastic Sequence Stratigraphy in Well Logs, Cores, and Outcrop: Concepts for High-Resolution

Correlation of Facies. American Association of Petroleum Geologists Methods in Exploration Series, pp. 55.

VINCENT, S.J., MORTON, A.C., CARTER, A., GIBBS, S. & BARABADZE, T.G. (2007) Oligocene uplift of the Western Greater Caucasus: an effect of initial Arabia–Eurasia collision. Terra Nova, 19(2), 160-166.

VINCENT, S.J., BRAHAM, W., LAVRISHCHEV, V.A., MAYNARD, J.R., & HARLAND, M. (2016) The formation and inversion of the western Greater Caucasus Basin and the uplift of the western Greater Caucasus: Implications for the wider Black Sea region. Tectonics, 35, 2948-2962.

VINCENT, S.J., GUO, L., FLECKER, R., BOUDAGHER-FADEL, M., ELLAM, R. & KANDEMIR, R. (2018) Age constraints on intra-formational unconformities in Upper Jurassic-Lower Cretaceous carbonates in northeast Turkey; geodynamic and hydrocarbon implications. Marine and Petroleum Geology, 91, 639-657.

WAGREICH, M. & KRENMAYR, H. (2005) Upper Cretaceous oceanic red beds (CORB) in the Northern Calcareous Alps (Nierental Formation, Austria): Slope topography and clastic input as primary controlling factors. Cretaceous Research, 26(1), 57-64.

WALKER, W., JOBE, Z. R., WOOD, L. & SARG, R. (2019) Progradational Slope Architecture and Sediment Partitioning in the Outcropping Mixed Siliciclastic-Carbonate Bone Spring Formation, Permian Basin, west Texas. EarthArXiv

WANG, C., HU, X., SARTI, M., SCOTT, R. & LI, X. (2005) Upper Cretaceous oceanic red beds in southern Tibet: A major change from anoxic to oxic, deep-sea environments. Cretaceous Research, 26(1), 21-32.

YOSE, L.A. & HELLER, P.L. (1989) Sea-level control of mixed-carbonate-siliciclastic, gravity-flow deposition: Lower part of the Keeler Canyon Formation (Pennsylvanian), southeastern California. Geological Society of America Bulletin, 101(3), 427-439.

ZELLER, M., VERWER, K., EBERLI, G.P., MASSAFERRO, J.L., SCHWARZ, E. & SPALLETTI, L. (2015) Depositional controls on mixed carbonate–siliciclastic cycles and sequences on gently inclined shelf profiles. Sedimentology, 62(7), 2009-2037.

ZONENSHAIN, L.P. & Le PICHON, X. (1986). Deep Basins of the Black-Sea and Caspian Sea as Remnants of Mesozoic Back-Arc Basins. Tectonophysics, 123 (1-4), 181-211.

ZONNEVELD, J.P., MOSLOW, T.F. & HENDERSON, C.M. (1997) Lithofacies associations and depositional environments in a mixed siliciclastic-carbonate coastal depositional system, upper Liard Formation, Triassic, northeastern British Columbia. Bulletin of Canadian Petroleum Geology, 45(4), 553-575.

FIGURE CAPTIONS

Figure 1: Simplified conceptual model showing how siliciclastic and carbonate systems may interact at a basin-scale in a deep-marine mixed siliciclastic-carbonate system. Carbonate material is shed from a shallower carbonate-producing platform that periodically received siliciclastic material; this is then deposited in the deep-marine by gravity flows during facies mixing in an interdigitating mixed system (after Mount, 1984; Chiarella et al., 2017). Note: source areas are not always separated and the different components of the source area can be opposite, parallel, perpendicular or oblique to each other.

Figure 2: Structural and stratigraphic framework of the Eastern Greater Caucasus (EGC) of Azerbaijan. A) Simplified geological map, location map inset, black box locates study area, lines B and C are located. B) Cross-section across the Cek-Hapit Valley, black box locates study area. C) Cross-section from Tahircal-Shahdag Mountain – Bazarduzu Mountain, black box locates equivalent stratigraphy to our studied section. Simplified structural contacts are shown for consistency with regional cross-sections (modified from Bochud, 2011).

Figure 3: Equal area stereographic projection showing bedding orientations for Cretaceous strata across the study area. Bedding planes shown as lines and poles to bedding shown as dots. Coloured by stratigraphy and location; LC- Lower Cretaceous (Aptian-Albian and Cenomanian – early Turonian stratigraphy), UC- Upper Cretaceous (mid Turonian and younger). Structural data reveal shallow-

moderate structural dips to the north-northeast and south-southwest, in agreement with the east-southeast – west-northwest trending structural zones of the Eastern Greater Caucasus.

Figure 4: Palaeocurrent (predominantly ripples) rose diagrams from the Cretaceous stratigraphy of the study area. Readings have been corrected for tectonic tilt and are subdivided by stratigraphy and location (see Figure 2).

Figure 5: Facies photographs. Due to the interbedding and mixing of these facies, it is not possible to document all facies in individual photographs and therefore multiple lithofacies appear in each photograph. Abbreviations on the figures refer to interpretations of lithofacies (Table 1): LDT; low-density turbidite, MDT; medium-density turbidite, Db; debrite (poorly-sorted clast-rich deposit); Tb; Turbidite, S; Siliciclastic, C; Calcareous. Scale is either lens cap (52 mm), person (1.74 m) or indicated. Letters in square brackets below refer to lithofacies definitions (Table 1) based on lithology and depositional features. A) Calcareous mudstone [J] B) Calcareous low-density turbidite [E and G] and mixed beds (of siliciclastic and calcareous low-density turbidites) [D] C) Two bi-partite beds [I] consisting of a lower turbidite and an upper debrite, in this case both siliciclastic, overlain by two siliciclastic low-density turbidites [H]. D) Evidence for facies-scale mixing (*sensu* Chiarella et al., 2017); calcareous turbidites were recognised in the field by their pale cream colour, while siliciclastic turbidites were brown-orange in colour and contained visual quartz granules. Calcareous turbidite probably accumulated slowly based on their grain-size, and were punctuated by siliciclastic gravity flows, forming mixed beds [D]. E) Siliciclastic low- [H] and medium- [F] density turbidites with cm-scale mud clasts weathered out. F) Mudstone [J] and low-density turbidites (both calcareous [G] and siliciclastic [H])) punctuated by metre-scale amalgamated conglomerates [A]. G) Chaotic, clast-rich deposit with deformed, non-extensive bedding [B]. Camera lens cap circled in green. H) Erosionally-based, crudely cross-laminated siliciclastic high-density turbidite [C] rich in mud-clasts.

Figure 6: Type examples of the seven recognised facies associations, divided into siliciclastic and mixed (siliciclastic and calcareous) associations, by orange and blue boxes respectively. Scale either lens cap (52 mm), person (1.74 m) or indicated. 10 m type log is taken from representative logged section of each facies association. Cretaceous Oceanic Red Beds; CORBS.

Figure 7: Quantitative facies analysis for the mid Turonian-Maastrichtian stratigraphy. The three columns represent three different logged sections from north to south that are representative of northern margin, axis and southern margin of the Buduq Syncline respectively. Charts compare bed

number (with 1 being at the base of the log and 200 at the top) to bed thickness (linearly in the top column and logarithmically in the middle column) and logged grain-size (in the basal column). Where grain-size varies within the bed average grain-size is used. In the top column thick beds are highlighted with a dashed line. Scales for bed number vary across the rows. Colours are for visual separation of data with greyscale used to for bed thickness (i.e. thicker beds are darker) and blue to orange used for grain-size (i.e. orange is coarser).

Figure 8: Quantitative facies analysis for Late Cretaceous event beds, divided into Cenomanian-early Turonian channelised siliciclastic deposition and mid Turonian–Maastrichtian mixed lobe deposition. Facies refer to HB: hybrid bed (bi/tri-partite beds); LDT: low-density turbidite; MDT: medium-density turbidite; HDT: high-density turbidite; Db: debrite (poorly-sorted clast-rich deposit) and Cg: conglomerate. Coloured by type log for different sub-environment. Density represents a probability density function.

Figure 9: Quantitative facies analysis of mid Turonian-Maastrichtian mixed stratigraphy comparing bed composition (carbonate or siliciclastic) against bed number (with 1 being at the base of the log and 200 at the top). Using the same logged sections as Figure 7, and thus a different number of beds per log resulting in variable bed number scale.

Figure 10: Pie charts showing composition of clasts within conglomerates per stratigraphic age, taken from 100 clasts from representative conglomeratic beds of over 1 metre thick. Percentage equates to absolute number of clasts, as 100 clasts were sampled. Carbonate clast content increases through time, discussed in text.

Figure 11: Evidence for palaeotopography. Scale is either person (1.74m), car (1.9 m) or indicated. A) Cretaceous stratigraphy thinning and onlapping Jurassic limestone, slope angle reconstructed. B) Evidence for opposing ripple directions suggesting flow deflection. C) Thickness and pinch-out variability of different deposits on a metre-scale laterally. D) Cliff section containing three conglomerate bodies that vary in architecture and termination style as indicated. E) Submarine landslide deposit showing evidence for slumping towards the south.

Figure 12: Evidence for collapse of the Jurassic carbonate platform. Scale is either person (1.74 m), car (1.9 m) or indicated. Onlap indicated by orange arrows, extent of clast or bedding surface shown in orange dashed line. A) Metre-scale limestone clasts within Coniacian mixed stratigraphy at

Kunkhirt. B) Campanian calcareous low-density turbidites abutting against a decametre-scale Jurassic limestone block at Cek. C) Stacked, inversely-graded submarine landslide deposits primarily composed of reworked Jurassic limestone blocks at Rük, upwards widening triangles indicate coarsening-upwards (inverse-grading). D) In situ break-up of the Jurassic platform at Cek. Clasts are fractured and separated but bedding planes (indicated in white) are still visible showing minimal displacement. For locations of villages see Figure 2.

Figure 13: Evidence and model for the generation of topography by an allochtonous block throughout the Cretaceous. A&B) Field examples of remobilised Jurassic stratigraphy forming topography throughout the Cretaceous influencing sediment routing. C) Schematic model showing formation of topography.

Figure 14: Evidence for allochtonous block model as the most likely for the generation of Cretaceous topography. Scale is either person (1.74 m) or indicated. Blocks are drawn around with black dashed line. A-C are examples of metre-decametre scale clasts around Cek. D) Shahdag Mountain, is interpreted as a kilometre-scale olistostrome (Bochud, 2011), which moved up to 20 km without significantly effecting the internal stratigraphy (Gavrilov, 2018). E) Block with both margins exposed and onlapped by mixed stratigraphy, black box locates C.

Figure 15: Evolutionary model for the Cretaceous of the study area. Studied stratigraphic sections highlighted. Topography, thought to be formed by a mega-clast, is present throughout the Cretaceous and influences deposition, discussed in text. Extract from the geological time scale, sea-level fluctuations (Haq, 2014) and local tectonic events highlighted on the left. Tectonic events are compiled by Bochud (2011), after Zonenshain & Le Pichon (1986), Philip et al. (1989), Nikishin et al. (2001), Brunet et al. (2003), Saintot et al. (2006a) and Barrier et al. (2008). The Pre-Albian was dominated by limestone blocks on a muddy slope. Thin-bedded siliciclastic turbidites of a distal lobe were deposited during the Aptian-Albian. Siliciclastic channels are prominent throughout the Cenomanian-early Turonian. In the mid Turonian-Maastrichtian mixed calcareous and siliciclastic lobes, of different sub-environments interact, and are likely sourced from the same northern margin, discussed in text. Locations in red boxes are stratigraphically, and not spatially, representative.

Figure 16: Seismic geomorphology of a mixed system offshore The Gambia, NW Africa. A) East-West two-way time seismic-section with key stratigraphic surfaces, location shown in C. B) Enlarged

two-way time seismic-section of carbonate blocks observed in the deep-marine mixed system. C) Depth structure map (contoured) with dip magnitude below of the diachronous regional composite unconformity surface displayed on seismic-section A, showing the heavily canyonised carbonate escarpment margin, canyon flow pathways (dashed white lines), lithological contact between siliciclastic and carbonate subcrop (solid white line) and onlap surface (dotted white line). D & E) RMS amplitude maps extracted from a +/- 12 ms window around two Late Cretaceous horizons in the basin. Location of maps shown on C.

Figure 17: Quantitative facies analysis for mid Turonian-Maastrichtian stratigraphy. Logs are the same as Figures 7 and 9. Logs 5C, 4A and 3A represent northern margin, axis and southern margin respectively. Each log is divided into carbonate and siliciclastic beds, and bed number is plotted against bed thickness (upper row) and grain-size (bottom row). Bold black lines indicate linear regression (trend line), r^2 value stated. Low-no correlation is observed suggesting no stacking patterns or modulation of any stacking patterns by interaction of both systems, discussed in text.

Figure 18: Interpreted RMS maps showing potential interactions of calcareous (blues) and siliciclastic (yellows/browns) lobes in mixed systems. A and B are from Figure 16, and have been overlain by schematic lobe complex geometries, based on seismic facies analysis and understanding of regional source area (see Casson et al., 2020). X and Y are representative logs, based on field observations where the lobe complexes interact in A and B respectively. X crosses the lobe fringe of the calcareous system and the lobe axis of the siliciclastic system and Y crosses the lobe fringe of both systems resulting in a thinner and finer-grained succession when compared to X. This variability highlights difficulties arising from exporting sub-environment terminology developed in siliciclastic systems (e.g., Prélat et al. 2009) into mixed systems. In both the calcareous (blue) and siliciclastic (yellow/browns) lobes darker colours are indicative of a more distal depositional environment.

TABLE CAPTION

Table 1: Summary of observations and interpretations of lithofacies, used to create facies associations.

SUPPLEMENTARY MATERIAL

Figure SM.1: Age of stratigraphic divisions of the 23 measured stratigraphic sections used in this study.

Figure SM 2: Topographic map of the Eastern Greater Caucasus (EGC), covering the same area as Figure 2a. Locations of the 23 measured stratigraphic sections shown in Figure SM.1, and used within this study.

Figure SM.3: Bed number (from bottom of stratigraphic section to top) against grain-size for all 23 measured stratigraphic sections from the study area. Figure SM.1 shows ages and SM.2 shows locations of each log. Colours are for visualisation purposes, blue (fine grain-size) to orange (coarse grain-size). Logs 3A, 4A, 5C used in Figures 7, 9 and 12. Logs 3A, 4A, 5C, 7A, 7B and 7C used for Figure 8. All logs used for facies and facies associations descriptions (Figures 5 and 6).

Figure SM.4: Bed number (from bottom of stratigraphic section to top) against facies for all 23 measured stratigraphic sections from the study area. Figure SM.1 shows ages and SM.2 shows location of each log. Colours are for visualisation purposes. Logs 3A, 4A, 5C used in Figures 7, 9 and 12. Logs 3A, 4A, 5C, 7A, 7B and 7C used for Figure 8. All logs used for facies and facies associations descriptions (Figures 5 and 6).

Figure SM.5: Bed number (from bottom of stratigraphic section to top) against bed thickness for all 23 measured stratigraphic sections from the study. Figure SM.1 shows ages and SM.2 shows locations of each log. Colours are for visualisation purposes, blue; thin beds, to red; thick beds. Logs 3A, 4A, 5C used in Figures 7, 9 and 12. Logs 3A, 4A, 5C, 7A, 7B and 7C used for Figure 8. All logs used for facies and facies associations descriptions (Figures 5 and 6).

Table SM.1: GPS locations of all logged sections used in this study.

Facies	Description	Interpretation
Conglomerates (A)	0.1 to 3 + m thick beds of poorly-sorted, disorganised conglomerates. Most commonly clast-supported consisting of sub-angular to sub-rounded boulder-, cobble- and pebble-grade clasts of carbonate (wackestone and micrite) and siliciclastic (sandstone and mudstone) material. Matrix comprises a poorly-sorted mix of all finer size fractions. Cm- 10 cms scale mud-clasts occur sporadically throughout the beds. Bed bases are often erosive and can be amalgamated. This facies often grades into thick-bedded sandstones (C).	Deposition from debris flows having cohesive as well as frictional strength (Fisher, 1971; Nemeck & Steel, 1984). The grading of conglomerates into thick-bedded sandstones reflects the transition of hyper-concentrated submarine debris flows into highly-concentrated turbulent flows (Mulder & Alexander, 2001; Sohn et al., 2002), due to the deposition of the coarsest size fraction and the entrainment of ambient water (Postma et al., 1988).
Poorly-sorted clast-rich deposit (B)	0.1 – 1+ m thick poorly-sorted deformed, matrix-supported units. Matrix can range from mudstone to coarse-sandstone sized clasts and is often poorly sorted and sheared. Clasts include cm-m scale carbonate and siliciclastic blocks, folded thin-bedded sandstones, sporadic pebbles and granules and frequent mud clasts. These deposits are commonly non-graded, but can show weak normal-grading.	The poorly-sorted matrix and large clast sizes are suggestive of 'flow freezing' (Inverson et al., 2010), indicating 'en masse' deposition from a cohesive debris flow (Nardin et al., 1979; Inverson, 1997; Sohn, 2000). Folded, remobilised, thin-bedded sandstones and intra-basinal clasts indicate localised mass failure and reworking.
Thick-bedded sandstones (C)	0.5 – 1+ m thick brown siliciclastic fine-granular sandstones. Normally-graded or non-graded and typically lacking primary depositional structures. Bases are often sharp and erosive. Parallel laminations are sometimes present at bed tops and mud-clasts can be observed throughout. Weak cross-lamination is infrequently observed.	The general massive nature of these deposits suggests that they represent rapid aggradation beneath a highly-concentrated but dominantly turbulent flow, and are thus interpreted as high-density turbidites (Lowe, 1982; Mutti, 1992; Kneller & Branney, 1995). In some instances, these may have been deposited by flows that evolved from laminar to turbulent, following the deposition of the coarsest grain fragment (Postma et al., 1988).
Mixed siliciclastic and calcareous sandstones (D)	0.1-1m beds of medium-bedded calcareous sandstones with punctuated interbeds of cm-scale thin-bedded siliciclastic sandstone, either as continuous beds or lenses. The medium-bedded calcareous sandstones are massive, and the siliciclastic beds are often erosively-based and show tractional structures (ripple and planar lamination). Siliciclastic beds can be	Medium-bedded calcareous sandstones are interpreted to represent deposition from a slowly aggrading dilute turbidity current. Periodic, thin-bedded siliciclastic sandstones represent deposition from a relatively quickly aggrading dilute turbidity current, which interacted with a much slower aggrading calcareous turbidity current. These facies represent lithofacies-scale mixing

	amalgamated with each other or isolated between calcareous siltstones or sandstones.	consistent with decimetre-scale alternations between siliciclastic and carbonate layers (Chiarella et al., 2017).
Medium-bedded calcareous sandstones (E)	0.1-1 m thick beige beds of calcareous siltstone -fine sandstone. Carbonate grains are normally-graded or non-graded. Planar lamination may be present, but other tractional structures are rare. Beds can be amalgamated.	Based on their tractional structures and normal-grading, beds are interpreted as having been deposited from dilute, slowly aggrading medium-density turbidity currents. These beds were deposited by thicker or more sustained flows than (G) (Remacha & Fernández, 2003).
Medium-bedded siliciclastic sandstones (F)	0.1 -0.5 m thick brown beds of very fine – granular grained, commonly normally-graded, sandstones. Inverse-grading is infrequently observed. Basal parts of the bed are often structureless containing infrequent cm-scale mud-clasts while tops are rich in tractional structures including parallel, ripple and hummock-like laminations. Bed bases are often erosive and can be amalgamated.	Based on their tractional structures and normal-grading, beds of this lithofacies are interpreted as deposition from a dilute turbidity current. These beds are interpreted as medium-density turbidites due to their bed thickness and common lack of structures in the lower part of the bed (e.g., Soutter et al., 2019).
Thin-bedded calcareous sandstones (G)	0.01 – 0.1 m thick beige beds of calcareous siltstone-fine sandstones. Carbonate grains can be normally-graded, often increasing in micrite percentage upwards, or non-graded. Planar laminations are infrequently observed but other tractional structures are typically absent. Individual beds are often amalgamated.	Thin-beds, fine grain-size and weak planar laminations represent deposition from a low-concentration turbidity current (Mutti, 1992; Jobe et al., 2012; Talling et al., 2012), indicating these beds are low-density turbidites. Fine grain-size, thicker beds compared to thin-bedded siliciclastic sandstone (H) and absence of ripple laminations suggest deposition by slowly aggrading, dilute remnants of a turbulent flow, (Remacha & Fernández, 2003; Bell et al., 2018a), which did not reach sufficient velocity to generate ripple laminations (Baas et al., 2016). Alternatively, ripples may not have been preserved, or may be extremely difficult to decipher due to lack of variety in grain-size or colour and early lithification (Imbrie & Buchanan, 1960).
Thin-bedded siliciclastic sandstones (H)	0.005 – 0.1 m thick brown beds of siliciclastic very fine- granular sandstones. Commonly normally-graded, occasionally inverse-graded. Tractional structures (planar, ripple, hummock-like and convolute	Thin-bedded, structured sandstones are interpreted to be deposited from low-concentration turbidity currents (Mutti, 1992; Jobe et al., 2012; Talling et al., 2012) and are therefore interpreted as low-density turbidites. Ripples indicating

	laminations) and sporadic mud-clasts are observed. Bases can be flat or weakly-erosive and sometimes contain granules. Bed tops are often flat. Ripples can show opposing palaeoflow directions.	opposing palaeoflow suggests topographic interference (e.g., Kneller et al. 1991).
Bi or tri-partite beds (I)	0.05-0.5 m thick beds that contain multiple parts. Typically consisting of a lower fine- to coarse-grained sandstone (division 1) overlain by a poorly-sorted muddy siltstone to medium-grained sandstone (division 2). Division 3 is sometimes present consisting of a siltstone-fine-sandstone loaded into division 2. Divisions 1 and 3 sometimes contain planar laminations and sporadic cm-scale mud-clasts. Division 2 is often highly deformed and rich in mud-clasts and very-coarse-grained sandstone to pebble-grade clasts. Sandstones can be calcareous or siliciclastic.	Tractional structures in division 1 and 3 indicate formation under turbulent flows. Poor sorting and mud content suggest division 2 was deposited under a transitional-laminar flow regime. These bi/tri-partite beds are hybrid beds (Haughton et al., 2009), generated by flow transformation from turbulent to laminar. Such transformation occurs through flow deceleration (Barker et al., 2008; Patacci et al., 2014) and by an increase in concentration of fines during flow run-out (Kane et al., 2017).
Mudstone (J)	0.005 – 8 m thick pale grey or red mudstone – fine-siltstone beds, which are friable and often inferred in areas of missing section. Planar laminations, discontinuous drapes and lenses of siltstone may be present. Commonly calcareous in composition. Red mudstones are common at the base of the Campanian stratigraphy. 'Mud' is used here as a general term, for mixtures of clay, silt and organic fragments.	Low-energy conditions, representative of background sedimentation via suspension fallout. Laminations may be present below the scale visible in outcrop, representing deposition from a dilute turbidity current (Boulesteix et al., 2019; 2020). Pale colour indicates low total organic carbon (TOC). Red mudstones are similar to Cretaceous Oceanic Red Beds (CORBS) described across Europe (Wang et al., 2005; Hu et al., 2005; Wagreich & Krenmayr, 2005) and represent deposition below the carbonate compensation depth (CCD) in a deep oceanic basin.

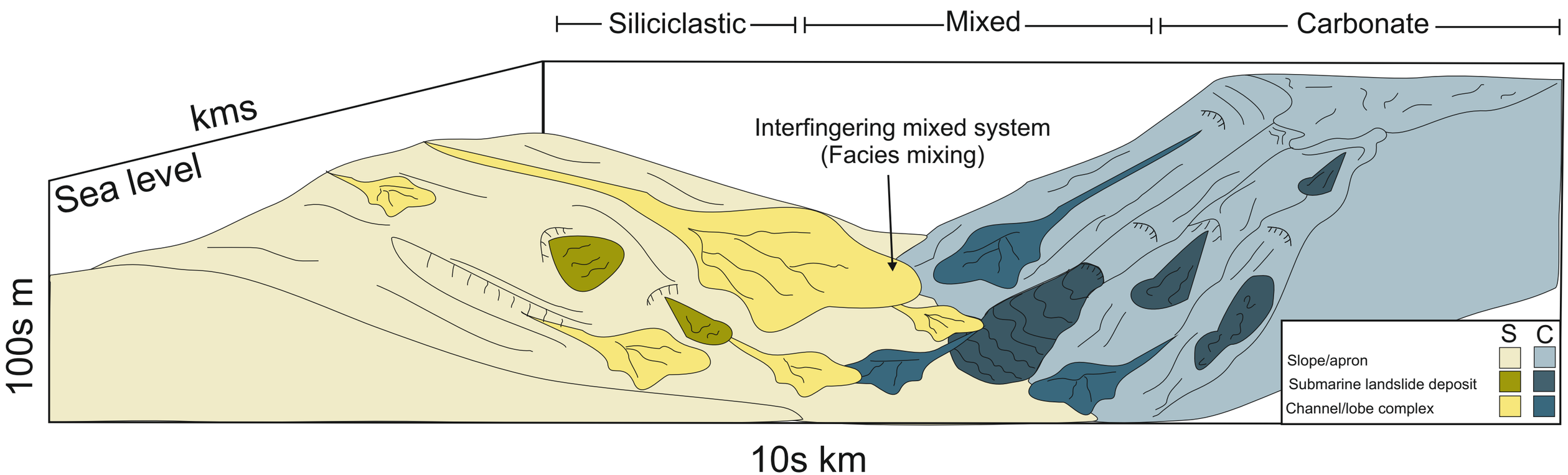
Siliciclastic
Mixed
Carbonate
kms
Sea level
100s m
Interfingering mixed system
(Facies mixing)
S
C
Slope/apron
Submarine landslide deposit
Channel/lobe complex
10s km

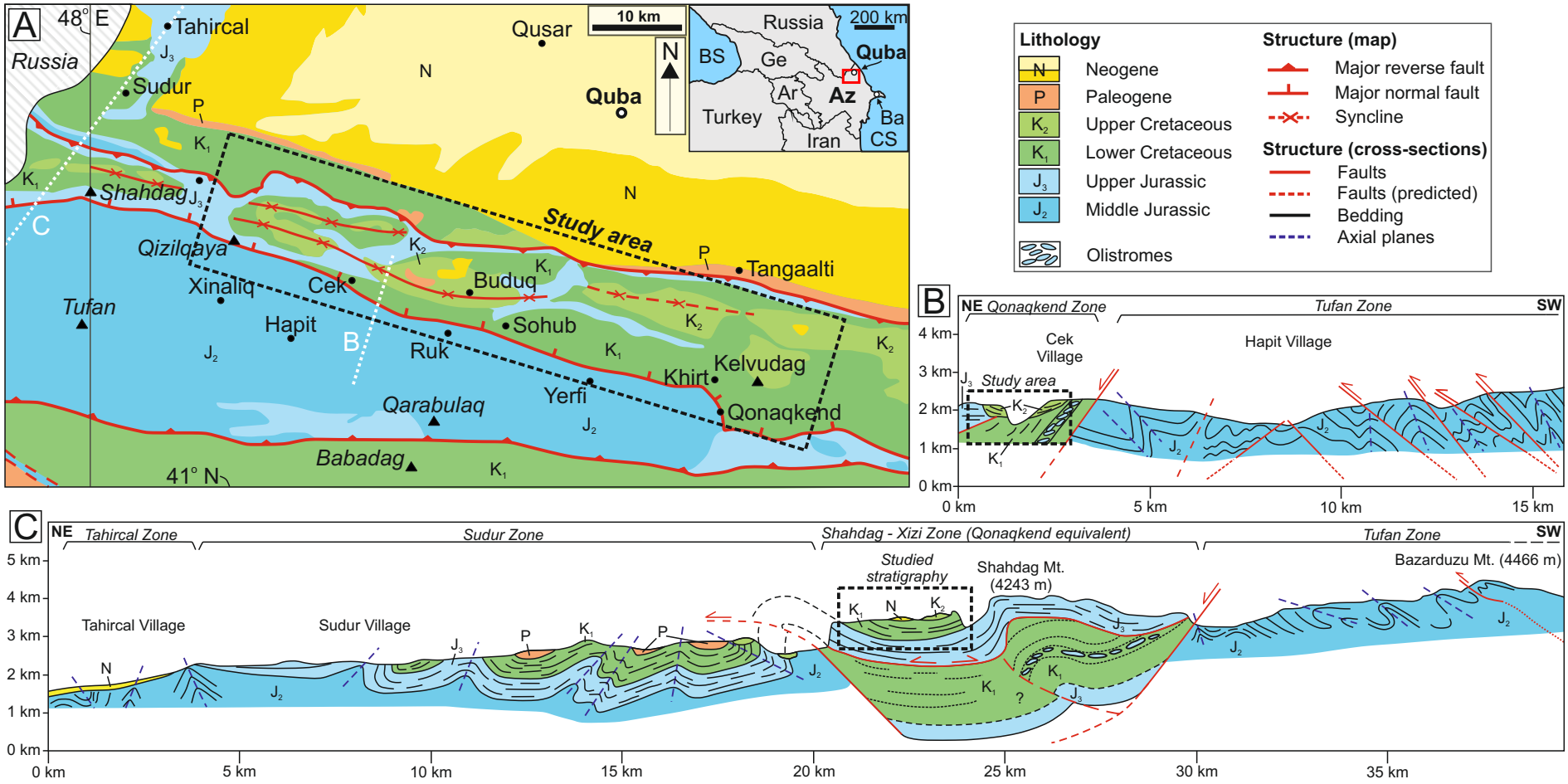
A
48° E
Russia
Tahircal
Sudur
Shahdag
Qizilqaya
Xinaliq
Tufan
Cek
Hapit
Buduq
Sohub
Ruk
Qusar
Quba
Study area
Tangaalti
Kelvudag
Khirt
Yerfi
Qonaqkend
Qarabulaq
Babadag
41° N
10 km
N
Russia
200 km
BS
Ge
Quba
Ar
Az
Turkey
Iran
Ba
CS
Lithology
Neogene
Paleogene
Upper Cretaceous
Lower Cretaceous
Upper Jurassic
Middle Jurassic
Olistromes
Structure (map)
Major reverse fault
Major normal fault
Syncline
Structure (cross-sections)
Faults
Faults (predicted)
Bedding
Axial planes
B
NE Qonaqkend Zone
Tufan Zone
SW
Cek Village
Hapit Village
Study area
4 km
3 km
2 km
1 km
0 km
0 km
5 km
10 km
15 km
C
NE
Tahircal Zone
Sudur Zone
Shahdag - Xizi Zone (Qonaqkend equivalent)
Tufan Zone
SW
Studied stratigraphy
Shahdag Mt. (4243 m)
Bazarduzu Mt. (4466 m)
Tahircal Village
Sudur Village
5 km
4 km
3 km
2 km
1 km
0 km
0 km
5 km
10 km
15 km
20 km
25 km
30 km
35 km

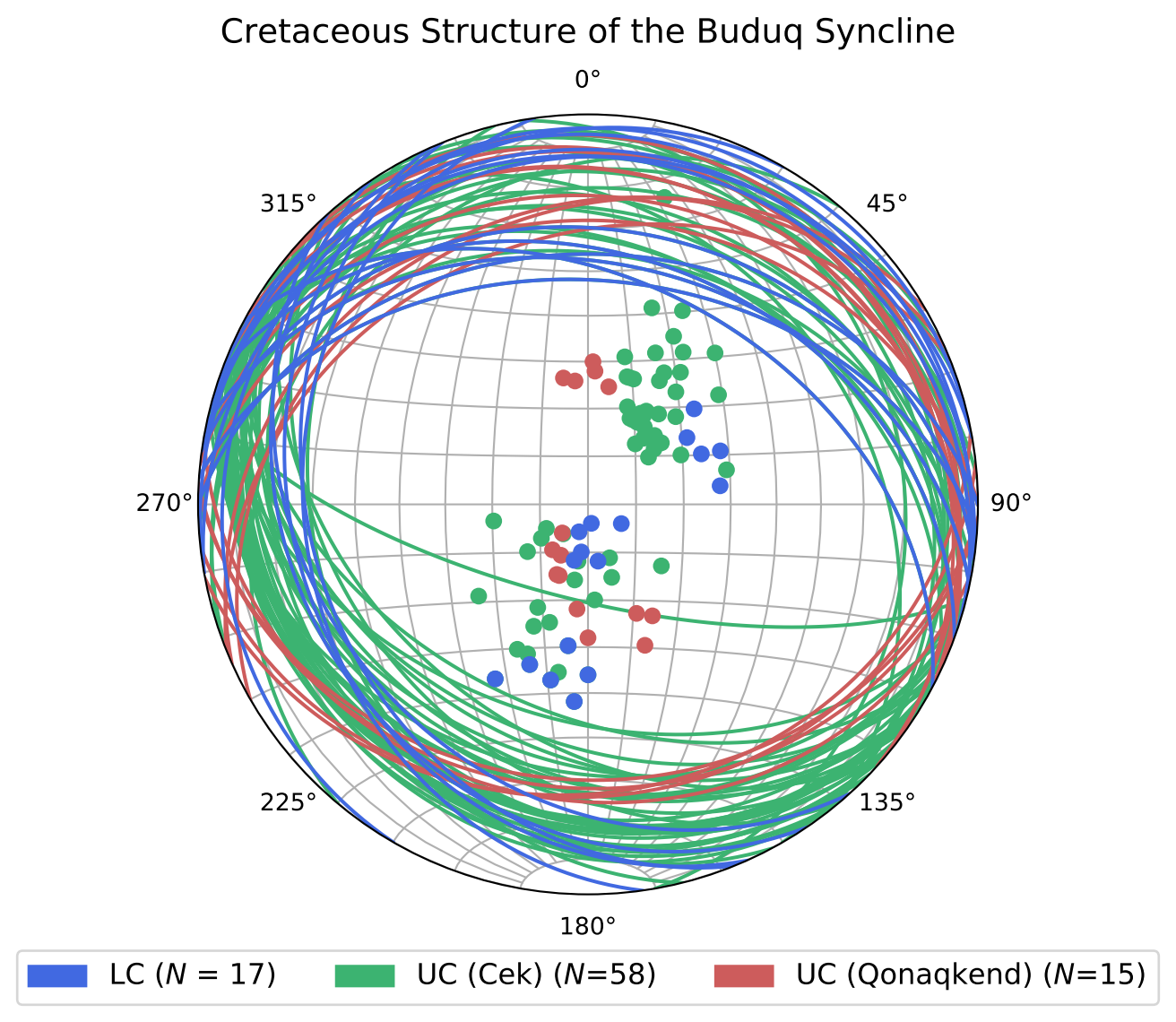
Cretaceous Structure of the Buduq Syncline
0°
45°
90°
135°
180°
225°
270°
315°
LC (N = 17)
UC (Cek) (N=58)
UC (Qonaqkend) (N=15)

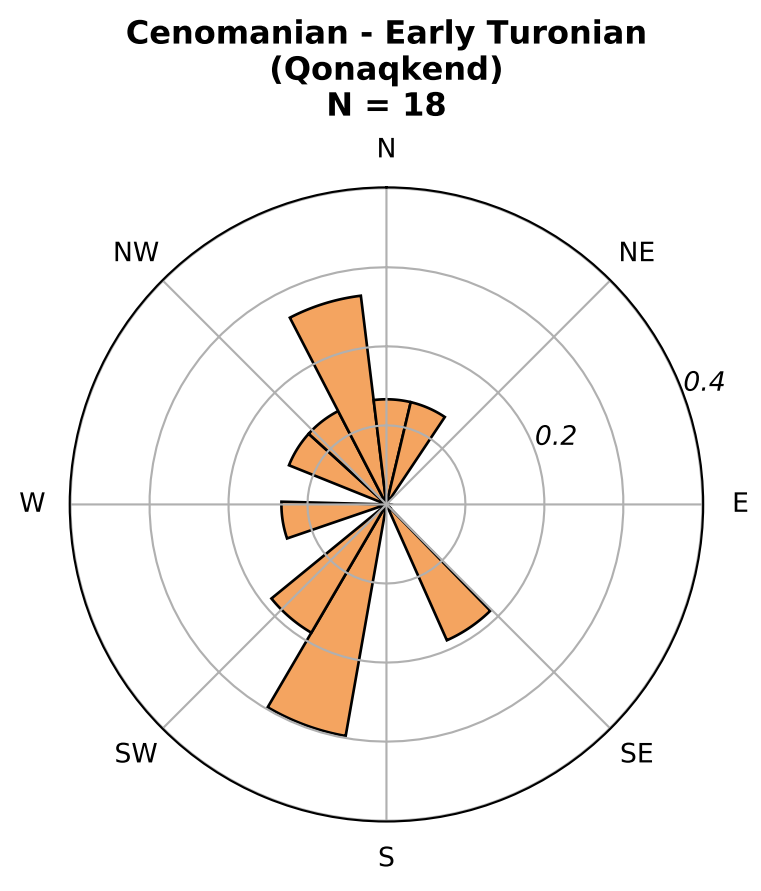
Cenomanian - Early Turonian
(Qonaqkend)
N = 18
N
NE
E
SE
S
SW
W
NW
0.2
0.4

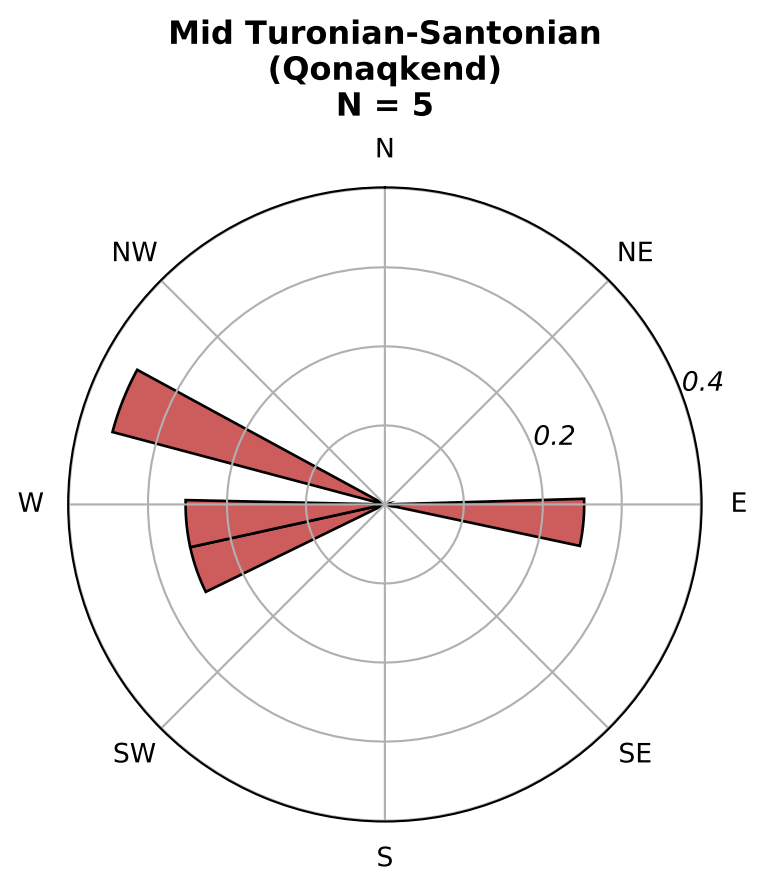
Mid Turonian-Santonian
(Qonaqkend)
N = 5
N
NE
E
SE
S
SW
W
NW
0.2
0.4

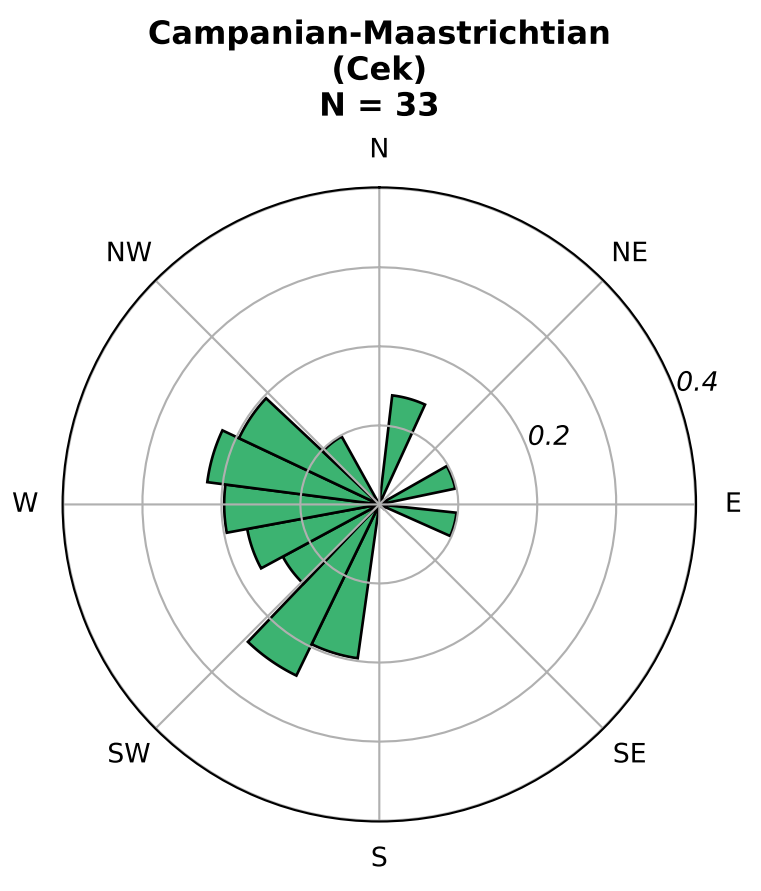
Campanian-Maastrichtian
(Cek)
N = 33
N
NE
E
SE
S
SW
W
NW
0.2
0.4


A

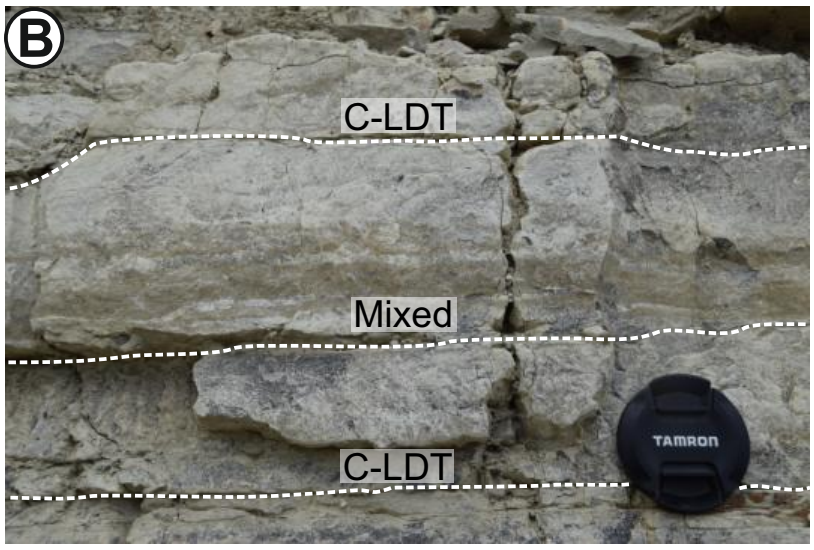
B
C-LDT
Mixed
C-LDT
TAMRON

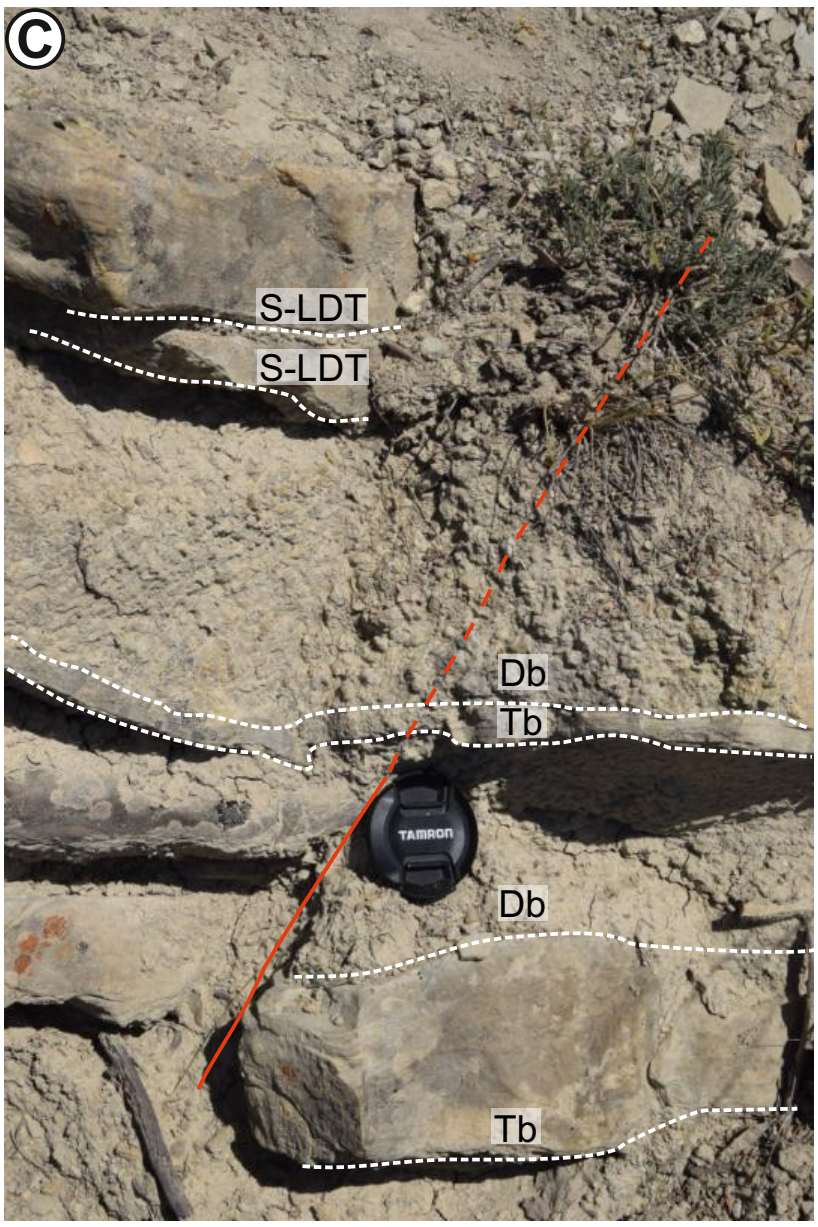
C
S-LDT
S-LDT
Db
Tb
TAMRON
Db
Tb

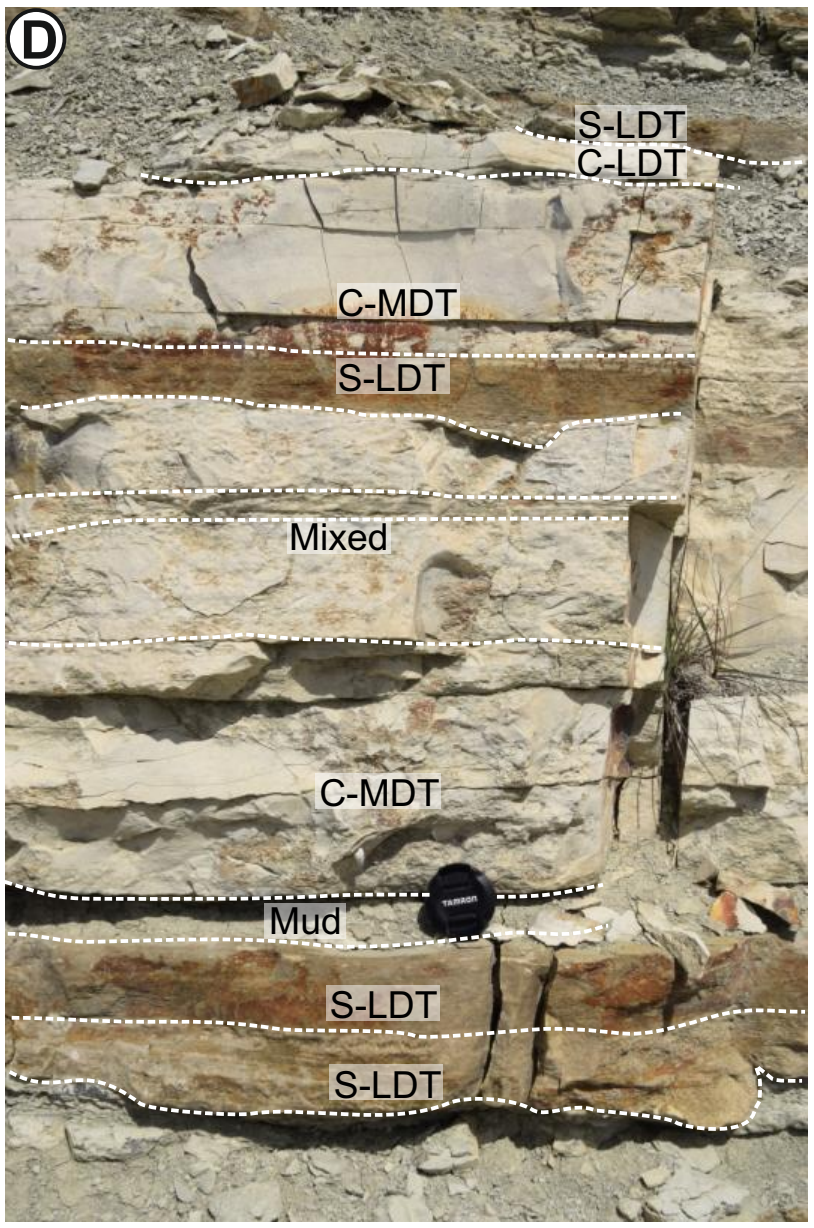
D
S-LDT
C-LDT
C-MDT
S-LDT
Mixed
C-MDT
Mud
S-LDT
S-LDT

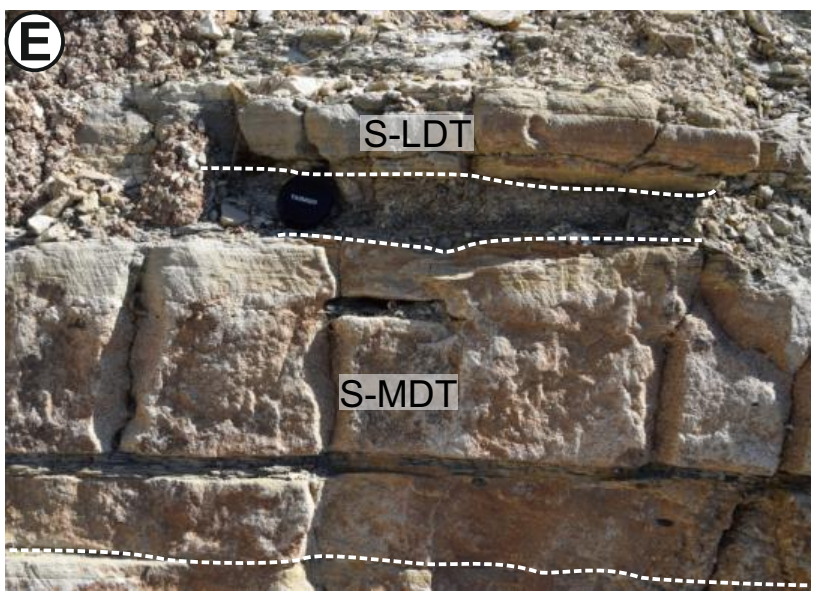
E
S-LDT
S-MDT

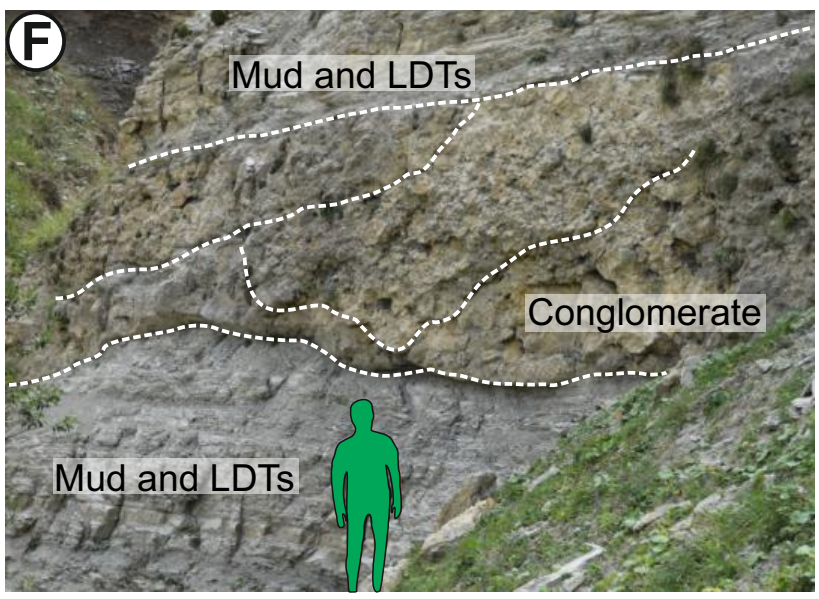
F
Mud and LDTs
Conglomerate
Mud and LDTs

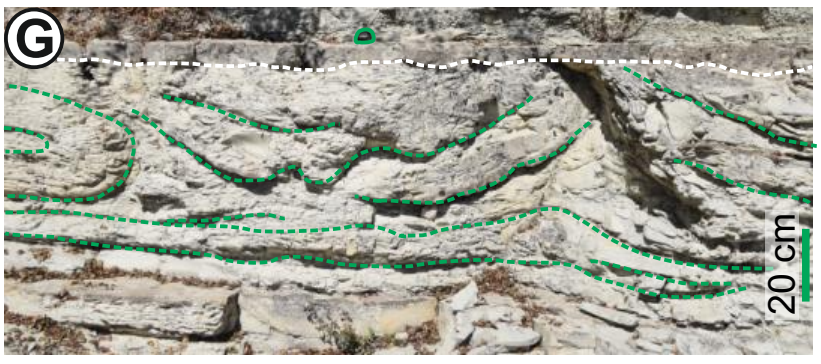
G
20 cm

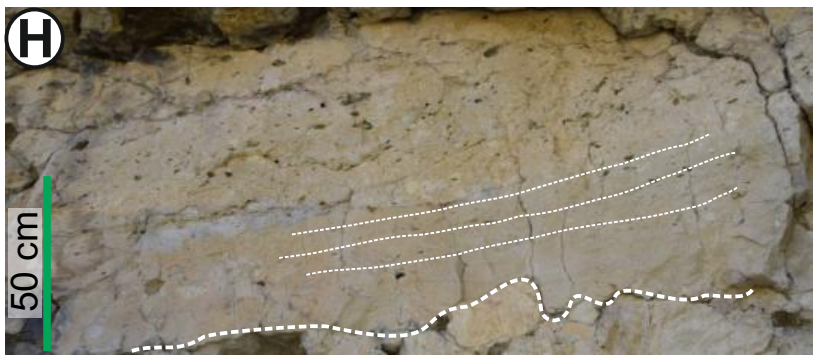
H
50 cm

Siliciclastic Facies Associations

Mixed Facies Associations

A) FA 1: Lobe Fringe

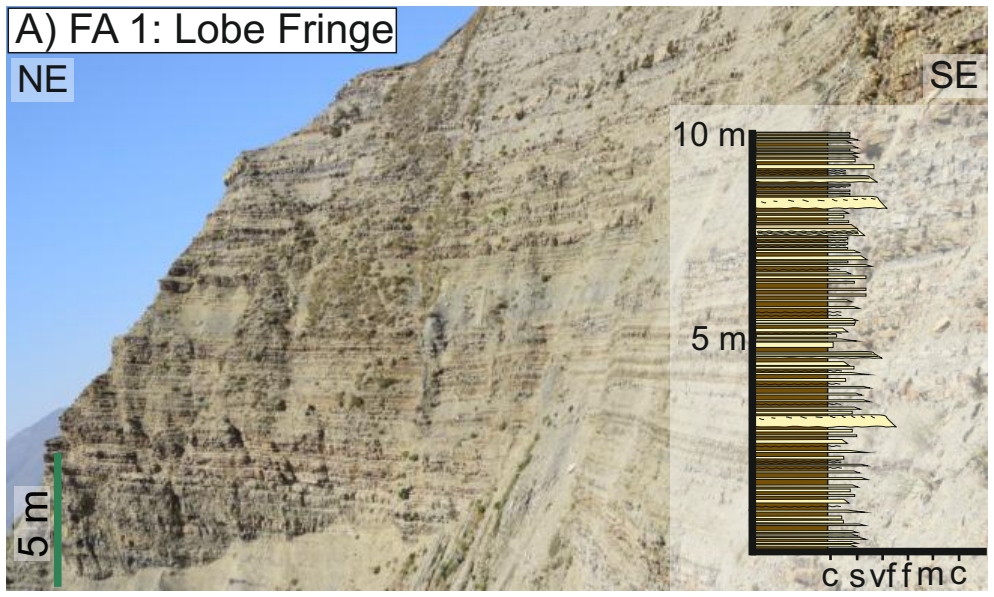

B) FA 3: Channel Margin

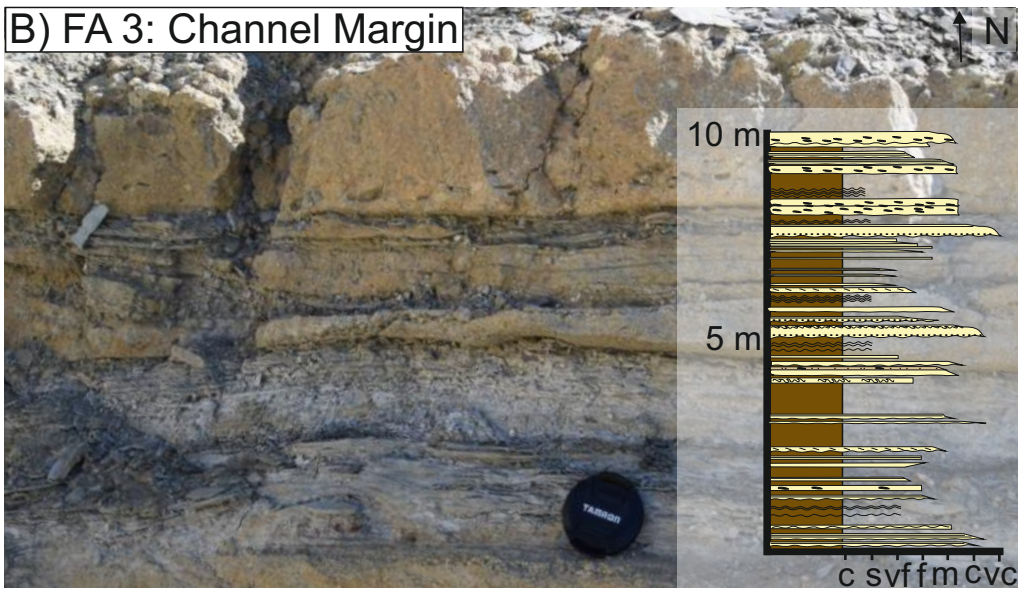

C) FA 2: Channel Axis

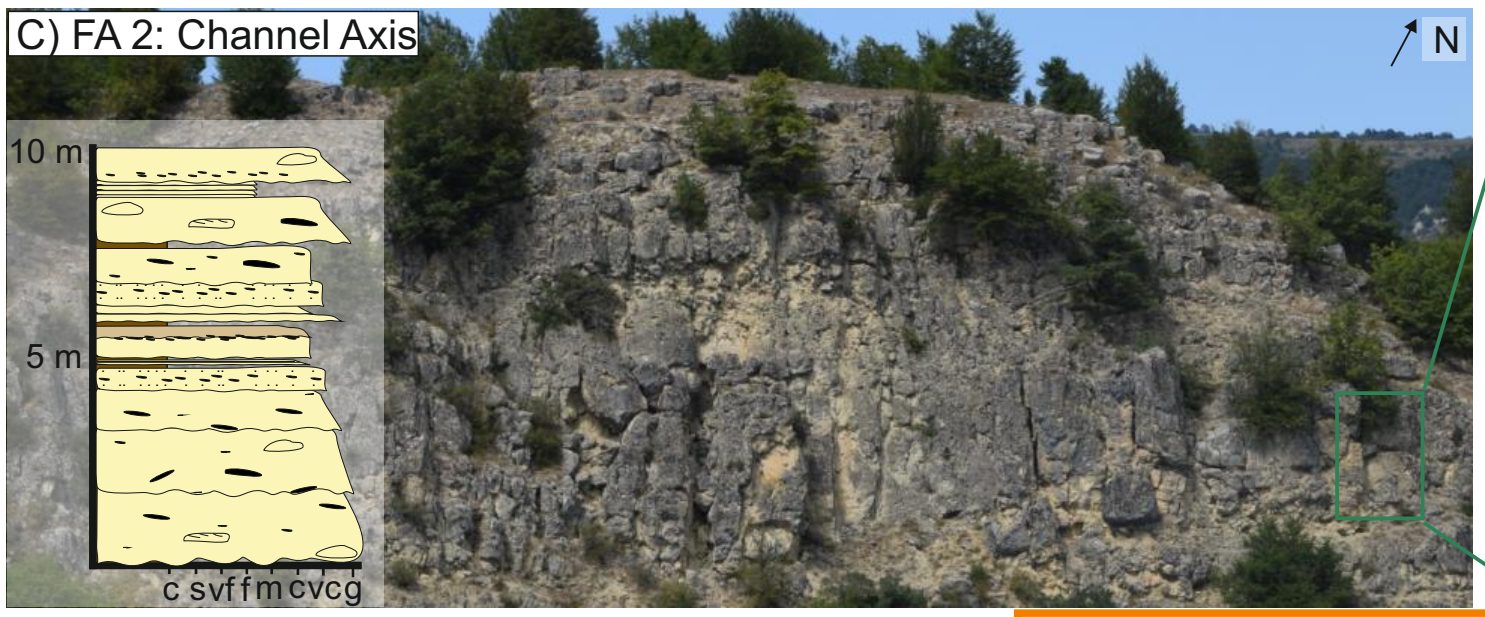

D) FA 4: Lobe Axis

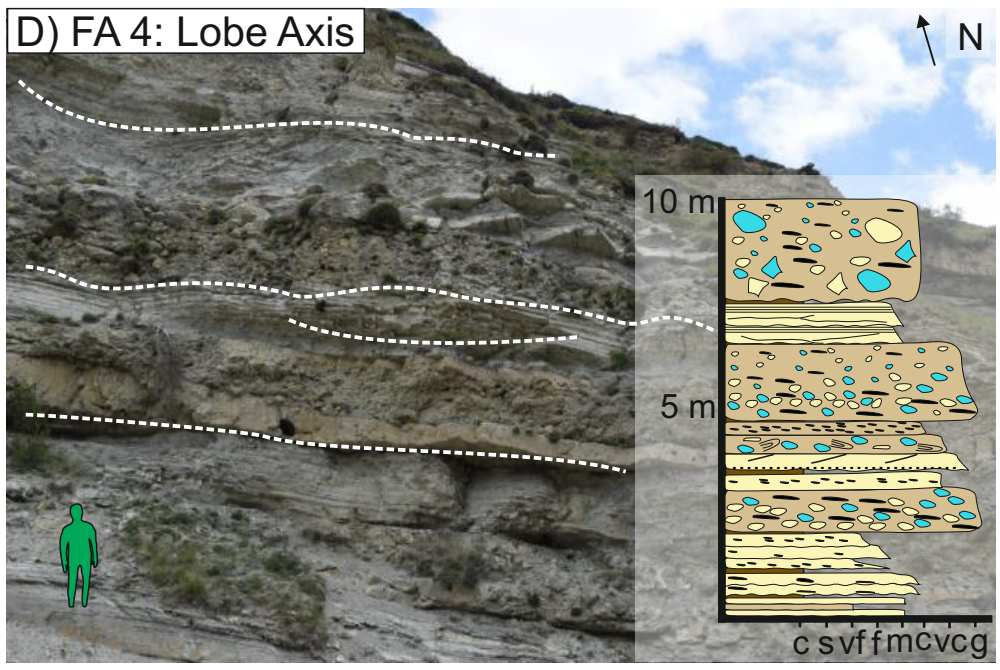

E) FA 5: Lobe off-axis

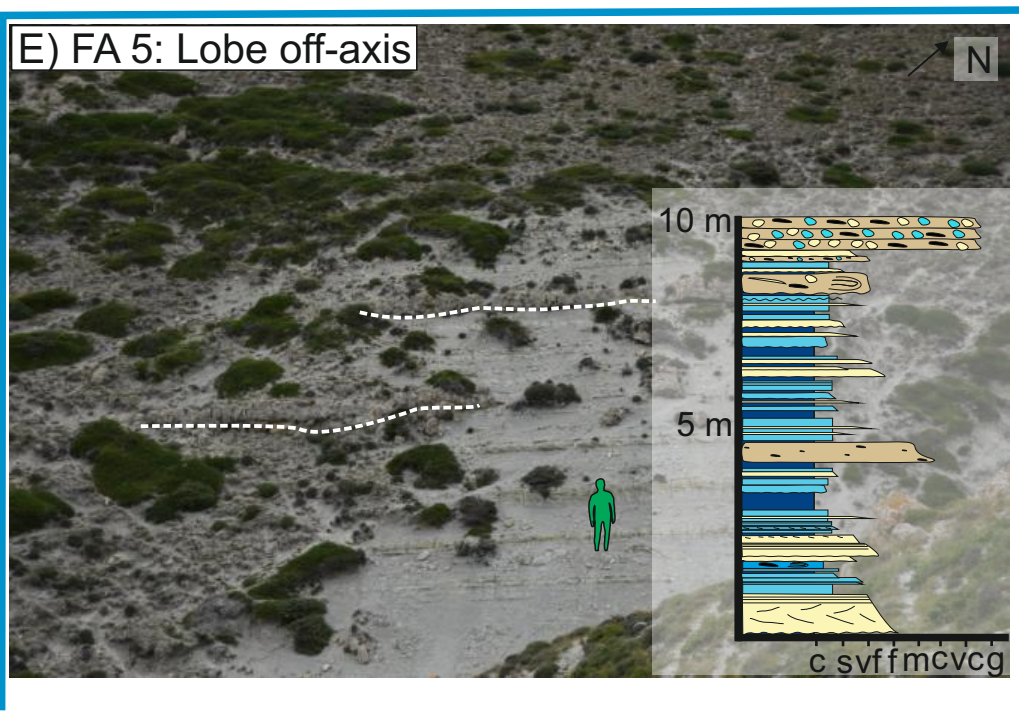

F) FA 6: Proximal Lobe Fringe

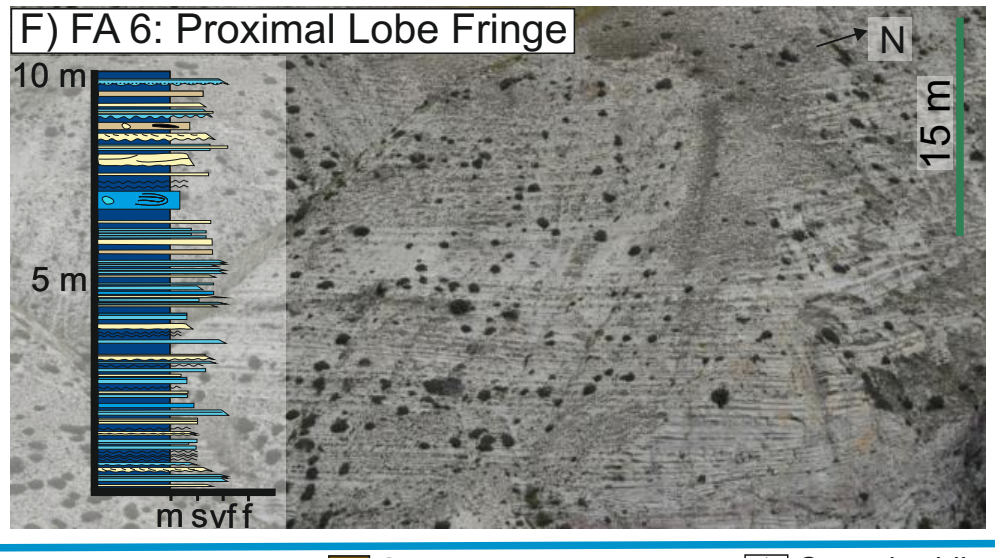

G) FA 7: Distal Lobe Fringe

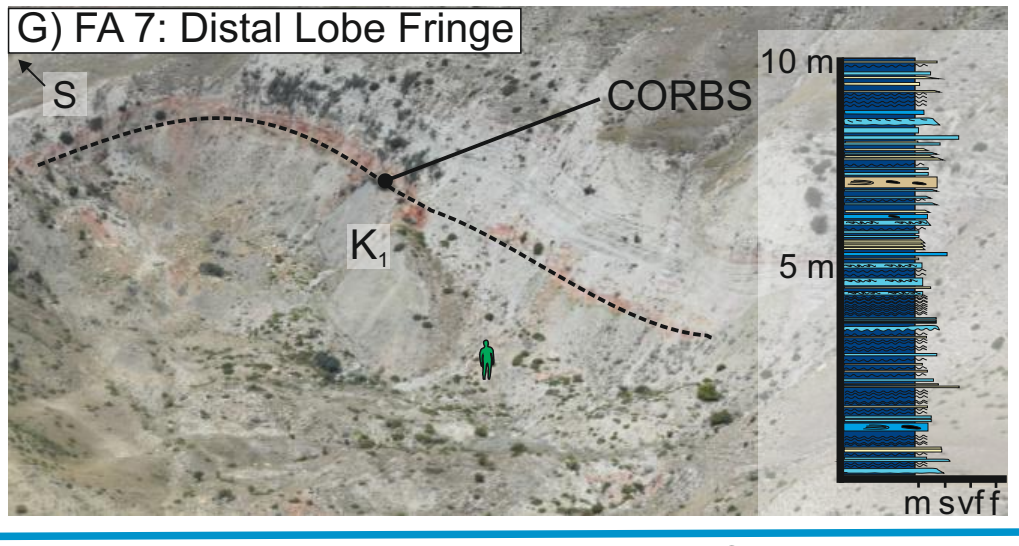

Key to all logs

- Calci-debrite
- Calci-turbidite
- Siliciclastic mudstone
- Siliciclastic debrite
- Siliciclastic turbidite
- Slump
- Cross bedding
- Granular horizon
- Amalgamation
- Ripple lamination
- Convolute lamination
- Wavy bedding
- Clasts (coloured by lithology)
- Beds <2 cm thick
- Sporadic pebble
- Mud clasts
- Planar lamination
- Erosional contact

Mid Turonian-Maastrichtian Bed Statistics

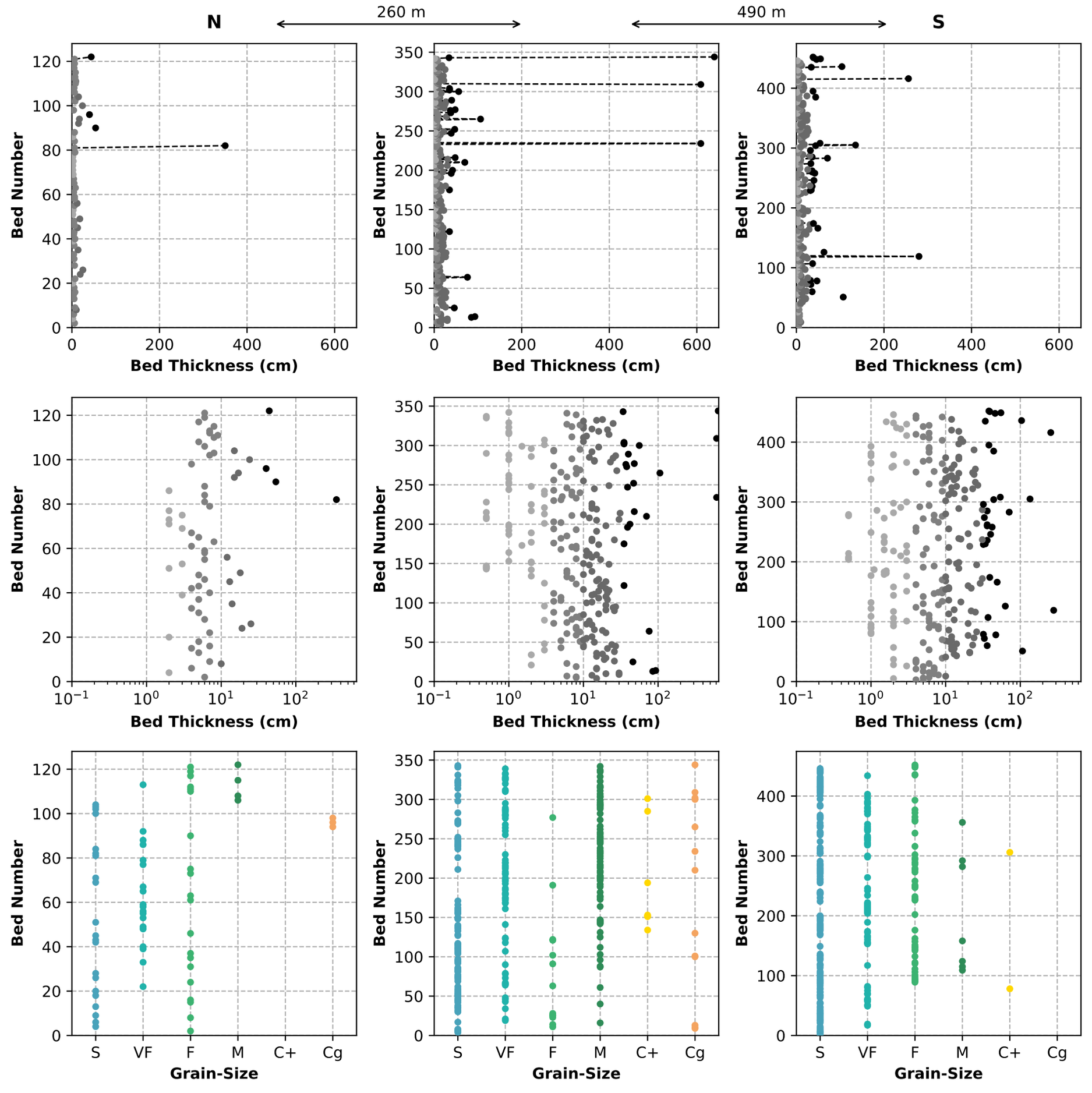

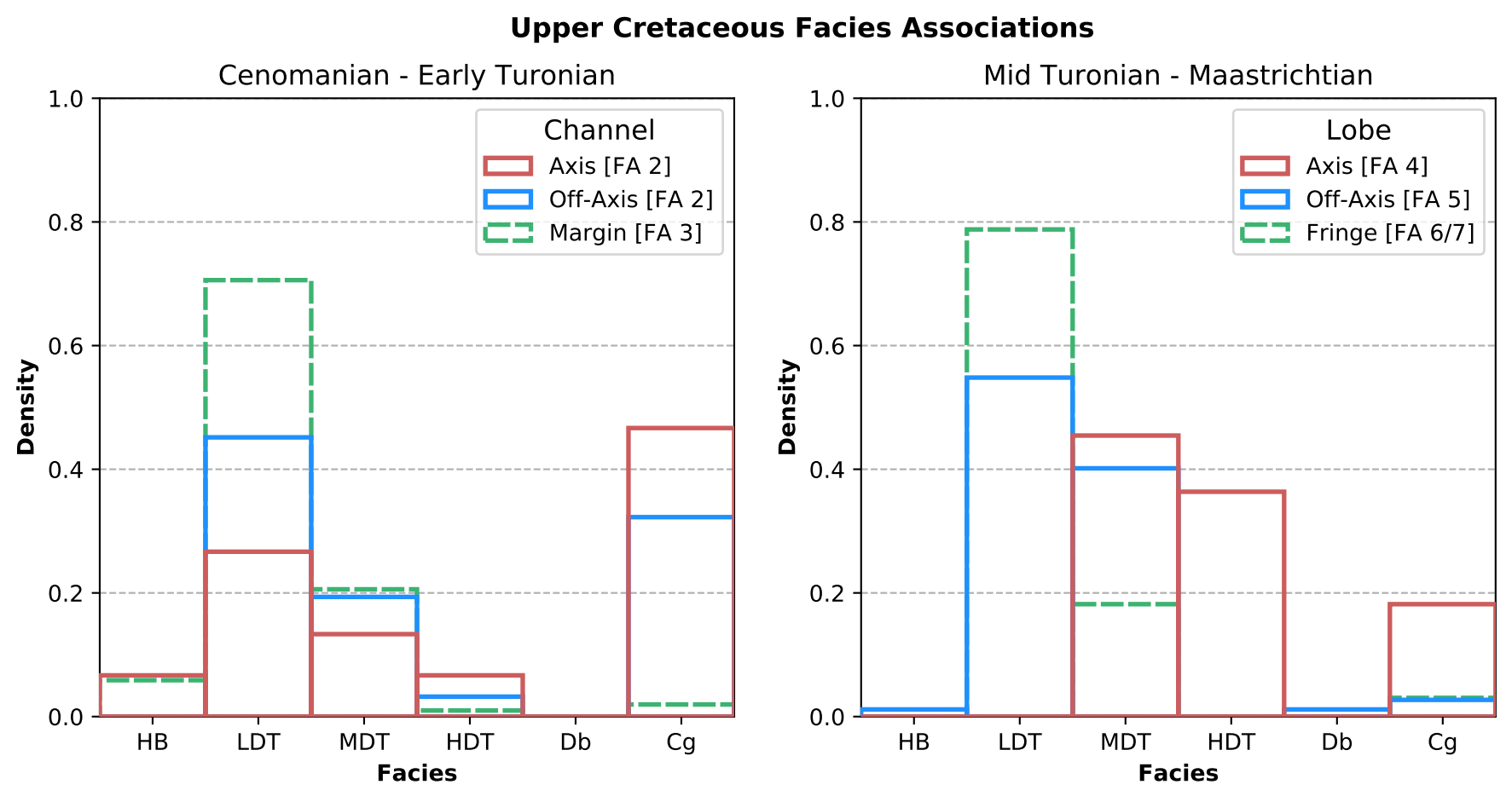
Upper Cretaceous Facies Associations
Cenomanian - Early Turonian
Mid Turonian - Maastrichtian
Density
Facies
HB
LDT
MDT
HDT
Db
Cg
0.0
0.2
0.4
0.6
0.8
1.0
Channel
Axis [FA 2]
Off-Axis [FA 2]
Margin [FA 3]
Lobe
Axis [FA 4]
Off-Axis [FA 5]
Fringe [FA 6/7]

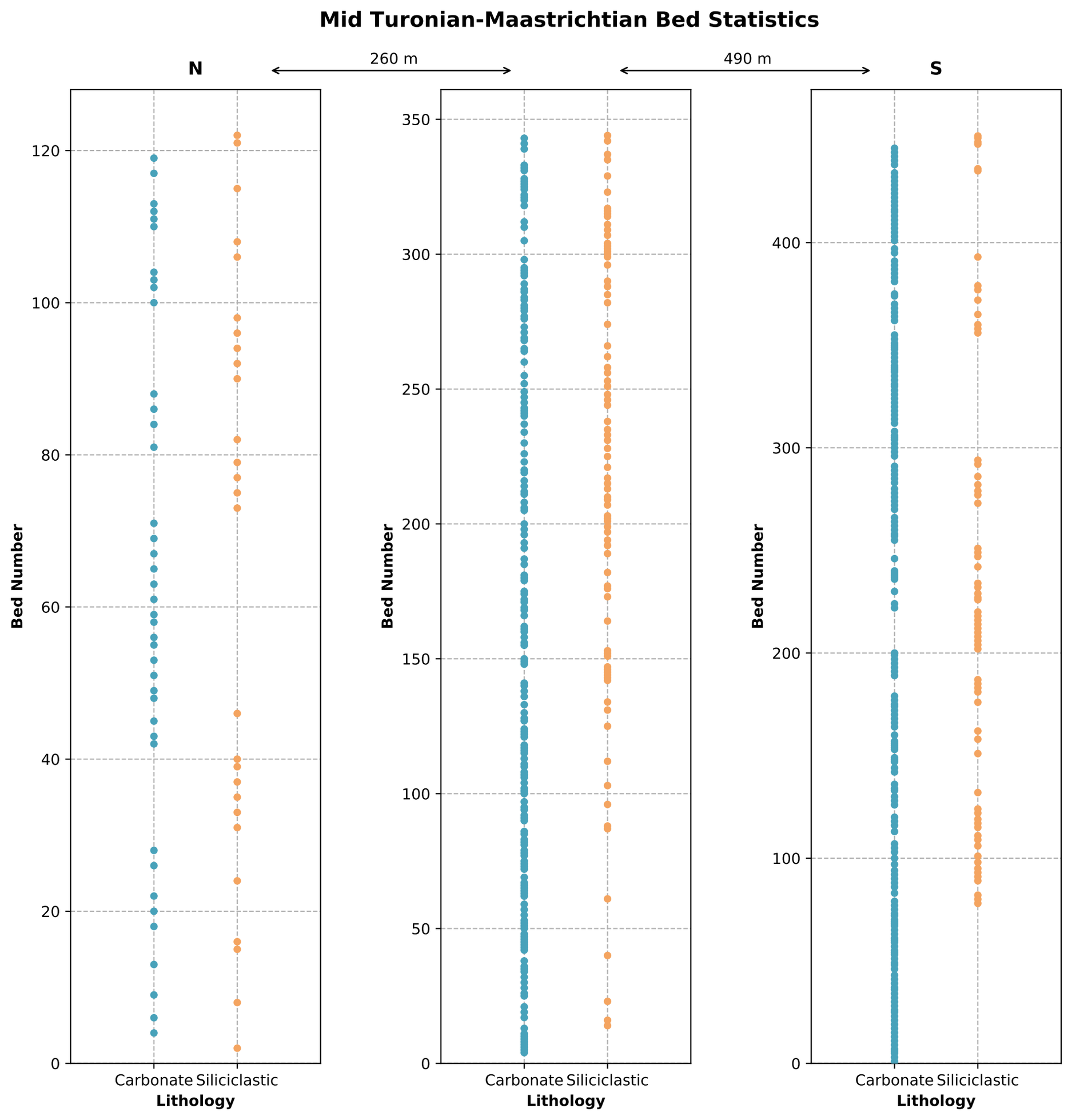
Mid Turonian-Maastrichtian Bed Statistics
N
260 m
490 m
S
Bed Number
Carbonate
Siliciclastic
Lithology

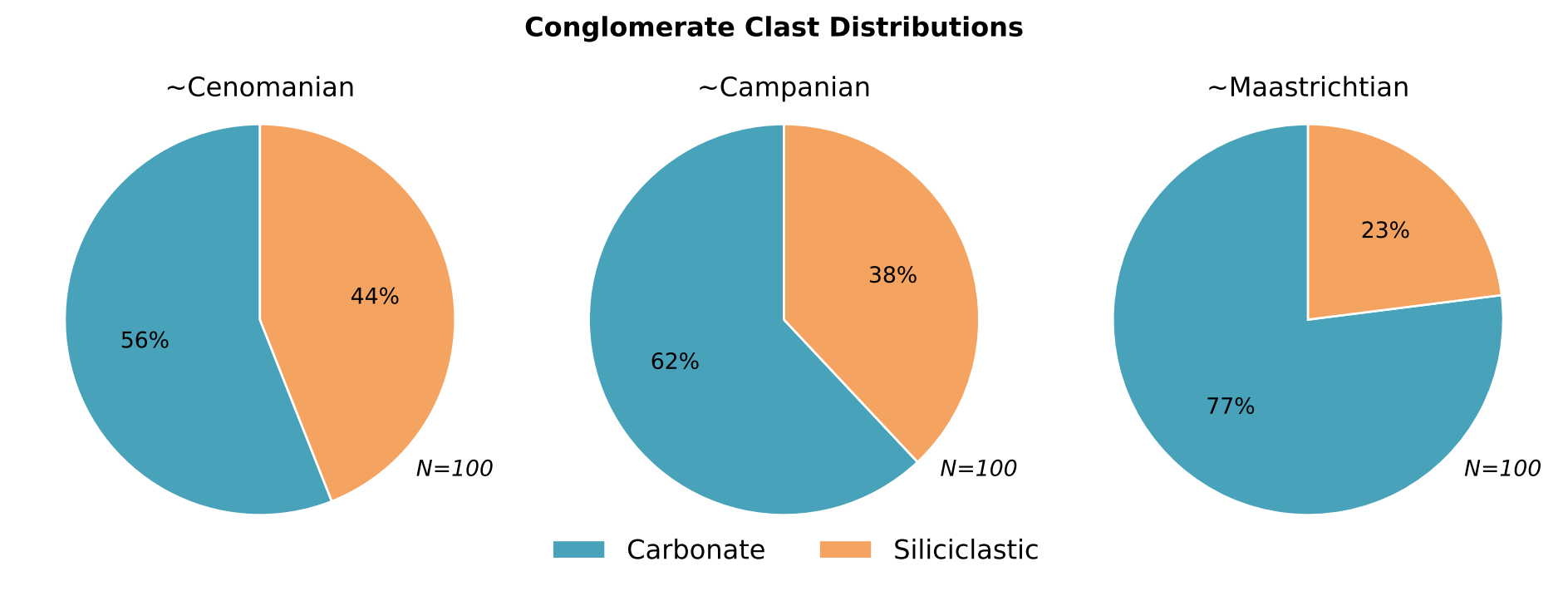
Conglomerate Clast Distributions
~Cenomanian
56%
44%
N=100
~Campanian
62%
38%
N=100
~Maastrichtian
77%
23%
N=100
Carbonate
Siliciclastic

A NE SE

Slope angle reconstruction

6°

32°-26° = 6°

Jurassic

Campanian 26°

Santonian 32°

B

5 cm

C

LDT running up topography

Conglomerate onlap

D NW NE

Downward pinch out

Isolated channelised conglomerate

Conglomerate

Conglomerate

Upward pinch out

E

Slumping to the south

5 m

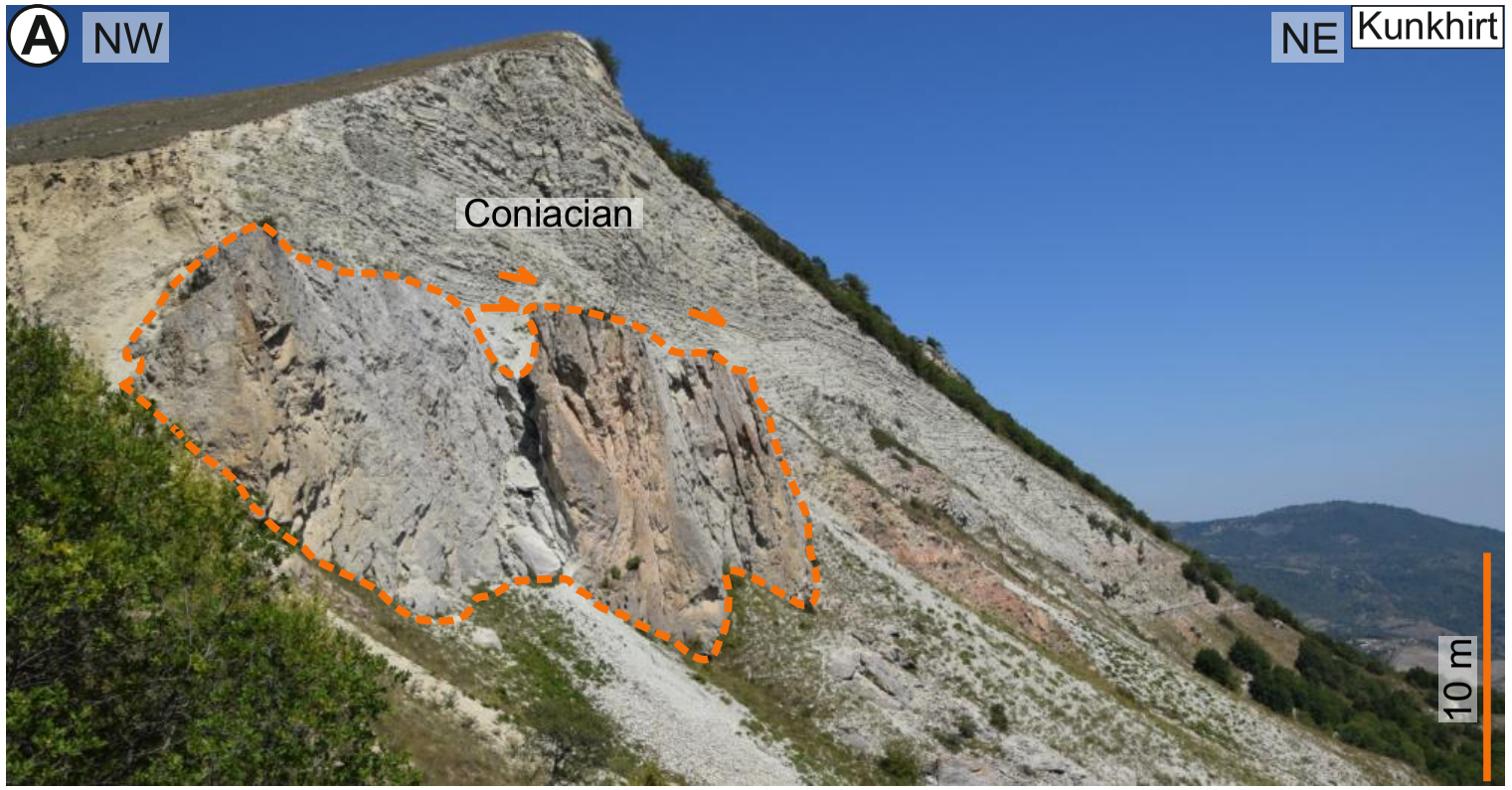
A
NW
NE
Kunkhirt
Coniacian
10 m

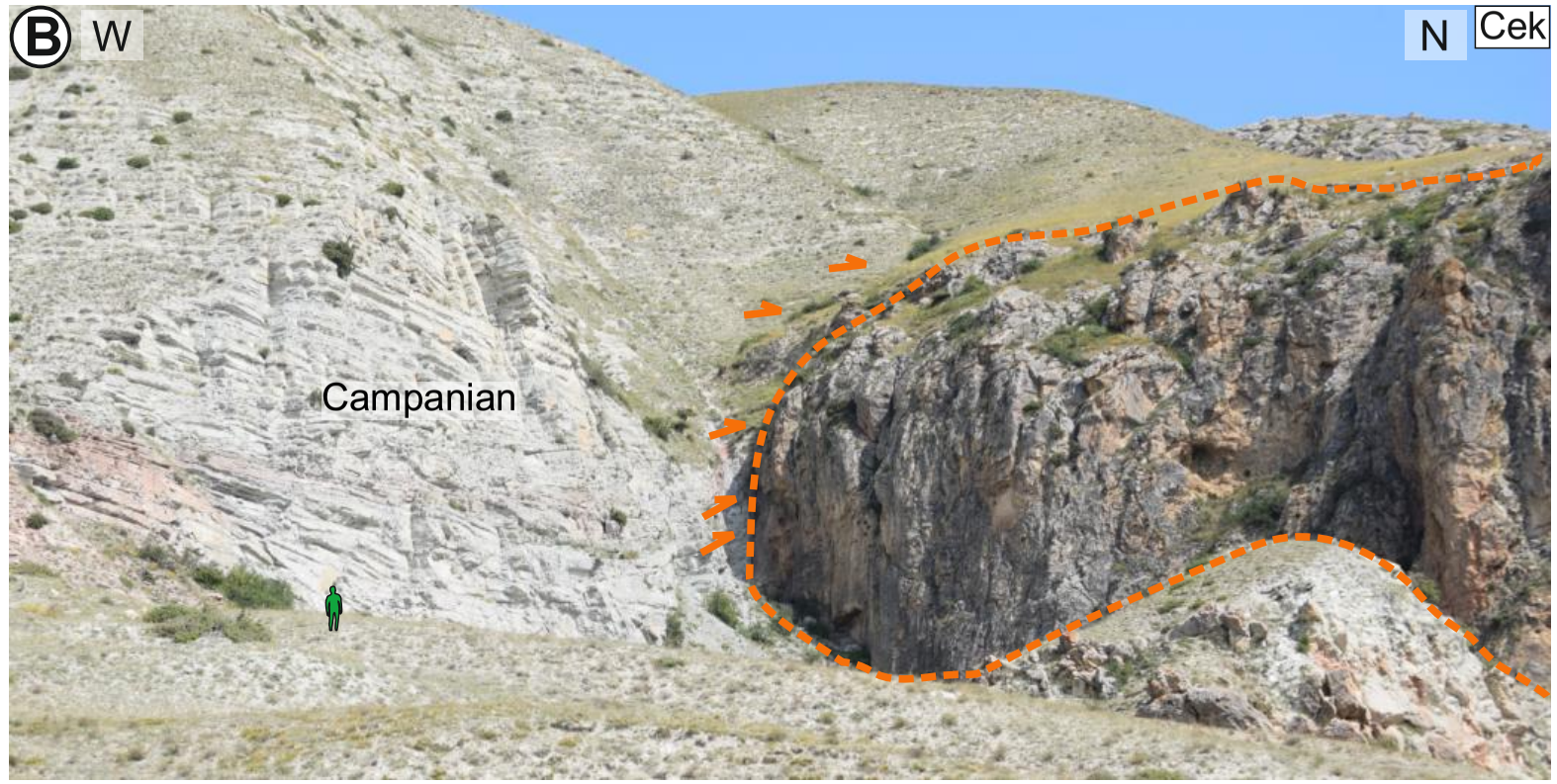
B
W
N
Cek
Campanian

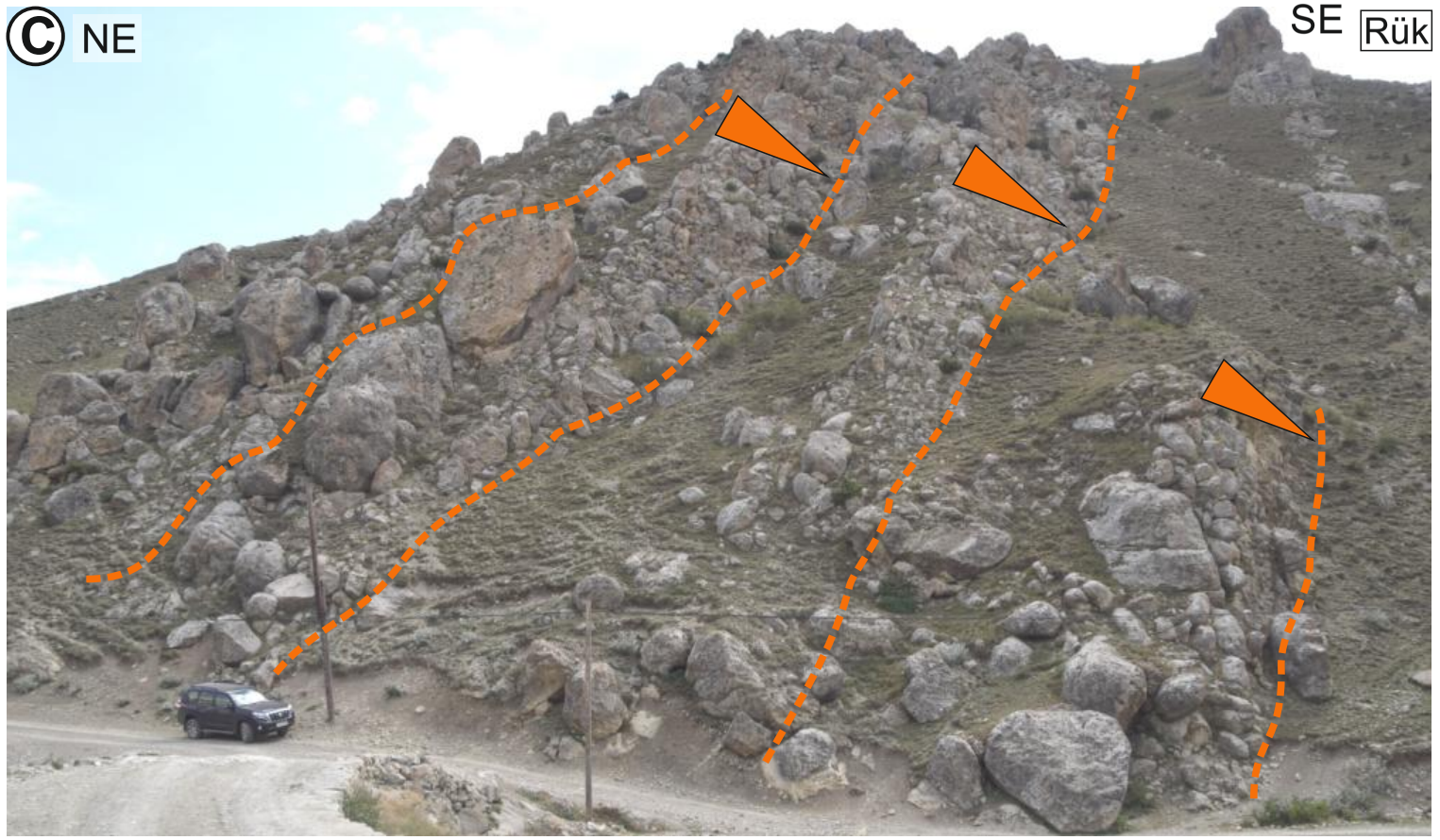
C
NE
SE
Rük

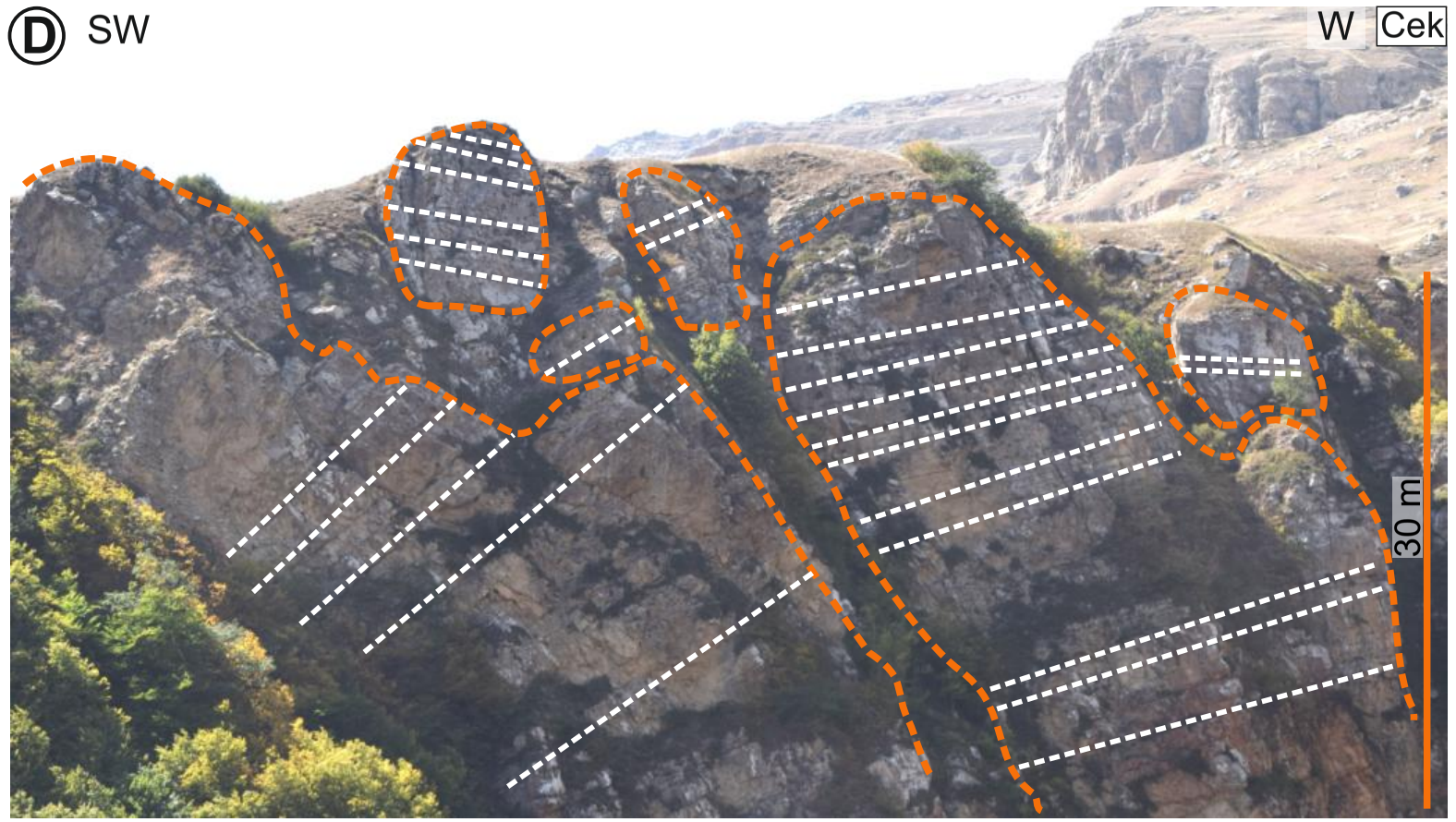
D
SW
W
Cek
30 m

Jurassic - Cretaceous contact

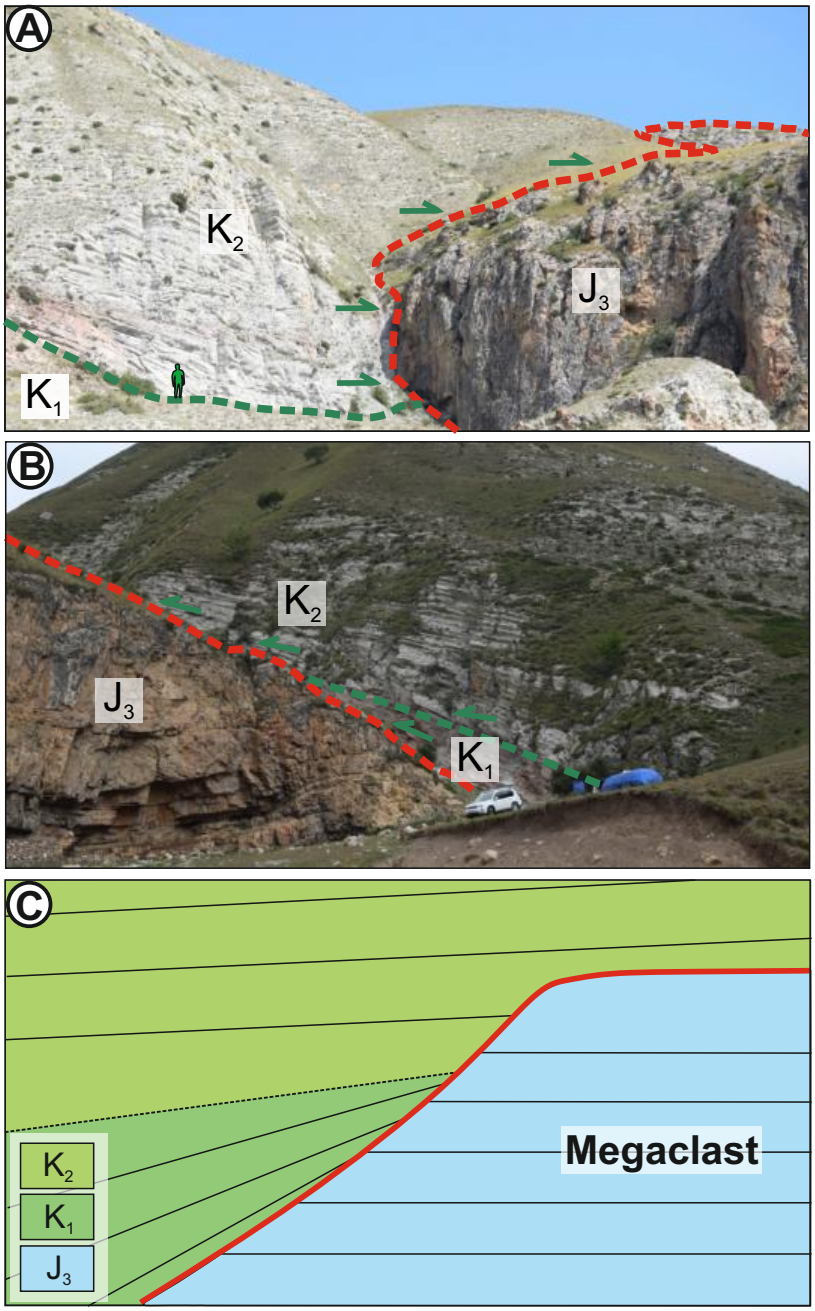


A
N


B
W
Village


C

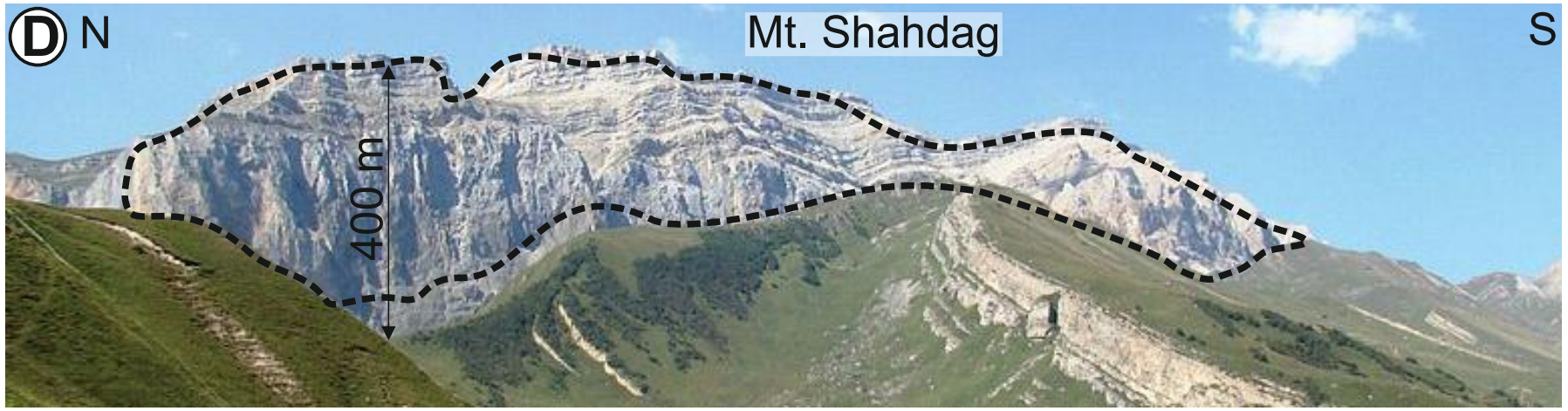
D
N
Mt. Shahdag
S
400 m

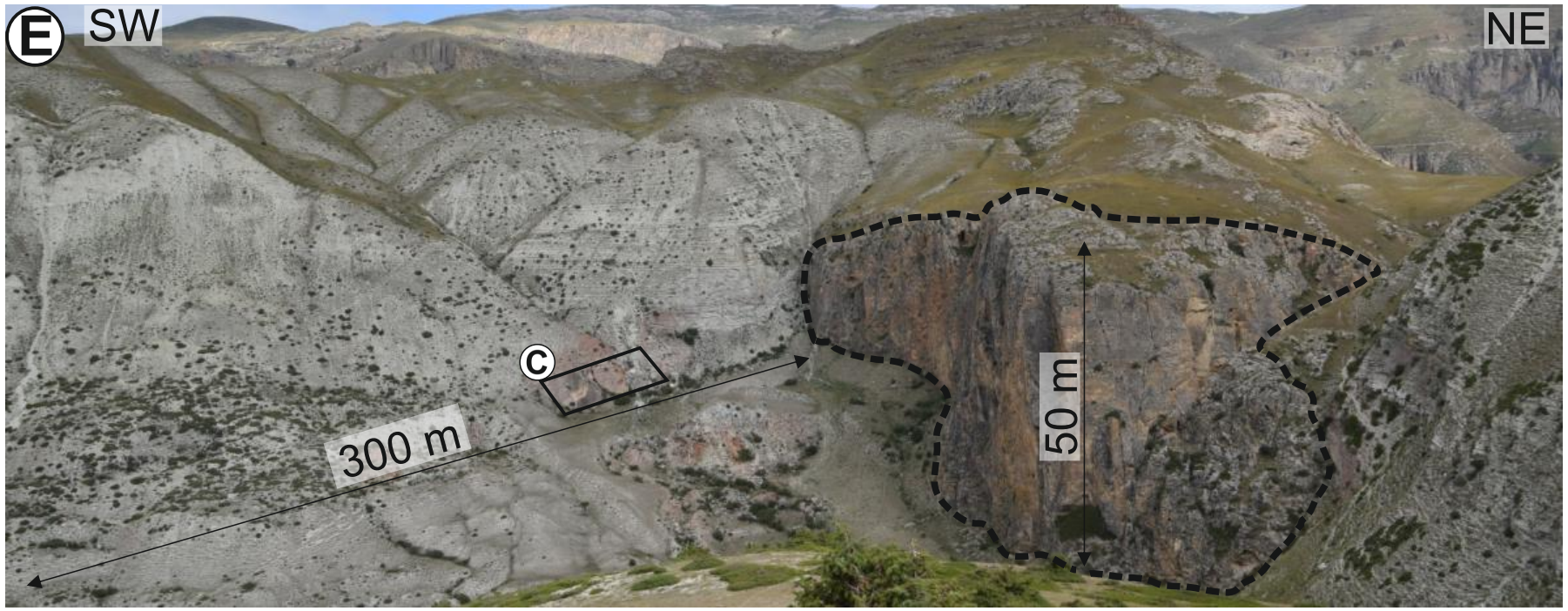
E
SW
NE
C
300 m
50 m

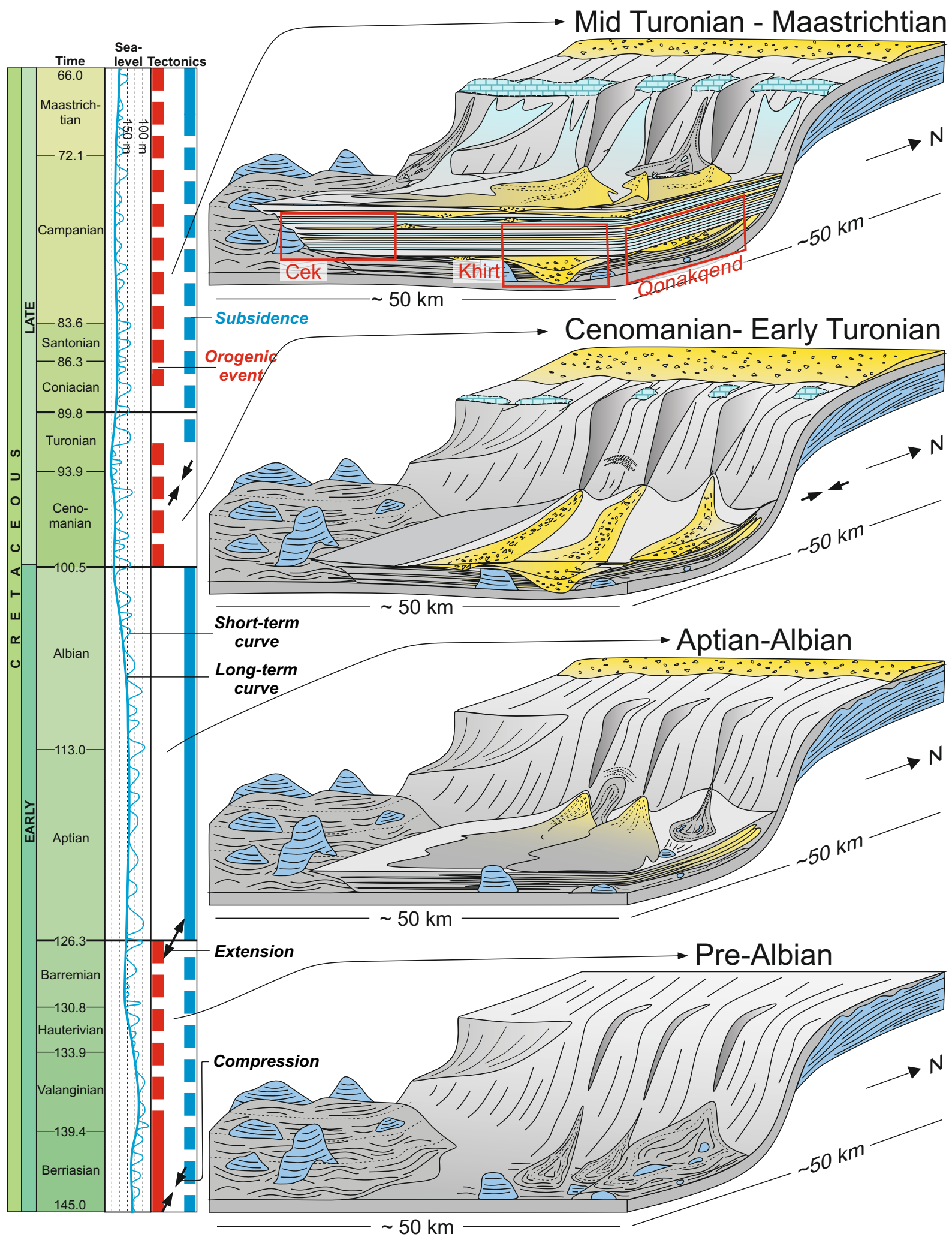
Time
Sea-level
Tectonics
66.0
Maastrich-tian
72.1
Campanian
83.6
Santonian
86.3
Coniacian
89.8
Turonian
93.9
Ceno-manian
100.5
Albian
113.0
Aptian
126.3
Barremian
130.8
Hauterivian
133.9
Valanginian
139.4
Berriasian
145.0
LATE
EARLY
CRETACEOUS
150 m
100 m
Subsidence
Orogenic event
Short-term curve
Long-term curve
Extension
Compression
Mid Turonian - Maastrichtian
Cek
Khirt
Qonakqend
~ 50 km
~50 km
N
Cenomanian- Early Turonian
Aptian-Albian
Pre-Albian

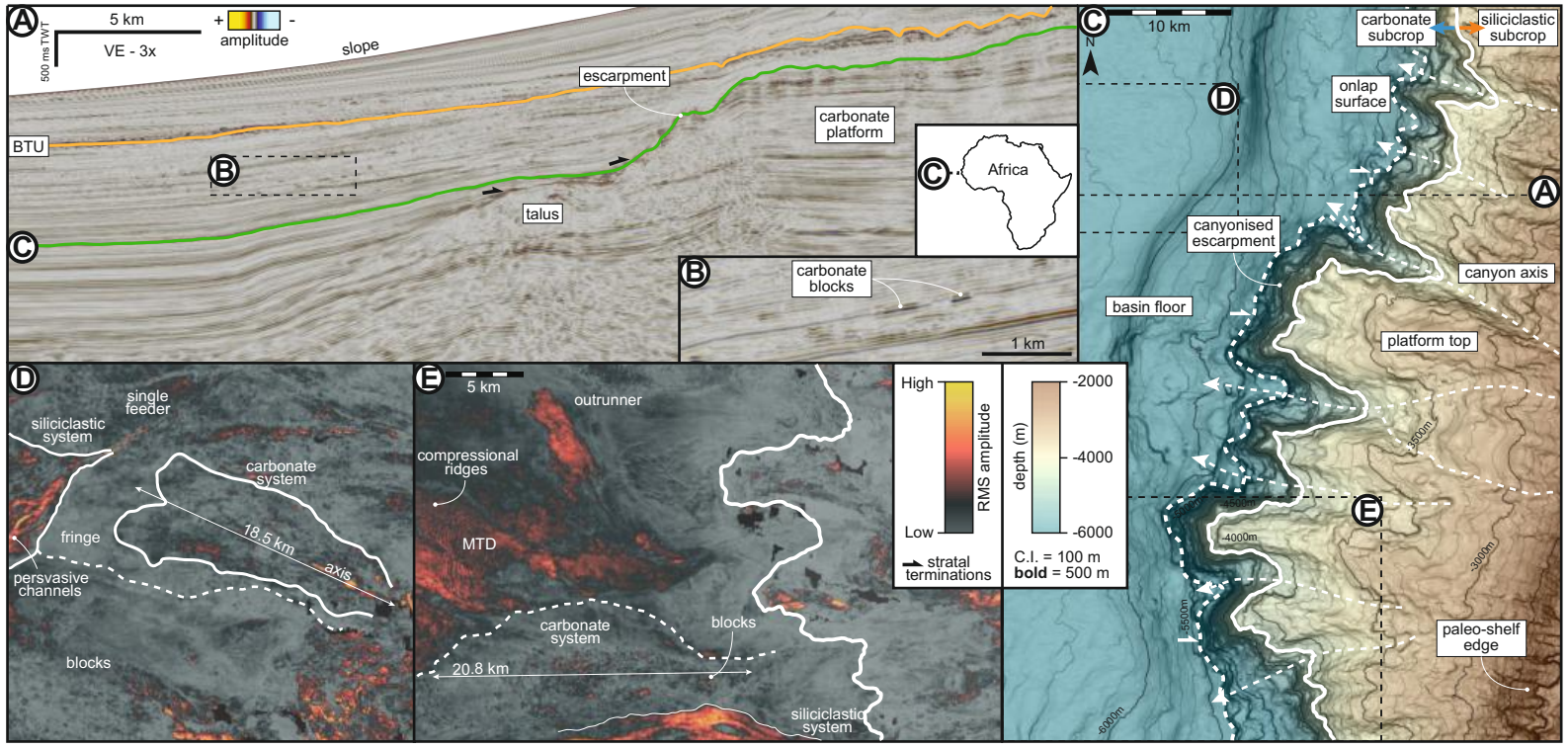
A
5 km
VE - 3x
500 ms TWT
+
amplitude
-
slope
escarpment
carbonate platform
BTU
B
talus
C
Africa
carbonate blocks
1 km
C
10 km
N
carbonate subcrop
siliciclastic subcrop
onlap surface
D
A
canyonised escarpment
canyon axis
basin floor
platform top
-5500m
-4500m
-4000m
-3000m
E
-5500m
-6000m
paleo-shelf edge
D
single feeder
siliciclastic system
carbonate system
fringe
18.5 km
axis
persvasive channels
blocks
E
5 km
outrunner
compressional ridges
MTD
carbonate system
blocks
20.8 km
siliciclastic system
High
Low
RMS amplitude
stratal terminations
depth (m)
-2000
-4000
-6000
C.I. = 100 m
bold = 500 m

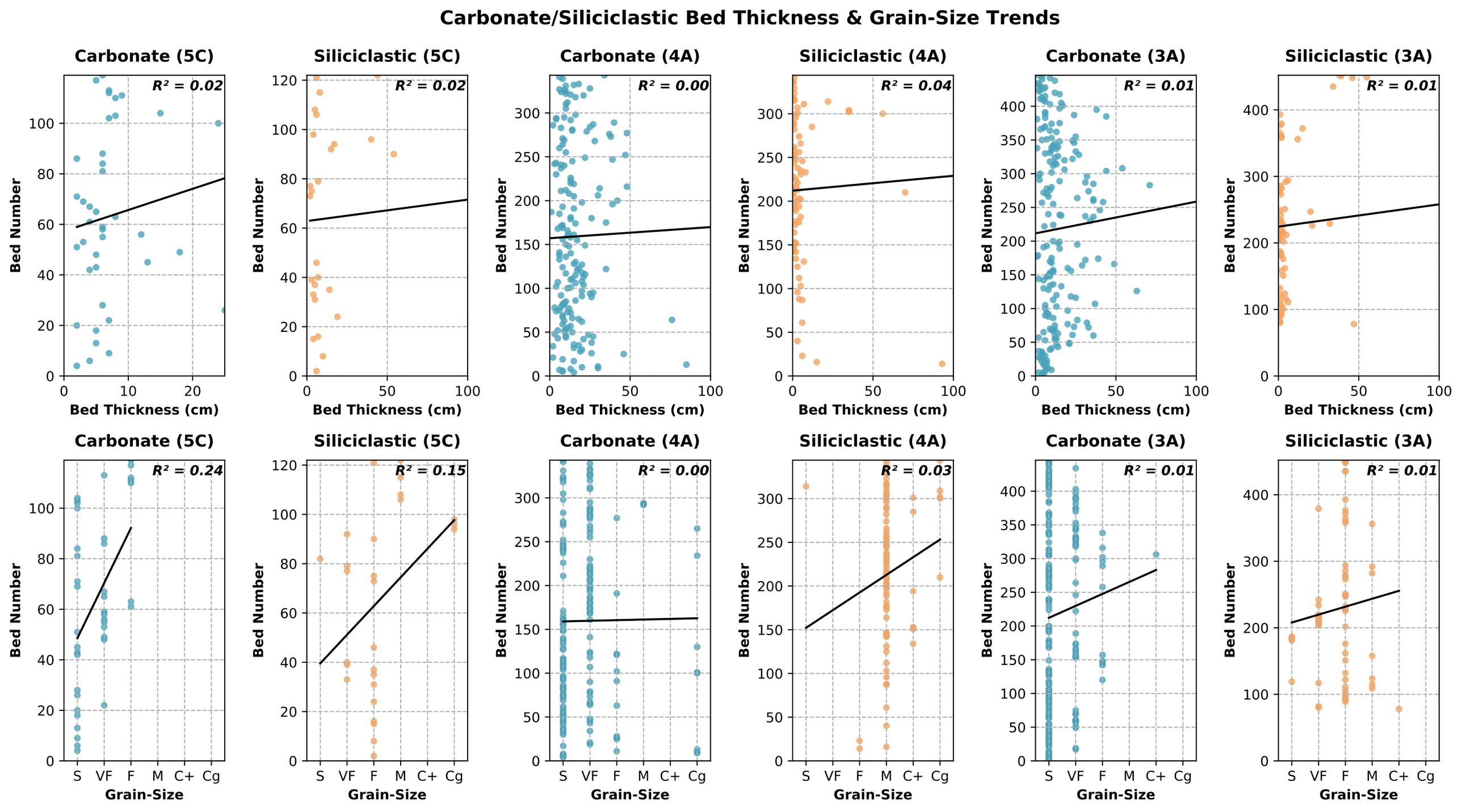
Carbonate/Siliciclastic Bed Thickness & Grain-Size Trends
Carbonate (5C)
Siliciclastic (5C)
Carbonate (4A)
Siliciclastic (4A)
Carbonate (3A)
Siliciclastic (3A)
R² = 0.02
R² = 0.02
R² = 0.00
R² = 0.04
R² = 0.01
R² = 0.01
Bed Number
Bed Thickness (cm)
R² = 0.24
R² = 0.15
R² = 0.00
R² = 0.03
R² = 0.01
R² = 0.01
S VF F M C+ Cg
Grain-Size

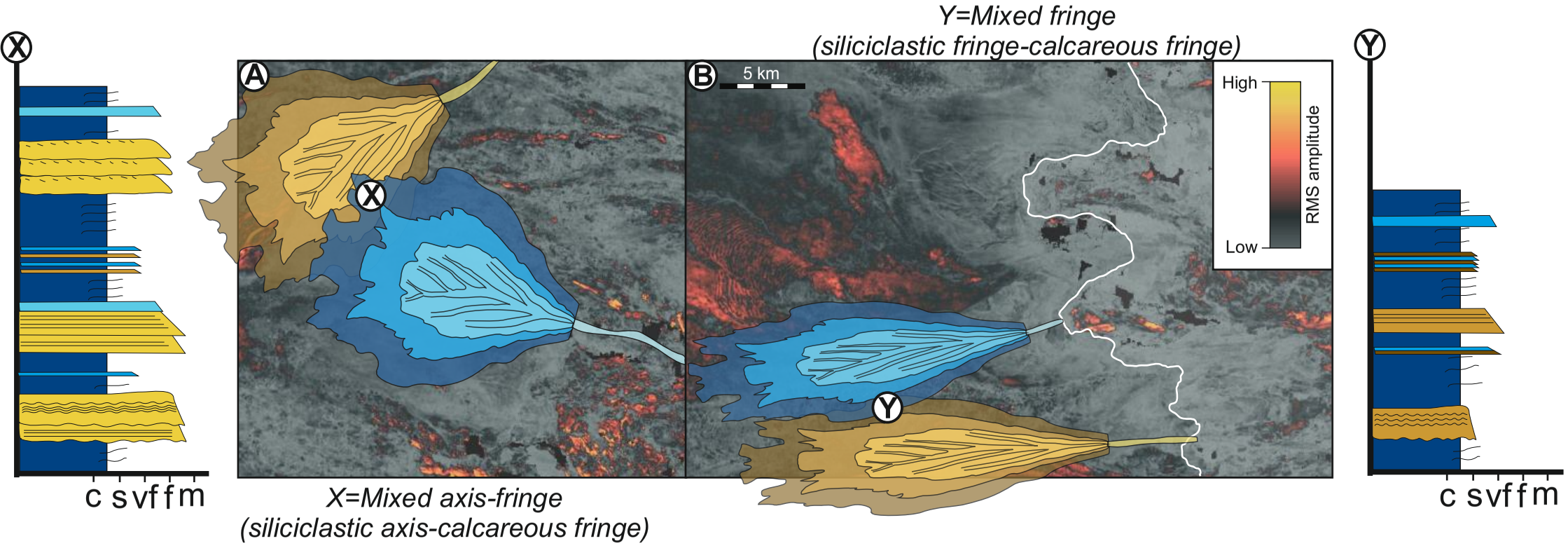

Y=Mixed fringe
(siliciclastic fringe-calcareous fringe)

X=Mixed axis-fringe
(siliciclastic axis-calcareous fringe)